PLOS | COMPUTATIONAL BIOLOGY

RESEARCH ARTICLE

Quorum-Sensing Synchronization of Synthetic Toggle Switches: A Design Based on Monotone Dynamical Systems Theory

Evgeni V. Nikolaev, Eduardo D. Sontag*

Department of Mathematics and Center for Quantitative Biology, Rutgers, The State University of New Jersey, Piscataway, New Jersy, United States of America

* eduardo.sontag@rutgers.edu

OPEN ACCESS

Citation: Nikolaev EV, Sontag ED (2016) Quorum-Sensing Synchronization of Synthetic Toggle Switches: A Design Based on Monotone Dynamical Systems Theory. PLoS Comput Biol 12(4): e1004881. doi:10.1371/journal.pcbi.1004881

Editor: Kobi Benenson, ETH Zürich, SWITZERLAND

Received: August 16, 2015

Accepted: March 23, 2016

Published: April 29, 2016

Data Availability Statement: All relevant data are within the paper and its Supporting Information files.

Funding: This work was funded by: Air Force Office of Scientific research FA9550-14-1-0060 http://www.wpafb.af.mil/afrl/afosr/; and Office of Naval Research 5710003367 http://www.onr.navy.mil/. The funders had no role in study design, data collection and analysis, decision to publish, or preparation of the manuscript.

Competing Interests: The authors have declared that no competing interests exist.

Abstract

Synthetic constructs in biotechnology, biocomputing, and modern gene therapy interventions are often based on plasmids or transfected circuits which implement some form of "on-off" switch. For example, the expression of a protein used for therapeutic purposes might be triggered by the recognition of a specific combination of inducers (e.g., antigens), and memory of this event should be maintained across a cell population until a specific stimulus commands a coordinated shut-off. The robustness of such a design is hampered by molecular ("intrinsic") or environmental ("extrinsic") noise, which may lead to spontaneous changes of state in a subset of the population and is reflected in the bimodality of protein expression, as measured for example using flow cytometry. In this context, a "majority-vote" correction circuit, which brings deviant cells back into the required state, is highly desirable, and quorum-sensing has been suggested as a way for cells to broadcast their states to the population as a whole so as to facilitate consensus. In this paper, we propose what we believe is the first such a design that has mathematically guaranteed properties of stability and auto-correction under certain conditions. Our approach is guided by concepts and theory from the field of "monotone" dynamical systems developed by M. Hirsch, H. Smith, and others. We benchmark our design by comparing it to an existing design which has been the subject of experimental and theoretical studies, illustrating its superiority in stability and self-correction of synchronization errors. Our stability analysis, based on dynamical systems theory, guarantees global convergence to steady states, ruling out unpredictable ("chaotic") behaviors and even sustained oscillations in the limit of convergence. These results are valid no matter what are the values of parameters, and are based only on the wiring diagram. The theory is complemented by extensive computational bifurcation analysis, performed for a biochemically-detailed and biologically-relevant model that we developed. Another novel feature of our approach is that our theorems on exponential stability of steady states for homogeneous or mixed populations are valid independently of the number N of cells in the population, which is usually very large ($N \gg 1$) and unknown. We prove that the exponential stability depends on relative proportions of each type of state only. While monotone systems theory has been used previously for systems biology analysis, the current work illustrates its power

for synthetic biology design, and thus has wider significance well beyond the application to the important problem of coordination of toggle switches.

Author Summary

For the last decade, outstanding progress has been made, and considerable practical experience has accumulated, in the construction of elementary genetic circuits that perform various tasks, such as memory storage and logical operations, in response to both exogenous and endogenous stimuli. Using modern molecular "plug-and-play" technologies, various (re-)programmable cellular populations can be engineered, and they can be combined into more complex cellular systems. Among all engineered synthetic circuits, a *toggle*, a robust bistable switch leading to a binary response dynamics, is the simplest basic synthetic biology device, analogous to the "flip-flop" or latch in electronic design, and it plays a key role in biotechnology, biocomputing, and proposed gene therapies. However, despite many remarkable properties of the existing toggle designs, they must be tightly controlled in order to avoid spontaneous switching between different expression states (loss of long-term memory) or even the breakdown of stability through the generation of stable oscillations. To address this concrete challenge, we have developed a new design for quorum-sensing synthetic toggles, based on monotone dynamical systems theory. Our design is endowed with strong theoretical guarantees that completely exclude unpredictable chaotic behaviors in the limit of convergence, as well as undesired stable oscillations, and leads to robust consensus states.

Introduction

In the short period since the pioneering milestones in synthetic biology [1, 2], outstanding progress has been made, and considerable practical experience has accumulated, in the construction of genetic circuits that perform various tasks, such as memory storage and logical operations, as well as support biomedical interventions and biotechnological manipulations in response to both exogenous and endogenous stimuli [3–9]. These circuits often include plasmids or transfected circuits which implement some form of "on-off" binary device, generically referred to as a *toggle switch*. For example, the expression of a protein used for gene therapy could be triggered by the recognition of some combination of inducers such as antigens, and memory of this event should be maintained across a cell population until a specific stimulus commands a coordinated shut-off [1, 3, 4]. In this context, as well as in many others, it is desirable for populations of cells to achieve coordinated static and/or dynamic functionalities. However, this coordination is hampered by molecular ("intrinsic") or environmental ("extrinsic") noise, which may lead to spontaneous changes of state in a subset of the population and is reflected in the bimodality of protein expression, as measured for example using flow cytometry.

To achieve robustness across a population, one may implement a "majority-vote" correction circuit that brings deviant cells back into the desired state. Much synthetic biology research focuses on single-cell microorganisms, often bacteria [4, 6–9]. Bacterial populations are relatively simple, and some aspects of their complex sociality can be rationally understood [10], providing a foundation for building more complex cellular systems. For bacteria, quorum-sensing (QS) has been suggested as a way for cells to broadcast their states to the population as

a whole so as to facilitate consensus. QS signaling pathways [11] can, for example, regulate bacterial gene expression in response to fluctuations in cell-population density. Bacteria produce and release various signaling molecules called autoinducers (AIs) [11–14]. The detection of a minimal threshold stimulatory concentration of an AI leads to an alteration in the host's gene expression. Both Gram-positive and Gram-negative bacteria use QS communication to regulate a diverse array of physiological activities. Synthetic biology design has adopted QS communication in its toolbox [15], because natural and artificially engineered QS modules can be used to interface synthetic circuits with exogenous and endogenous cues [4], and a systematic modular approach to standardize engineering toggle genetic circuits that would allow programmed cells to be designed for various specific purposes and to communicate their states to other cells was suggested as a bioengineering "plug-and-play" modular approach [4]. The design of such QS-toggle combinations is the focus of this paper.

A Known Design and Its Drawbacks

We benchmark our design by comparing it to Toggle B2 [4], see Fig SI-1.1 in S1 Text. Despite remarkable properties of design B2, observed experimentally in controllable experimental settings [4], and studied theoretically [16, 17], the fact that their functional repertoire includes not only a bistable long-term memory but also the generation of stable oscillations suggests that the environment-toggle system must be tightly controlled in order to avoid spontaneous switching, not merely between different expression states but even between different functions.

To address this challenge, we propose a novel design, which is endowed with mathematically guaranteed properties of stability and auto-correction. Our approach is closely guided by concepts and theory from the powerful framework of *monotone dynamical systems* pioneered by M. Hirsch and H. Smith [18–23].

We employ monotone theory to provide guarantees of global convergence to steady states, thus ruling out unpredictable ("chaotic") behaviors and sustained oscillations. These theorems are valid no matter for all values of parameters and are based only on the network structure. We also provide an extensive computational bifurcation analysis of the corresponding biochemically-detailed and biologically-relevant mathematical models. Our results for homogeneous or mixed populations are valid independently of the number of cells in the population ($N \gg 1$), and depend only on the relative proportions of each type of state.

The Components

As a basic design, we chose a genetic toggle switch consisting of two mutually repressing genes, *lacI* and *tetR* [1]. We use two acylated homoserine lactones (Acyl-HSLs), (*i*) *N*-butanoyl-l-homoserine lactone (C4-HSL) secreted by *Pseudomonas aeruginosa* [24], and (*ii*) *N*-(3-hydroxy-7-*cis*-tetradecenoyl)-L-homoserine lactone (3-OH-C14-HSL) produced by *Rhizobium leguminosarum* [13] as a means of coordinating toggle-host activity. Our design has two QS arms built-in the toggle in such a way that each promoter-repressor pair is controlled by its own QS signaling pathway symmetrically. Because of this "mirror-like" toggle symmetry, we call our design a symmetric toggle or an "S" design.

To benchmark the new S toggle design and the monotone systems approach, we compare the S design to the well-studied asymmetric B2-strain (Fig SI-1.1 in S1 Text) which has one QS arm only [4, 16]. In this work, we call the asymmetric B2-strain the "A" design. Our S design cannot be reduced to the A design by removing one QS arm, and, thus, the S design cannot be viewed as a straightforward extension of the A design. From a theoretical standpoint, it is worth remarking that the A design is non-monotone.

Under certain experimentally controllable conditions (*e.g*, unsaturated levels of AAA+ proteases ClpXP, *etc.*), the S vs. A toggle comparative results obtained in this work can be summarized as follows:

- The S toggle design completely excludes any unpredictable chaotic behaviors, as well as stable oscillations. Typical trajectories converge globally to stable equilibria. This conclusion is valid for all parameter values, and provides a strong theoretical guarantee missing from other synthetic biology designs.
- We refer to mixed states leading to bimodal distributions as *spontaneous synchronization errors*. We find that the S toggle design is able to self-correct (or, auto-correct) synchronization errors, while the non-monotone A toggle design is not.
- We show how monotone systems theory can predict not only the dynamics of an S toggle population but it also explains certain monotonically increasing or decreasing parametric dependencies of population steady states. Some of these predictions can facilitate self-synchronization and, thereby, reduce the chance for synchronization errors to emerge spontaneously.

Organization of Paper

In Models, the S toggle and A toggle mathematical models are introduced. The basic formalism and fundamental mathematical results of monotone systems theory, including Strong Monotonicity and Hirsch's Theorem [18–21, 23] are as well reviewed. Reference values of dimensionless parameters, scaling, and selection and interpretation of bifurcation parameters are discussed. We also formalize a concept of spontaneous synchronization errors by considering three types of equilibrium populations: One homogeneous population, and two heterogeneous (mixed) populations (bimodal distributions) with both equally (1:1)-mixed and not-equally (N_1:N_2)-mixed transcriptional signatures, $N_2 \ll N_1$, the latter giving rise to spontaneous synchronization errors, where $N = N_1 + N_2$, and N is the number of cells in the given population.

In Results and Discussion, we proceed to a comparative theoretical and computational analysis of the S and A toggle designs. We begin this section with results on the application of monotone systems theory to the S design, as these results constitute the main conceptual and practical subject motivating this work (Application of Monotone Systems Theory to the S Design). We then explain how monotone systems theory allows one to predict, based on qualitative knowledge only, that generically all solutions converge to equilibria, with no possible oscillations [16] nor chaotic behavior [25], no matter what the kinetic parameters are. This is in contrast to the A design, which may admit oscillations [16]. Next, we analyze single S and A toggles decoupled from the environment (Bistability in Single S and A Toggles), and observe that the S toggle remains bistable even if "redundant" repressor genes are removed from the corresponding plasmids. To show how the S design is more robust than the A design, we carry out a comparative bifurcation analysis of populations consisting of coupled S or A toggles. We select a free (bifurcation) dimensionless parameter which can be interpreted in terms of experimental interventions [6] leading to (*a*) changes in the membrane permeability, or (*b*) changes in the half-lives of repressor proteins, or (*c*) changes in the specific growth rate of the host cell. We finally test the toggle design capabilities to self-correct spontaneous synchronization errors by sampling the basin of attractor of the corresponding equilibrium solutions. We find that the S toggle design is able to self-correct synchronization errors far better than the A toggle design.

The paper also has Supplemental Information (SI) materials S1–S8 which can be found in S1 text (the file S1-text.pdf).

In SI-1 Toggle B2 (see S1 Text), we discuss the relationship between A design and its prototype, the *E. coli* strain "B2" developed by Kobayashi et al [4] who considered a number of genetic toggle switches, interfaced with a QS signaling pathway.

In SI-2 Model Derivation (see S1 Text), we derive mathematical models and carry out a nondimensionalization procedure, the conclusions of which are used in the main text (Scaling).

In SI-3 Estimation of Parameter Values (see S1 Text), we discuss ranges of biologically meaningful parameter values based on data available in the existing literature. Values of biologically meaningful parameters depend upon experimental conditions and other factors controlled by an experimenter, as reviewed in [6]. Therefore, we provide an example of a concrete estimation of the values of dimensionless parameters, which we interpret in terms of interventions reviewed in [6].

In SI-4 Alternative Definitions of Monotone Systems and Order Preservation (see S1 Text), balanced graphs, relation to graph partitions, and order presentation by flows are explained.

In SI-5 Symmetry (see S1 Text), we formalize symmetry of the S design and discuss interpretation of symmetric results with respect to nonsymmetric perturbations typical for experimental systems.

In SI-6 Exponential Stability of Cellular Populations (see S1 Text), we prove a number of general theorems to analyze exponential stability [26] of both homogeneous and heterogeneous (mixed) population equilibrium states, independently of the number N of cells in the given population, which (*i.e.,* the value of $N \geq 2$) can be *a priori* unknown.

In SI-7 Additional Figures (see S1 Text), we provide additional bifurcation diagrams.

In SI-8 Modification of the S and A Models to Describe Sequestration of AAA+ protease ClpXP (see S1 Text), additional (modified) mathematical models describing competition of ssrA-tagged protein molecules for AAA+ proteases ClpXP are described.

Models

Although our main objective in this paper is to present a conceptual and general organizing principle for the construction of self-correcting "majority-vote" multistable synthetic systems, we instantiate our ideas through a very concrete set of genes and protein products, all being standard molecular parts in synthetic biology [1, 2, 4, 7–9, 27–31]. We do that in order to emphasize the fact that our constructs can be realistically implemented with currently available molecular components. However, replacing these components with others does not change the basic mathematical framework.

To facilitate a conceptual and quantitative comparison of the S and A toggle designs, the corresponding genetic circuits are assumed to be built from the same tightly controlled *lac-tet* transcription entities [7–9, 32–37], which have been intensively used in a number of experimental and theoretic-modeling studies in the context of synthetic biology [1, 2, 4, 7–9, 28–31]. Below, we briefly characterize relevant molecular details and then form the corresponding mathematical models.

Toggle Designs

For the sake of completeness of our description, we begin our discussion of the S toggle and A toggle designs (Fig 1) with two classical orthogonal repressors (Table 1):

1. LacI from *E. coli* which inhibits the transcription of the second repressor gene, tetR from the tetracycline-resistance transposon Tn10;
2. TetR which represses the transcription of the first repressor gene *lacI*.

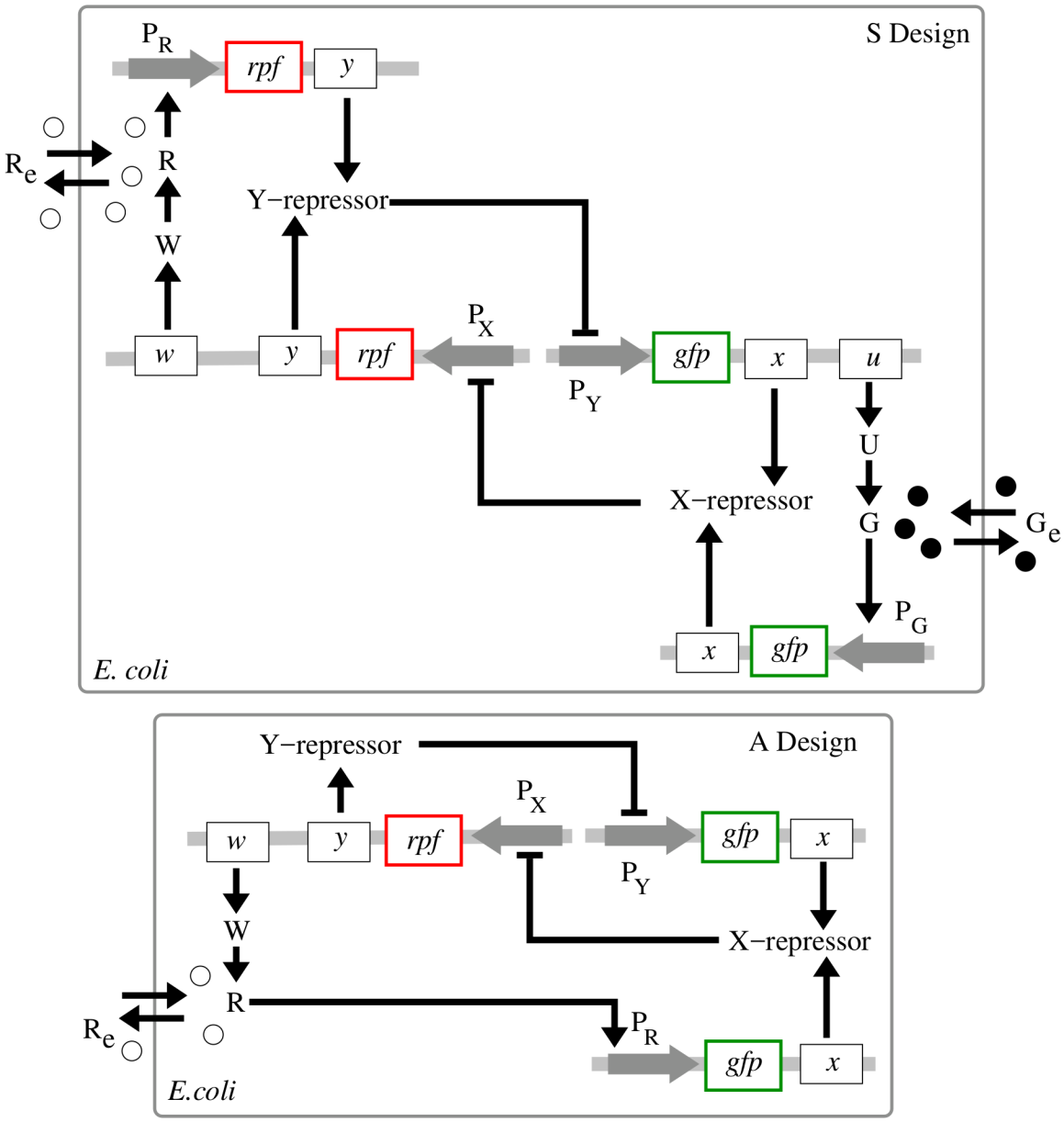

Fig 1. Monotone-symmetric and nonmonotone-asymmetric toggle designs. S design (*top panel*): Activation of the expression of gene *x* (*lacI*) occurs by binding of autoinducer G (C14-HSL) to promoter P_G (P_{cin}). Inhibition of the expression of both genes *x* (*lacI*) and *u* (*cinI*) occurs by binding of the gene product *Y* (TetR) of gene *y* (*tetR*) to a single promoter P_Y (P_{tet}). Symmetrically, activation of the expression of gene *y* (*tetR*) occurs by binding of autoinducer R (C4-HSL) to promoter P_R (P_{rhl}), while inhibition of the transcription of both genes *y* (*tetR*) and *w* (*rhlI*) occurs by binding of X (LacI) to a single promoter P_X (P_{lac}). **A design** (*bottom panel*): Activation of the expression of gene *x* (*lacI*) occurs by binding of autoinducer R (C4-HSL) to promoter P_R (P_{rhl}). Expression of genes *y* (*tetR*) and *w* (*rhlI*) is driven by a common single promoter P_X. Gene products *U* and *W* are synthases CinI and RhiI, respectively. Gray horizontal strips correspond to integration plasmids. Genes *gfp* and *rfp* correspond to green and red florescent proteins, GFP and RFP, respectively.

doi:10.1371/journal.pcbi.1004881.g001

Next, the communication network among all toggles (Fig 1) is built upon two quorum-sensing (QS) signaling molecules (Table 1):

1. *N*-(3-hydroxy-7-*cis*-tetradecenoyl)-L-homoserine lactone (3-OH-C14-HSL);
2. *N*-butanoyl-l-homoserine lactone (C4-HSL).

Table 1. A toggle molecular part catalog (explanations of variables are given in S model).

Name	variable	Function	Description	References
lacI	–	repressor gene	lactose-inducible transcriptional repressor from *E. coli*	[1, 2, 6, 33]
tetR	–	repressor gene	from the tetracycline-resistance transposon Tn10	[1, 2, 33, 36]
cinI	–	autoinducer gene	encodes protein CinI which synthesizes C14-HSL	[11, 13, 14]
rhlI	–	autoinducer gene	encodes protein RhlI which synthesizes C4-HSL	[11, 12]
LacI	x_i	lactose inhibitor	a DNA-binding protein encoded by *lacI*	[1, 2, 33, 37]
TetR	y_i	repressor protein	a basic element of tetracycline-controlled regulation	[1, 2, 34, 36]
CinI		synthase	the gene product of gene *cinI*	[11, 13, 14]
RhlI		synthase	the gene product of gene *rhlI*	[11, 12]
C14-HSL	g_i, g_e	autoinducer	*N*-(3-hydroxy-7-*cis*-tetradecenoyl)-L-Homoserine Lactone	[13]
C4-HSL	r_i, r_e	autoinducer	*N*-butyryl-L-Homoserine Lactone	[12, 24]

doi:10.1371/journal.pcbi.1004881.t001

For the sake of brevity, the QS signaling molecules are called autoinducers G (C14-HSL) and R (C4-HSL). Note that the G- and R-signals (acylated homoserine lactones) are natural biological signals secreted by Gram-negative bacteria, including *E. coli*, as a means of coordinating cellular activity [4, 11].

Finally, to drive the autoinducer concentrations, two synthases are used (Table 1):

1. CinI, the gene product of *cinI*, driving the concentration of C14-HSL;
2. RhlI, the gene product of *rhlI*, driving the concentration of C4-HSL.

Using the above molecular species, we implement and study two different toggle designs called *symmetric* (S) and *asymmetric* (A) designs, respectively, (Fig 1):

1. In the S design, each of the two autoinducers activates symmetrically the transcription of the corresponding repressor gene through a single promoter, that is, promoter P_{cin} (P_G) for gene *lacI* (x) and promoter P_{rhl} (P_R) for gene *tetR* (y);
2. In the A design, the same repressor genes (as used in the S design) antagonistically repress one another directly, while there is only one autoinducer that asymmetrically facilitates communication between all toggles.

The genetic circuit topology used in the A design (Fig 1) is taken from [16]. In order to keep making a fair comparison with the S design, we have replace the *luxR-luxI* system considered in [16] by the *lacI-tetR* system suggested in [1], see SI-1 Toggle B2 in S1 Text. Note that both CinI and RhiI are homologous to LuxI [38].

To host the S and A toggles, we use *E. coli*, a bacterial cell which has been well-studied in a huge number of relevant experimental and modeling works [32, 39–50], and which has been widely used to implement and test various synthetic circuits [1, 2, 4, 7–9, 15]. A practical modeling reason for this selection is narrowing-down our search for biologically-meaningful parameters to values known from the *E. coli* studies. However, our conclusions do not depend in any way on biological properties of the host.

As a readout of the toggle state in individual cells, we further assume that each *E. coli* cell contains a gene encoding a spectrally distinct fluorescent reporter, GFP for gene *lacI*, and RFP for gene *tetR*, driven by promoters that respond to the autoinducers C14-HSL and C4-HSL, respectively. We do not simulate the processes of bio-synthesis and degradation of the fluorescent proteins explicitly, using appropriate cascade models, for two reasons: *(i)* the "reporter" submodel does not affect the dynamics of the entire model, and *(ii)* the half-lives of the reporter proteins can be made similar to the half-lives of the repressor proteins [2].

Finally, because each toggle can either be in a state where *(a)* LacI protein is abundant, while TetR protein is scarce, or in a state where *(b)* TetR protein is abundant, while LacI protein is scarce, we call state *(a)* a green state or, simply, a G-state and state *(b)* a red state or, simply, an R-state, respectively.

S model. A mathematical model describing a population of identical S toggles is

$$\frac{dx_i}{dt} = \gamma_x + \frac{a_1}{1+y_i^{n_Y}} + \frac{a_3\, g_i^{n_G}}{1+g_i^{n_G}} - x_i, \tag{1}$$

$$\frac{dy_i}{dt} = \gamma_y + \frac{a_2}{1+x_i^{n_X}} + \frac{a_4 r_i^{n_R}}{1+r_i^{n_R}} - y_i, \tag{2}$$

$$\frac{dg_i}{dt} = \gamma_g + \frac{a_5}{1+y_i^{n_Y}} + d(g_e - g_i) - \delta_g g_i, \tag{3}$$

$$\frac{dr_i}{dt} = \gamma_r + \frac{a_6}{1+x_i^{n_X}} + d(r_e - r_i) - \delta_r r_i, \quad i = 1, \ldots, N, \tag{4}$$

$$\frac{dg_e}{dt} = \frac{\rho}{N}\sum_{i=1}^{N} d(g_i - g_e) - \delta_e g_e, \quad 0 \le \rho \le 1, \tag{5}$$

$$\frac{dr_e}{dt} = \frac{\rho}{N}\sum_{i=1}^{N} d(r_i - r_e) - \delta_e r_e. \tag{6}$$

Here, all state variables and parameters are dimensionless, and are obtained from the corresponding biologically meaningful state variables and parameters describing the *lac-tet* system (Table 1) after an appropriate nondimensionalization, see SI-2 Model Derivation in S1 Text.

In the S model Eqs (1)–(6), t is dimensionless time; x_i and y_i are the dimensionless concentrations (levels) of intracellular repressor proteins LacI and TetR, respectively; g_i and r_i are the dimensionless concentrations of intracellular autoinducers C14-HSL and C4-HSL, respectively; g_e and r_e are the dimensionless concentrations of extracellular autoinducers C14-HSL and C4-HSL, respectively.

The dimensionless rate constants a_i, $i = 1, \ldots, 6$, depend on the copy numbers of the plasmids that bear the corresponding genes, see relationships Eqs (18) and (19) given in Scaling; n_X, n_Y, n_G, and n_R are the corresponding Hill coefficients; d is the dimensionless diffusion coefficient; δ_g and δ_r are the dimensionless lumped dilution-degradation rates due to the exponential cell growth and degradation of the corresponding species; γ_x, γ_y, γ_g, and γ_r are the corresponding leakiness coefficients [16, 17].

The degradation rate constants for repressor species x_i and y_i are scaled out to unity, as it is done in [1, 2, 16, 17], see SI-3 Estimation of Parameter Values in S1 Text; δ_e is the dilution rate due to flow in the medium; ρ is a population density; and N is the number of cells in the given population.

A model. A dimensionless mathematical model describing a population of identical A toggles is

$$\frac{dx_i}{dt} = \gamma_x + \frac{a_1}{1+y_i^{n_Y}} + \frac{a_4\, r_i^{n_R}}{1+r_i^{n_R}} - x_i, \tag{7}$$

$$\frac{dy_i}{dt} = \gamma_y + \frac{a_2}{1 + x_i^{n_X}} - y_i, \tag{8}$$

$$\frac{dr_i}{dt} = \gamma_r + \frac{a_6}{1 + x_i^{n_X}} + d(r_e - r_i) - \delta_r r_i, \quad i = 1, \ldots, N, \tag{9}$$

$$\frac{dr_e}{dt} = \frac{\rho}{N} \sum_{i=1}^{N} d(r_i - r_e) - \delta_e r_e. \tag{10}$$

Here, all state variables and parameters are as defined for the S model Eqs (1)–(6). The A model is mathematically identical to the *minimal* (simplified) model developed in [16] for the *E.coli* strain (toggle) B2 [4], shown in Fig SI-1.1 in S1 Text.

Modeling assumptions. Since the intention of our work is to illustrate the application of monotone dynamical systems theory to the S design and, also, to compare the S design with other known designs, we have developed two *simplified minimal* models, described in S model and A model, respectively. However, because a practical implementation of synthetic toggles is still far from being a routine exercise [6], care should be taken to explain the assumptions used to construct the models.

First of all, we compare the new *monotone* S design with a well accepted *non-monotone* toggle design, the *E.coli* strain B2 [4], which we call the A design, and for which a substantial modeling work has been done [16, 17] (SI-1 Toggle B2 in S1 Text). Therefore, for a careful comparison of these two different designs, we have accepted the corresponding modeling simplifications and assumptions [16, 17]. We discuss them in SI-1 Toggle B2 and SI-2.1 Mass-Balance Equations in S1 Text.

Models always involve simplifications of reality. The impact of several such simplifications and assumptions, particularly those impacting monotonicity properties and bistabiliy regions, are: (*i*) a reduced promoter leakiness [2, 4, 51], (*ii*) unsaturated levels of AAA+ proteases ClpXP [9], and (*iii*) small values of Hill coefficients [7–9, 16]. Because the impact of the variation in the values of the Hill coefficients and leakiness parameters on the bistability region in the A model is carefully analyzed in [16], we validate variations in these parameters for the S model only.

Other assumptions refer to the cells growth conditions, *e.g.*, whether the cells are in solid culture, liquid culture, in a micro-chemostat, on plates, etc. To this end, the A model [16] corresponds to the strain B [4] for which a detailed description of the growth conditions can be found in the corresponding experimental protocol [4]. We can thus assume that both S and A models correspond to the same growth condition, that is, the aerobic growth in LB medium on plates [4].

In both S and A models, there is no time-dependence of dilution or degradation [16]. However, depending on the growth phase of the bacteria, the effects of dilution will not be constant [40, 47–49, 52]. We use the stationary exponential growth assumption for the sake of simplicity [16].

Model Parameters

Uncertainty about the values of parameters characterizing molecular components of synthetic circuits always presents a significant difficulty in circuit design [2]. Here, we discuss reference values of dimensionless parameters obtained using an appropriate scaling procedure. We also explain how we select and interpret parameters for our bifurcation analysis.

Model parameters. Reference values of all parameters used in our modeling studies are estimated in SI-3 Estimation of Parameter Values in S1 Text, and these correspond to half-lives

of all proteins in the range 4–10 min., which are close to a typical mRNA half-life in *E. coli* [2]. Also, to avoid competition for ribosomes [43], only a few plasmids bearing four promoters P_X, P_Y, P_G, and P_R can be used, and we use 1–2 copies per cell, see SI-3 Estimation of Parameter Values in S1 Text. The *E. coli* replication period is assumed to be around 25 min.

Despite the fact that much is known about *E. coli* [39–41, 45, 47, 48, 50], it is not possible to model behavior in a quantitatively precise way, since not enough is yet known about molecular interactions between the toggle and the host cell to make such a description realistic [6]. Instead, we hope to identify classes of toggle designs and dynamic behaviors to determine which of the designs could lead to an improved self-synchronization reliability and an improved capability for self-correction of spontaneous synchronization errors, when a small fraction of cells flips to the opposite (undesirable) transcriptional signature state, see Spontaneous Synchronization Errors. We will also make some predictions that might help to facilitate engineering toggles with desired robust traits.

In our computational analysis, the following set of *reference* parameter values is used:

$$\gamma_x = \gamma_y = \gamma_g = \gamma_r = 0, \tag{11}$$

$$a_1 = a_2 = 20, \quad a_3 = a_4 = 10, \quad a_5 = a_6 = 3, \tag{12}$$

$$n_{\mathrm{X}} = n_{\mathrm{Y}} = n_{\mathrm{G}} = n_{\mathrm{R}} = 3, \tag{13}$$

$$\delta_g = \delta_r = 1.0, \quad \delta_e = 0.5, \quad \rho = 0.8. \tag{14}$$

Groups of parameters with identically the same values are used to introduce the toggle mirror (involutive) symmetry into the S model as discussed in SI-5 Symmetry in S1 Text. We find that the working values of parameters estimated in Eqs (11)–(14) are within the range of equivalent parameters (rate constants, Hill coefficients, *etc.*) used earlier for genetic circuits built from similar (*e.g.*, homologous) molecular entities [1, 2, 4, 7–9, 16, 17, 28–31, 53].

However, there is a variability in the estimation of values for some important parameters in the literature. Specifically, the values of the Hill coefficients (n_G and n_R) for the binding of C4-HSL and C14-HSL to the corresponding promoters are equal to 4 (estimated *ad hoc*) in the model developed in [9]. On the other hand side, the values of the Hill coefficients for C6-HSL and C12-HSL are estimated in the range of values 1–2 in [7, 8]. Because it may be unlikely to have high values of the Hill coefficients, and because the analytical and computational analyses of the impact of the Hill coefficients on the bistability regions for the A model have been done in great detail in [16], we have selected a compromising *reference* values of all Hill coefficients equal to 3 [16].

Another important parameter (γ) is the promoter leakiness [2, 4, 51]. To this end, very small dimensionless values of the corresponding leakiness parameters are used in the relevant modeling studies [16, 17]. Because we compare our S model with the A model [16], and because the zero reference value for the leakiness parameters is used in [16], we also use the zero *reference* value for the leakiness parameters in both the S and A models. The tightness of the promoter control has been reported in the literature, *e.g.*, see [2, 4, 12, 51], and the reduction in the promoter leakiness is the subject of active ongoing research with the promise to reduce this leakiness even further dramatically [51].

To probe the robustness of the developed theory in the cases when: (*i*) the Hill coefficients can take on different values, (*ii*) the promoter leakiness can be allowed to take on nonzero values, and (*iii*) the S model can lose its "perfect" mirror symmetry property, we additionally analyze the S model with the following modified parameter values while all other parameter values

are kept intact as in the reference set Eqs (11)–(14),

$$\gamma_x = \gamma_y = \gamma_g = \gamma_r = 0.01, \tag{15}$$

$$a_1 = a_2 = 100, \tag{16}$$

$$n_{\mathrm{X}} = n_{\mathrm{Y}} = 2,\ n_{\mathrm{G}} = 1, \text{ and } n_{\mathrm{R}} = 2. \tag{17}$$

Specifically, condition $n_{\mathrm{G}} \neq n_{\mathrm{R}}$ removes the mirror symmetry from the S model. We will also use the set of modified parameters in the case when the monotonicity property is violated by the sequestration of AAA+ proteases ClpXP (Monotone Parametric Dependencies in the S Design).

Scaling. One of the goals of a model nondimensionalization and scaling is to reduce the number of (correlated) parameters by lumping original parameters into a smaller parameter set. In this case, interpretation of changes in the values of dimensionless parameters should be done carefully, as the set of dimensionless parameters is usually not in one-to-one correspondence with the set of original parameters. For example, mathematical models used for synthetically engineered systems often contain parameters representing multiple biological parts and, so, tuning a dimensionless parameter in the corresponding mathematical model can be implemented experimentally in a number of different ways [6].

The dimensional and dimensionless parameters used in the S and A toggle models are related to one another by the following relationships (see SI-2 Model Derivation in S1 Text):

1. For the dimensionless rate parameters, we obtain:

$$a_1 = \frac{b_x k_x [\mathrm{P_Y}]}{K_{\mathrm{X}}(r_d + \mu)}, \quad a_2 = \frac{b_y k_y [\mathrm{P_X}]}{K_{\mathrm{Y}}(r_d + \mu)}, \quad a_3 = \frac{b_x k_x [\mathrm{P_G}]}{K_{\mathrm{X}}(r_d + \mu)}, \tag{18}$$

$$a_4 = \frac{b_y k_y [\mathrm{P_R}]}{K_{\mathrm{Y}}(r_d + \mu)}, \quad a_5 = \frac{b_u k_u k_{\mathrm{G}} [\mathrm{P_Y}]}{K_{\mathrm{G}}(r_d + \mu)^2}, \quad a_6 = \frac{b_w k_w k_{\mathrm{R}} [\mathrm{P_X}]}{K_{\mathrm{R}}(r_d + \mu)^2}. \tag{19}$$

2. For the dimensionless diffusion and degradation parameters, we obtain:

$$d_g = \frac{D_{\mathrm{G}}}{r_d + \mu}, \quad d_r = \frac{D_{\mathrm{R}}}{r_d + \mu}, \tag{20}$$

$$\delta_g = \frac{r_{\mathrm{G}} + \mu}{r_d + \mu}, \quad \delta_r = \frac{r_{\mathrm{R}} + \mu}{r_d + \mu}, \quad \delta_e = \frac{\mu_e}{r_d + \mu}. \tag{21}$$

Let us briefly discuss Eqs (18), (19), (20) and (21). Here, the burst parameter b_x for the protein X or, equivalently, LacI, depends on the efficiency of translation, controlled by strength of ribosome-binding sites (RBS) [1, 6], and the mRNA half-life time [54]; $[\mathrm{P_X}]$ is the number of promoters per cell for gene x; k_x is an average transcription rate for gene x (*lacI*); K_{X} is the number of LacI proteins required to half-maximally repress $\mathrm{P_{lac}}$; k_G is the maximum production rate of C14-HSL by CinI, D_{G} is the export rate of C14-HSL; μ is the intracellular specific dilution rate due to the host cell growth, $\mu = \ln 2/T$, T is the division period. Parameters for other proteins and QS signaling molecules are defined similarly, see SI-2 Model Derivation and SI-3 Estimation of Parameter Values in S1 Text. Based on the fact that N-Acyl Homoserine Lactone Lactonase (AHL-lactonase) hydrolyzes C4-HSL effectively [55], we also assume that specific degradation rate constants for the signaling molecules, C14-HSL and C4-HSL, can be

set experimentally [6], corresponding to the parameter values used in our models. We pick these specific promoters and autoinducers in order to be concrete and to justify biologically meaningful values of the model parameters. However, we wish to emphasize that our results are generic for the architectures shown in Fig 1.

Bifurcation parameters. In our bifurcation analysis, we use almost all dimensionless parameters given in Eqs (11)–(14) as free parameters allowed to be varied to detect changes in stability of the corresponding solutions. Whenever a new bifurcation point is detected, we provide an appropriate interpretation in terms of interventions reviewed in [6], which can potentially lead to the corresponding effect.

For example, suppose that d is the free parameter used in bifurcation analysis. Due to the relationships Eqs (20)–(21), changes in the values of d may correspond to different and independent experimental interventions [6] leading to: (*a*) changes in the membrane permeability (*i.e.*, D_G and D_R), or (*b*) changes in the half-lives of repressor proteins, or (*c*) changes in the specific growth rate of the host cell. As such, both higher values of protein half-lives and diffusion permeability as well as lower values of the specific growth rate (longer replication periods) correspond to higher values of the parameter d. Recall that the value of the parameter d characterizes the strength of the interaction between cells in the given population, which facilitates self-synchronization [15–17, 25, 56].

More broadly, we can rely upon the fact that all dimensionless parameters are defined via appropriate combinations of the original dimensional parameters Eqs (18), (19), (20) and (21) in our interpretation of results obtained from bifurcation analysis as follows.

The values of dimensionless rate parameters (*i.e.*, a-parameters) can be changed by decreasing or increasing translational efficiency, which depends on the nucleotide sequence of the ribosome binding sites (RBS) located within the upstream noncoding part of the mRNA [1, 50]. The values of dimensionless rate parameters can also be changed by decreasing or increasing the lifetime values of appropriate proteins. Indeed, a carboxy-terminal tag, based on ClpX, the ATP-dependent unfoldase/translocase of ClpXP recognizing specific protein substrates bearing *ssrA* tags [9, 57], can be inserted at the 3W end of each repressor gene [2]. Proteases in *E. coli* recognize this tag and target the attached protein for destruction. Such tags are used to reduce the half-life of the proteins from more than 60 min to around 4 min, which makes it possible and (also convenient) to set the half-life times for all toggle proteins (approximately) equal to one another and close to the half-lives of mRNAs [2, 15]. We assume that all *ssrA* tagged proteins do not compete for AAA+ protease ClpXP [9], in which case the sequestration of AAA+ protease ClpXP is negligible small and is not modeled. To this end, both RBS and carboxy-terminal tags are the principal tools by which the parameters of an engineered gene network can be adjusted experimentally [1, 2, 6].

Stability and Bifurcation in Cellular Populations

A number of powerful concepts and software tools have been developed to efficiently analyze bifurcations of equilibrium solutions in small-scale and medium-sized dynamical models [58–61]. To this end, however, the analysis of bifurcations in the A and S models already becomes a formidable task in terms of CPU loads at $N = 10$. For example, the S model describing 10 coupled toggles includes 42 ODEs. Therefore, special conceptual and computational approaches need to be developed to interpret results of modeling with A and S models for cellular populations consisting of thousands or even millions of cells.

Fortunately, due to the special structure of the Jacobian matrices for the corresponding linearizations of the A and S models, the computation of the characteristic polynomials, which are used to evaluate stability and bifurcation [26, 62], can first be conceptually and, then, numerically simplified, by employing Schur's formula [63]. As a result, (*i*) the stability and bifurcation analyses of

homogeneous populations for any $N \geq 2$ can be rigorously reduced to the case of a population consisting of only *two* toggles, (*ii*) the analysis of a (1:1)-mixed state for any even $N \geq 4$ can be rigorously reduced to the case of only *three* toggles, and (*iii*) the analysis of a (N_1: N_2)-mixed state with any $N_1 \neq N_2$ and $N_1 + N_2 = N$ can be rigorously reduced to the case of only *four* toggles as described in SI-6 Exponential Stability of Cellular Populations in S1 Text.

Schur's formula [63] also helps to solve another important nontrivial specificity of the A- and S-population models caused by multiplicity of eigenvalues due to the model's symmetry discussed in SI-6 Exponential Stability of Cellular Populations in S1 Text. Computationally, in the case of multiple eigenvalues caused by symmetry, the standard tools [58–61] cannot be used in a straightforward way, when a special care should be taken. Our theoretic developments can aid in the analysis and interpretation of all such and similar cases arising in modeling of cellular populations, see SI-6 Exponential Stability of Cellular Populations in S1 Text for more rigorous definitions and results.

Indeed, the exact (very large) number of cells, N, in a cell culture is usually unknown, as cells can die or even be washed out. In such cases, the population density parameter ρ is used, and, therefore, stability of and bifurcation in populations with respect to the variability in their densities is done. The corresponding changes in the integer parameter N that reflect changes in ρ assume a formal study of stability with respect to changes in the number of differential equations in the corresponding models. This is an ill-defined perturbation in the number of equations, and we show how it can be avoided by using the stability approach developed in SI-6 Exponential Stability of Cellular Populations in S1 Text.

Spontaneous Synchronization Errors

Capabilities of toggles to fail and recover from spontaneous synchronization errors can be formalized in terms of a *multistability* concept, that is, as a co-existence of bistable *homogeneous* populations and various *heterogeneous* populations (Fig 2), also called *mixed* states, under the same conditions. Recall that mixed states are known to lead to bistable distributions [4].

Following [4], we call a population heterogeneous or, equivalently, mixed if it comprises toggles with *different* transcription signatures for the *same* genes: (*i*) the repressor gene *lacI* is active (G-state), while *tetR* is repressed, and (*ii*) *lacI* is repressed, while the repressor gene *tetR*

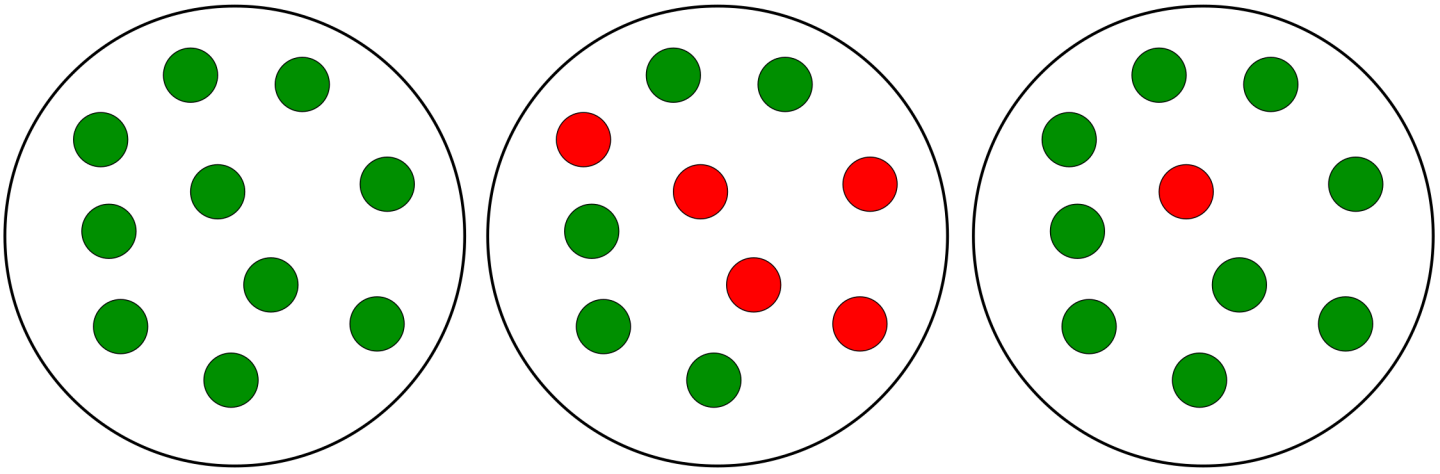

Fig 2. Homogeneous and heterogeneous (mixed) populations. An example of a population consisting of 10 cells is shown. The left panel demonstrates a homogeneous G-population. The center panel demonstrates a heterogeneous (1:1)-population, where the homogeneous G- and R-subpopulations have equal number of cells. The right panel demonstrates a heterogeneous (9:1)-population formed of two unequal subpopulations which represent a *spontaneous synchronization error*, when one or a few toggles spontaneously flip from green (G) to red (R) states.

doi:10.1371/journal.pcbi.1004881.g002

is active (R-state), see Toggle Designs. In other words, a homogeneous population is fully characterized by either transcription signature (*i*) or (*ii*), while a heterogeneous population is characterized by mixed signatures (*i*) and (*ii*) simultaneously present in the population (Fig 2).

Different heterogeneous populations can be characterized by transcription signature "mixtures" with ratio (p:q), $p + q = 1$, describing the fraction of toggles in the G-state versus the fraction of toggles in the R-state within the same population. For homogeneous populations, we, therefore, have either (1:0) or (0:1) transcriptional signature (Fig 2).

With these concepts, we can formulate more precisely our objective: to find conditions under which heterogeneous (mixed) population equilibrium solutions can loose their stability or can even be eliminated completely.

As a proof of concept, an example of an (9:1)-heterogeneous population (Fig 2) will be used, where the number of toggles in the first, Green-subpopulation (G) (*tetR* is suppressed) is 9 times bigger that the number of toggles in the second, Red-subpopulation (R) (*lacI* is suppressed). In this simplest case, the G-subpopulation comprises 9 cells ($p = 0.9$ or 90%-fraction of all cells), while the R-subpopulation comprises one cell ($q = 0.1$ or 10%-fraction of all cells).

Note that our analysis of (9:1)-mixed states does not depend on the number of cells N in the entire population, which is usually unknown in experiments. In other words, our results hold for any integers N, N_1, and N_2, such that $N = N_1 + N_2$, and N_1: $N_2 = 9$: 1, where the fractions of cells with different transcription signatures are defined by the numbers $p = N_1/N$ and $q = N_2/N$, respectively, see SI-6 Exponential Stability of Cellular Populations in S1 Text.

Monotone Systems Formalism

The systems considered here are described by the evolution of states, which are time-dependent vectors $x(t) = (x_1(t), \ldots, x_n(t))$. The components x_i represent concentrations of chemical species (such as proteins, mRNA, metabolites, and so forth), the dynamics of which are given by a system of ODE's:

$$\begin{aligned}
\frac{dx_1}{dt}(t) &= f_1(x_1(t), x_2(t), \ldots, x_n(t)),\\
\frac{dx_2}{dt}(t) &= f_2(x_1(t), x_2(t), \ldots, x_n(t)),\\
&\vdots\\
\frac{dx_n}{dt}(t) &= f_n(x_1(t), x_2(t), \ldots, x_n(t)).
\end{aligned}$$

We also write simply $dx/dt = f(x)$, where f is a differentiable vector function with components f_i. The coordinates $x_i(t)$ are non-negative numbers. We write $\varphi(t, x_0)$ for the solution of the initial value problem $\dot{x}(t) = f(x(t))$ with $x(0) = x_0$, or just $x(t)$ if x_0 is clear from the context, and assume that this solution $x(t)$ exists and remains bounded for all $t \geq 0$.

Definition of monotone systems. A system is said to be *monotone* if there exists a partition of the set of indices of state variables:

$$\{1, 2, \ldots, n\} = S_+ \bigcup S_- \quad (S_+ \bigcap S_- = \emptyset)$$

with the following properties:

1. for each pair of indices $\{i, j\} \in S_+$ $(i \neq j)$ and each pair of indices $\{i, j\} \in S_-$ $(i \neq j)$,

$$\frac{\partial f_i}{\partial x_j}(x) \geq 0 \quad \forall\ x$$

2. and for each pair of indices $\{i, j\}$ such that $i \in S_+$ and $j \in S_-$ and each pair of indices $\{i, j\}$ such that $i \in S_-$ and $j \in S_+$,

$$\frac{\partial f_i}{\partial x_j}(x) \leq 0 \quad \forall\ x\,.$$

Observe that the definition does not impose any constrains on diagonal entries $\frac{\partial f_i}{\partial x_i}(x)$. These may have arbitrary signs, even depending on x.

Monotone systems [23, 64, 65] were introduced by Hirsch, and constitute a class of dynamical systems for which a rich theory exists. (To be precise, we have only defined the subclass of systems that are "monotone with respect to some orthant order" but the notion of monotone dynamics can be defined with respect to more general orders.)

We assume from now on that our system satisfies the following property: for each pair of distinct nodes i and j, one of these holds:

1. $\frac{\partial f_i}{\partial x_j}(x) > 0$ for all states x
2. $\frac{\partial f_i}{\partial x_j}(x) < 0$ for all states x
3. $\frac{\partial f_i}{\partial x_j}(x) = 0$ for all states x.

Of course, there are many models for which partial derivatives may change sign depending on the particular point x. With assumptions (1–3), however, the main results that we need from monotone dynamical systems theory will be particularly easy to state.

Monotone systems cannot admit any stable oscillations [19, 21, 66]. Under a stronger property, described next, only convergence to steady states is generically possible.

Strong monotonicity. The directed *species influence graph* G associated to a system with n state variables is defined as follows. The graph G has n nodes (or "vertices"), which we denote by $v_1, \ldots, v_n$, one node for each species. If

$$\frac{\partial f_i}{\partial x_j} > 0 \text{ (activation)},$$

we introduce an edge labeled "1" from v_j into v_i. If, instead,

$$\frac{\partial f_i}{\partial x_j} < 0 \text{ (inhibition)},$$

we introduce an edge labeled "−1" (or just "−") from v_j into v_i. Finally, no edge is drawn from node v_j into node v_i if the partial derivative $\frac{\partial f_i}{\partial x_j}(x)$ vanishes identically (no direct effect of the jth species upon the ith species). An alternative is to write a normal arrow "→" or a blunted arrow "⊣" (or an arrow labeled "−") respectively for the first two cases. The graph G is an example of a *signed graph* [67], meaning that its edges are labeled by signs.

No self-edges (edges from a node v_i to itself) are included in the graph G, whatever the sign of the diagonal entry $\partial f_i/\partial x_i$ of the Jacobian. The sign of this derivative may be positive,

negative, or even be state-dependent. Results will not depend on signs of diagonals of the Jacobian of f.

The graph G is said to be *strongly connected* if, given an arbitrary pair of different indices $\{i, j\}$, there is a some, possibly indirect, effect of i on j. Formally, we ask that there is a sequence of indices $i = k_0, k_1, \ldots, k_r = j$ such that

$$\frac{\partial f_{k_{s+1}}}{\partial x_{k_s}} \neq 0 \quad \text{for } s = 0, \ldots, r-1 .$$

A system is said to be *strongly monotone* if it is monotone and, in addition, its species influence graph G is strongly connected. (As with the definition of monotonicity, one can extend strong monotonicity to far more general classes of systems, but we use a more restrictive notion that makes results less technical to state.) Even when there are multiple steady-states, the Hirsch Generic Convergence Theorem [21, 23, 64, 65] is a fundamental result.

Hirsch's Theorem. Even though they may have arbitrarily large dimensionality, monotone systems behave in many ways like one-dimensional systems: Hirsch's Theorem asserts that generic bounded solutions of strongly monotone differential equation systems must converge to the set of (stable) steady states. "Generic" means here "for every solution except for a measure-zero set of initial conditions." In particular, no nontrivial attractors arise. The genericity qualifier is needed in order to exclude the unstable manifolds of saddles as well as behavior on lower-dimensional sets [18].

The general theory of monotone systems applies to a class of differential equations somewhat larger than the one considered here. What we defined as monotone systems are, to be more precise, "systems monotone with respect to an orthant order". It is possible to, more generally, define systems that are monotone with respect to orders induced by arbitrary convex proper cones. However, the generality that one obtains in that fashion comes at the cost of conditions which are typically very difficult to verify in examples and, in any event, this generality is not needed for the purpose of analyzing the systems that are the focus of this paper.

Results and Discussion

To carry out computational bifurcation analysis, MatCont [59, 68] has been used. A technical description of bifurcation points can be found in [58, 59, 62, 68].

Application of Monotone Systems Theory to the S Design

To apply monotone systems theory to the S toggle model Eqs (1)–(6), we first rewrite the model in the following convenient general form with $4N + 2$ variables:

$$\begin{aligned}
\frac{dx_i}{dt} &= h_x(x_i, y_i, g_i), \\
\frac{dy_i}{dt} &= h_y(x_i, y_i, r_i), \\
\frac{dg_i}{dt} &= h_g(y_i, g_i, g_e), \\
\frac{dr_i}{dt} &= h_r(x_i, r_i, r_e), \\
\frac{dg_e}{dt} &= H_g(g_e, g_1, \ldots, g_N), \\
\frac{dr_e}{dt} &= H_r(r_e, r_1, \ldots, r_N).
\end{aligned}$$

Here, $i = 1, \ldots, N$, all the functions in the right-hand side are differentiable, and the following signs hold for partial derivatives, everywhere in the state space:

$$\frac{\partial h_x}{\partial x_i} < 0, \quad \frac{\partial h_x}{\partial y_i} < 0, \quad \frac{\partial h_x}{\partial g_i} > 0, \quad \frac{\partial h_x}{\partial a_1} > 0, \quad \frac{\partial h_x}{\partial a_3} > 0, \tag{22}$$

$$\frac{\partial h_y}{\partial x_i} < 0, \quad \frac{\partial h_y}{\partial y_i} < 0, \quad \frac{\partial h_y}{\partial r_i} > 0, \quad \frac{\partial h_y}{\partial a_2} > 0, \quad \frac{\partial h_y}{\partial a_6} > 0, \tag{23}$$

$$\frac{\partial h_g}{\partial y_i} < 0, \quad \frac{\partial h_g}{\partial g_i} < 0, \quad \frac{\partial h_g}{\partial g_e} > 0, \quad \frac{\partial h_g}{\partial a_5} > 0, \quad \frac{\partial h_g}{\partial \delta} < 0, \tag{24}$$

$$\frac{\partial h_r}{\partial x_i} < 0, \quad \frac{\partial h_r}{\partial r_i} < 0, \quad \frac{\partial h_r}{\partial r_e} > 0, \quad \frac{\partial h_g}{\partial a_6} > 0, \quad \frac{\partial h_r}{\partial \delta} < 0, \tag{25}$$

$$\frac{\partial H_g}{\partial g_i} > 0, \quad \frac{\partial H_g}{\partial g_e} < 0, \quad \frac{\partial H_g}{\partial \delta_e} < 0, \tag{26}$$

$$\frac{\partial H_r}{\partial r_i} > 0, \quad \frac{\partial H_r}{\partial r_e} < 0, \quad \frac{\partial H_r}{\partial \delta_e} < 0, \quad i = 1 \ldots, N. \tag{27}$$

Next we observe that the S system is monotone, because we may partition its state variables as follows. One set consists of

$$x_i,\ g_i,\ g_e,\ i = 1, \ldots, N\,, \tag{28}$$

and another set consists of

$$y_i,\ r_i,\ r_e,\ i = 1, \ldots, N\,. \tag{29}$$

Moreover, the corresponding graph is strongly connected, as we have the following paths, for each two indices i, j:

$$x_j \dashv r_j \to r_e \to r_i \to y_i \dashv g_i \to g_e \to g_i \to x_i \tag{30}$$

which shows that one can reach any node from any other node by means of a directed path. Thus, the S model Eqs (1)–(6) is strongly monotone. We conclude as follows.

Theorem 1 *Typical solutions of the S model* Eqs (1)–(6) *converge to steady states.*

This fundamental result is robust to parameters as well as to the functional form of the equations. It ensures that our proposed design has theoretically guaranteed global stability properties. No stable oscillations [16] can exist, nor can other (for, example, "chaotic" [25]) solution regimes arise. In addition to these global properties, it is also possible to use the theory of monotone systems in order to make qualitative predictions about bifurcation diagrams as discussed in the next section.

The monotonicity property of the S system has important consequences regarding its transient as well as asymptotic behavior. We discuss in an appendix how Kamke's Theorem characterizes order relations for monotone systems. We explain now what these mean, explicitly, for the S system. Let $z_i(t)$ characterize the state of the i-th S toggle at time $t \geq 0$, that is, $z_i(t) = (x_i(t), y_i(t), g_i(t), r_i(t))$, $i = 1, \ldots, N$. Let $Z(t)$ characterize the state of the population of cells, $Z(t) = (z_1(t), \ldots, z_N(t), g_e(t), r_e(t))$. Suppose that we have two initial sets, $Z(0)$

and $\tilde{Z}(0)$, of values for the various expression levels of the repressor proteins, LacI and TetR, and we consider the behavior of $Z(t)$ and $\tilde{Z}(t)$ for $t > 0$.

Now suppose that we wish to understand what is the effect of a perturbation in one of the components of the initial state $z_i(0)$ for S toggle i with some fixed i, $1 \leq i \leq N$. (A similar argument can be applied to perturbations in other components of the initial state, or even simultaneous perturbations in all the components.) Suppose, for example, that we are interested in understanding the behavior starting from a state in which $\tilde{x}_3(0) \geq x_3(0)$ in the 3rd toggle z_3. This gives rise to a new population-wide solution $\tilde{Z}(t)$, and we use a tilde to denote its coordinates, that is, $\tilde{Z}(t) = (\tilde{z}_1(t), \ldots, \tilde{z}_N(t), \tilde{g}_e(t), \tilde{r}_e(t))$, where $\tilde{z}_i(t) = (x_i(t), y_i(t), g_i(t), r_i(t))$, $i = 1, \ldots, N$. Then, using the information provided by the partition shown in Eqs (28) and (29), we can predict that, for all $t > 0$: $\tilde{x}_i(t) \geq x_i(t)$, $\tilde{y}_i(t) \leq y_i(t)$, $\tilde{g}_i(t) \geq g_i(t)$, $\tilde{r}_i(t) \leq r_i(t)$, $\tilde{g}_e(t) \geq g_e(t)$, and $\tilde{r}_e(t) \leq r_e(t)$ for all $i = 1, \ldots, N$. As we will see shortly below, a similar conclusion can also be made with respect to perturbations in parameters, not merely initial states.

Monotone Parametric Dependencies in the S Design

As a first step, we can include the eight parameters, a_i ($i = 1, \ldots, 6$), δ_g, and δ_r, as constant state variables by formally adding the corresponding equations $da_i/dt = 0$ ($i = 1, \ldots, 6$), and $d\delta_g/dt = d\delta_r/dt = 0$ to the S-model Eqs (1)–(6). The extended S-model is a monotone system. However, this extended model has no strong monotonicity property, because the nodes corresponding to the parameters cannot be reached from other nodes, as the parametric extension violates the strong connectivity relationships Eq (30). However, this is not of any consequence, as the global stability properties of the S system are determined by constant values of the parameters. We only introduced the extended model in the context of bifurcation analysis. One might add additional constant variables to represent other parameters, such as the d's. These other parameters do not lead to monotonicity, and this lack of monotonicity will have important consequences in bifurcation analysis, as we discuss later.

Dependencies between the S-model state variables and parameters Eqs (22)–(27) are shown in Fig 3 (Top Panel). Here, the set of all molecular entities in the S design is partitioned into two "orthogonal" subsets, S^- and S^+ (Definition of monotone systems). Solid arrows and lines highlighted in light brown color correspond to S^-, while solid arrows and lines highlighted in cyan color correspond to S^+. Although interactions within each subset contribute to its activate state, the orthogonal subsets repress one another. Here, ClpXP is a pool of AAA+ proteases ClpXP that use the energy of ATP binding and hydrolysis to perform mechanical work during targeted protein degradation within the cell. The corresponding inhibitory (degradation) interactions are shown, using dashed gray lines. If the circuit operates near the saturation condition for the pool of AAA+ proteases ClpXP, the S design may loss its monotone properties.

However, there is a substantial body of literature that gives theorems to the effect that "small" perturbations of monotone systems retain the properties of monotone systems, for example, a smooth regular perturbation of a strongly monotone system also has generic convergence properties [65]. A similar result as well holds for singular perturbations [69].

An example of three identical S toggles interacting via common autoinducers and operating far from the saturation of AAA+ proteases ClpXP is shown in Fig 3 (Bottom Panel).

The monotonicity of the extended model implies that stable loci in bifurcation diagrams depend monotonically on parameter variations. They will increase when the parameter being varied belongs to the component as the variable being analyzed, and will decrease if they are in different components. This property is a consequence of the general order preserving properties of monotone systems, as we explain now.

Suppose that $\bar{x}_0$ is a steady state corresponding to a parameter value p_0, that is to say, $f(\bar{x}_0, p_0) = 0$. Suppose that we now consider p_1 that is very close to p_0 and larger than p_0, $p_1 > p_0$. Suppose in addition that $\bar{x}_1$ is a steady state for the parameter value p_1, $f(\bar{x}_1, p_1) = 0$, and that $\bar{x}_1$ is stable. Now pick the solution $x_1(t)$ of $\dot{x} = f(x, p_1)$ that has initial condition $x_1(0) = \bar{x}_0$. Suppose that the extended system $\dot{x} = f(x, p)$ and $\dot{p} = 0$ is monotone. Now, we may consider the following two initial states for the extended system: $(\bar{x}_0, p_0)$ and $(\bar{x}_0, p_1)$. Since the second state is larger (in the sense of Kamke's Theorem as earlier explained) in the monotone order, it follows that the solutions satisfy $x_1(t) \geq \bar{x}_0$ for all $t > 0$, and therefore, taking limits, we conclude that $\bar{x}_1 > \bar{x}_0$, as desired.

Using Fig 3 in conjunction with the dimension analysis in terms of the relationships Eqs (18), (19), (20) and (21), certain qualitative predictions can be made about the parametric

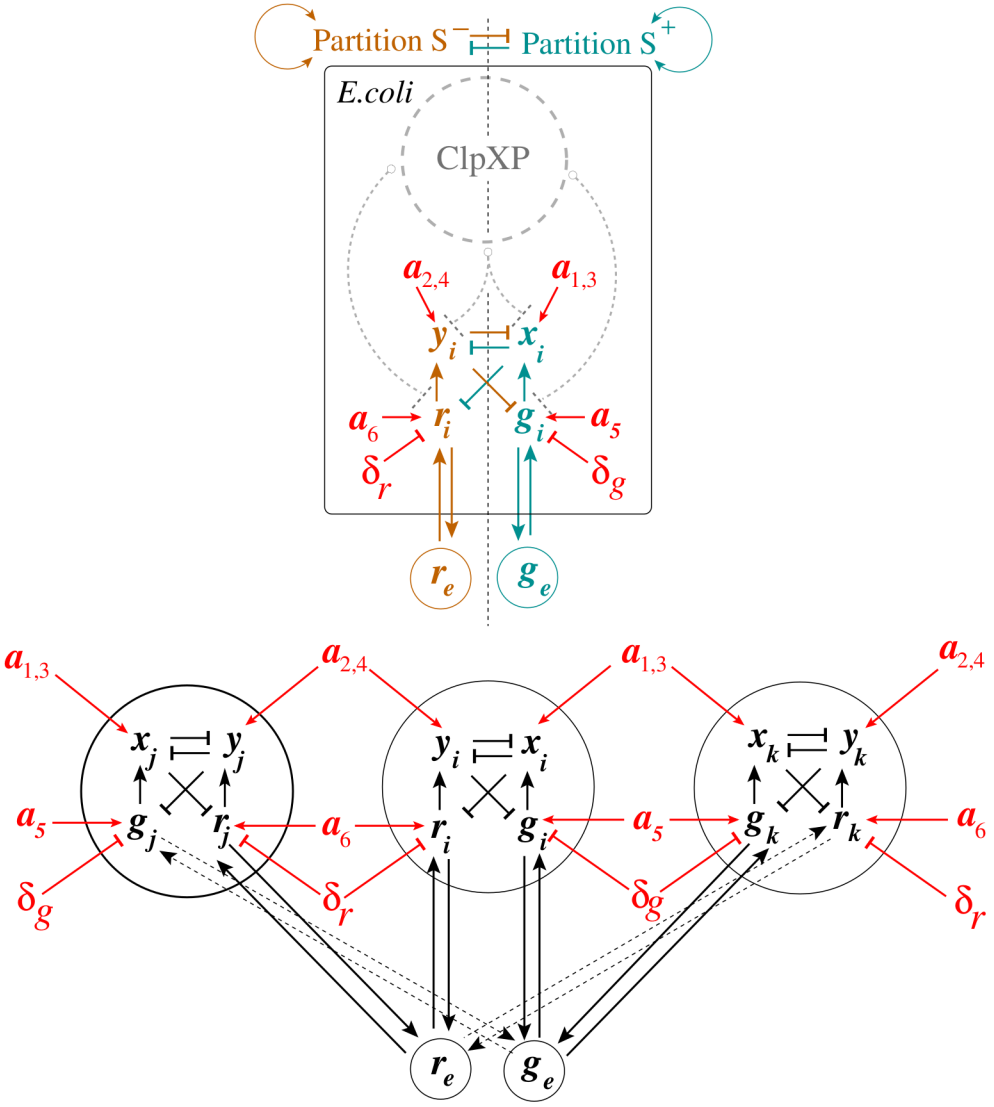

Fig 3. Application of Monotone Systems Theory to the S design. The top panel presents a monotonicity diagram for a single-cell S design, while the bottom panel represents an example of three identical S toggles interacting via common autoinducers, see the main text for details. In all cases, solid arrows and lines highlighted in red color correspond to monotone parameter dependencies. In the bifurcation analysis, the values of all monotone parameters are varied for all cells simultaneously.

doi:10.1371/journal.pcbi.1004881.g003

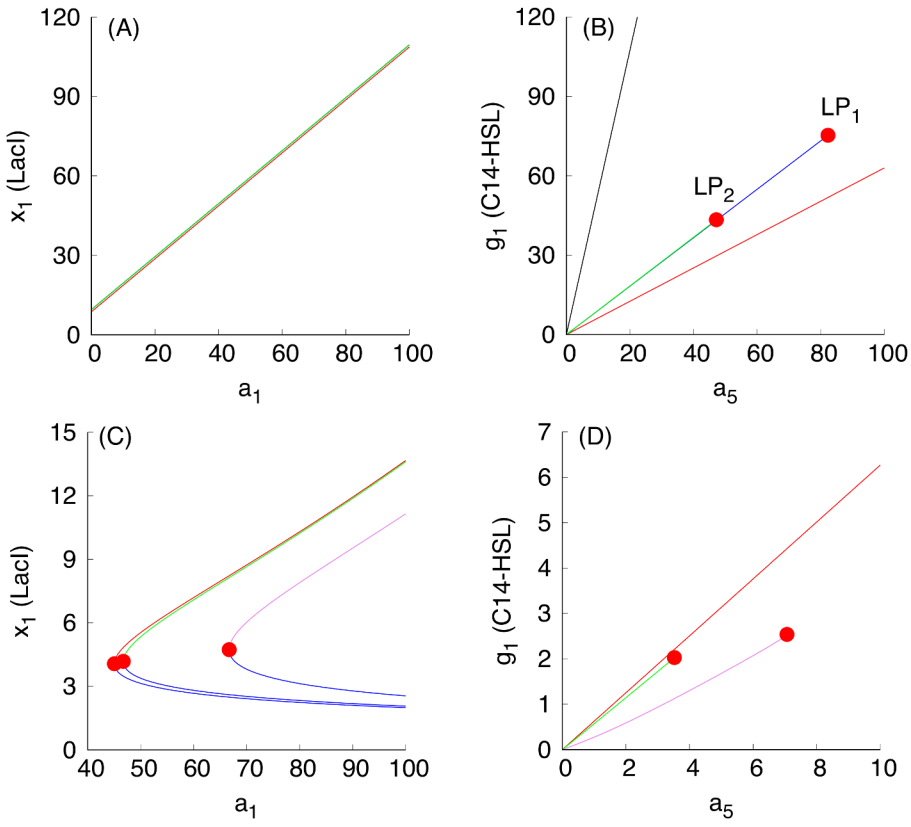

Fig 4. Examples of monotone parametric dependencies. Panels (A) and (B) correspond to the unsaturated S design, while Panels (C) and (D) correspond to the saturated S design. **Panels (A) and (B)**. The following color coding schema is used: (*i*) black plots are used for G-homogeneous solutions at $d = 0.1$; (*ii*) red plots are used for G-homogeneous solutions at $d = 10$; (*iii*) blue plots are used for (1:1)-mixed states at $d = 0.1$; and (*iv*) green plots are used for (9:1)-mixed states at $d = 0.1$. Red filled circles in panel (B), labeled with LP_1 and LP_2, correspond to Limit Point (LP) (or, equivalently, Saddle-Node) bifurcation points. Here, the blue curve connecting the origin (0, 0) and the LP_1-point corresponds to the stable branch of the (1:1)-mixed state. The green curve connecting the origin (0, 0) with the LP_2-point corresponds to the stable branch of the (9:1)-mixed state. Because the green curve was plotted after plotting the blue curve, a part of the blue curve is hidden beneath the green curve. Projections of the corresponding plots on 2D-planes often overlap, mixing different colors, which should not lead to any difficulty in recognizing similar monotone ("overlapping") dependencies. **Panels (C) and (D)**. The following color coding schema is used: (*i*) red plots correspond to stable homogeneous G-states, (*ii*) violet plots correspond to stable (1:1)-mixed states, and (*iii*) green plots correspond to stable (9:1)-mixed states. In all cases, blue plots correspond to unstable states. All red filled circles correspond to the LP bifurcations. In the panel (D), the unstable branches for both (1:1) and (9:1)-mixed states are not shown because they overlap with the stable ones.

doi:10.1371/journal.pcbi.1004881.g004

dependencies based on monotone systems theory. To benchmark the approach, we have selected, as an example, a subset of dependencies shown in Fig 3, presented in Fig 4A and 4B. Fig 4C and 4D correspond to the case when the S toggle operates under the saturation condition for the pool of AAA+ proteases ClpXP (SI-8 Modification of the S and A Models to Describe Sequestration 617 of AAA+ protease ClpXP in S1 Text.)

In Fig 4, three different stable populations are chosen: (1) an G-homogeneous population; (2) an (1:1)-mixed population; here, the levels of LacI and C14-HSL from one subpopulation (within which LacI is over-expressed) are shown; and (3) a (9:1)-mixed population (a spontaneous synchronization error); here, again, the levels of LacI and C14-HSL from the largest subpopulation (within which LacI is over-expressed) are shown. Because the stable mixed populations do not exist for large values of the parameter d in the cases shown in Fig 4A and 4B, we use both

$d = 0.1$ (weak coupling) for all populations and, additionally, we use $d = 10$ (strong coupling) for the G-homogeneous population only. In the cases shown in Fig 4C and 4D, the mixed populations turn out to be more robust and exist at $d = 10$.

Using the S-model Eqs (1)–(6) and its sequestration version (SI-8.1) (see SI-8.1 Modification of the S Model in S1 Text) with the values of fixed parameters given in Eqs (11)–(14) and (15)–(17), respectively, we find that Fig 3 predicts monotonically increasing dependencies.

The loss of stability and disappearance of the mixed states shown in Fig 4B and 4D as a_5 increases can be interpreted intuitively by the fact that an increase in a_5 leads to an increase in the intracellular levels of the corresponding QS signaling molecules, which, in turn, lead to an increase of extracellular levels of the QS molecules via diffusion, thereby facilitating self-synchronization of the given population of all toggles under conditions corresponding to a stronger interaction among all toggles. In particular, the strong interaction and coupling condition eliminates spontaneous synchronization errors in terms of suppressing the emergence of undesired (9:1)-mixed states.

This result is similar to a well-known fact for oscillators coupled via a common medium that a transition from an unsynchronized to a synchronized regime emerges as the strength of coupling increases [15–17, 25, 56]. Indeed, many microbial species accomplish this via quorum sensing, which entails the secretion and detection of diffusible molecules (autoinducers), whose concentration serves as a proxy for population density [10].

Using the expression for the dimensionless parameter a_5 given in Eqs (18) and (19), see Scaling, we can conclude that the increase in the values of the parameter a_5 leading to the bifurcation point LP_2 (Fig 4) can be achieved by the following experimental interventions:

- stabilization of cell division with lower values of the specific growth rate μ (or, equivalently, higher division periods T);
- stabilization of relevant proteins, using lower values of r_d (or, equivalently, higher half-lives);
- an increase in the maximum production rate (k_G) of C14-HSL by enzyme CinI, see SI-3 Estimation of Parameter Values in S1 Text;
- an increase in the sensitivity (K_G) of promoter P_{cin} with respect to the number of molecules C14-HSL to half-activate P_{cin}, see Table SI-3.2 given in SI-3 Estimation of Parameter Values in S1 Text.

We have used bifurcation analysis with respect to changes in the values of the parameter a_5 as a way to illustrate predictions from monotone systems theory, and in the process we obtained conclusions regarding improvements of S toggle self-synchronization properties by eliminating the (9:1)-mixed state. To this end, we note that there is no need to further increase values of a_5 to move the system to the bifurcation point LP_1 at which the (1:1)-mixed state loses it stability and disappears, because we do not interpret the (1:1)-mixed state as a spontaneous synchronization error, see Spontaneous Synchronization Errors. Additional parametric dependencies with respect to changes in other parameters are shown in Figs SI-7.1 and SI-7.1 in S1 Text.

We then repeat the analysis of the same parametric dependencies for a (1:1)-mixed state, illustrated in Fig 5 and Fig SI-7.3 in S1 Text. Like in the previous case, we observe that all dependencies are in line with the predictions suggested by Fig 3. To this end, we will not provide here reproduced similar results for the saturated S design (SI-8.1 Modification of the S Model in S1 Text), because in all computationally investigated cases, the parameter monotone dependencies are predicted by the theory and Fig 3.

The LP-bifurcation point (Fig 5) can be interpreted as follows. Decreasing values of both parameters δ_g and δ_r leads to an increase in the intracellular and extracellular levels of the

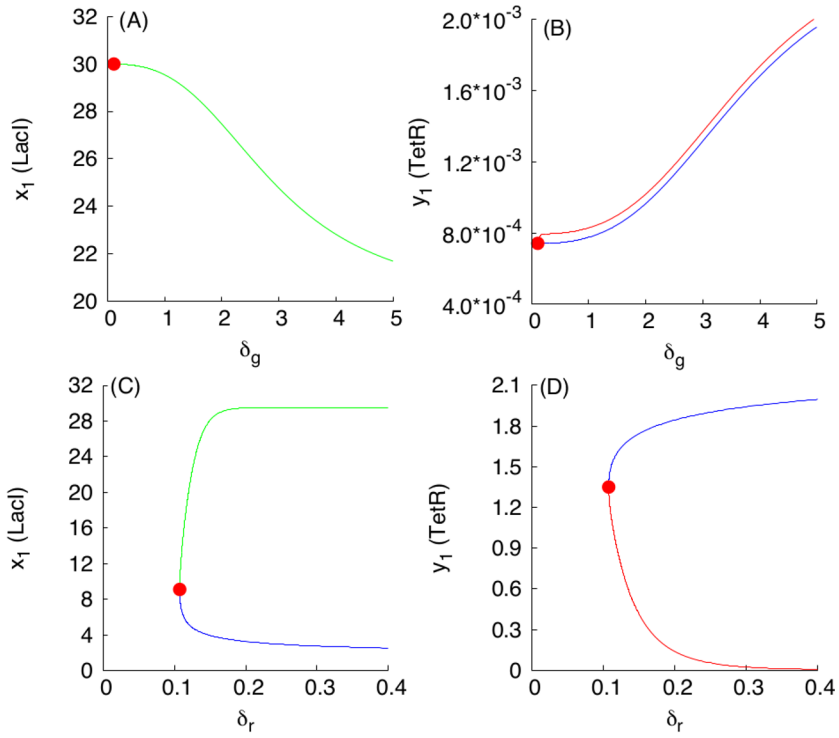

Fig 5. Examples of monotone parametric dependencies for a (1:1)-mixed state. Panels (A) and (B) correspond to dependencies of LacI and TetR levels on parameter δ_g, respectively. Panels (C) and (D) correspond to dependencies of LacI and TetR levels on parameter δ_r, respectively. The dependencies for the G-subpopulation are shown only, within which LacI is activated, while TetR is repressed. Green and red solid curves correspond to stable branches of (1:1)-equilibrium solutions, while all blue curves correspond to unstable branches of the solutions. Red filled circles correspond to an LP-bifurcation point. In panel (A), projections of stable and unstable branches coincide and, so, only the stable branch is shown.

doi:10.1371/journal.pcbi.1004881.g005

corresponding QS signaling molecules, which, in turn, leads to stronger interactions among all toggles. Indeed, it follows from Eqs (20) and (21) (see Scaling) that the described changes in the values of dimensionless parameters δ_g and δ_r can be achieved by increasing half-lives of the corresponding QS signaling molecules.

To this end and similarly to the interpretation provided earlier, as the values of the parameters δ_g and δ_r decrease, the (1:1)-mixed state loses its stability and disappear via an LP-bifurcation (Fig 5), the effect which is similar to the well-known fact that oscillators coupled via common medium synchronize as the strength of coupling increases [15, 25, 56].

We note that the parametric dependencies for unstable solutions are not described by Fig 3. To explain this observation, we recall that our proof of monotone dependence on parameters applies to stable solutions only, see above.

Finally, the monotone parametric dependencies for (9:1)-mixed states corresponding to spontaneous synchronization errors are illustrated in Figs SI-7.4 and SI-7.5 in S1 Text. In this case, by increasing the strength of interactions between the toggles from the large subpopulation, the spontaneous error can also be eliminated, corresponding to the existence of the LP-points in panels (A) and (B) of Figs SI-7.4 and SI-7.5 in S1 Text. At the same time, increasing the strength of interactions between the toggles from the small population, the corresponding spontaneous error cannot be eliminated.

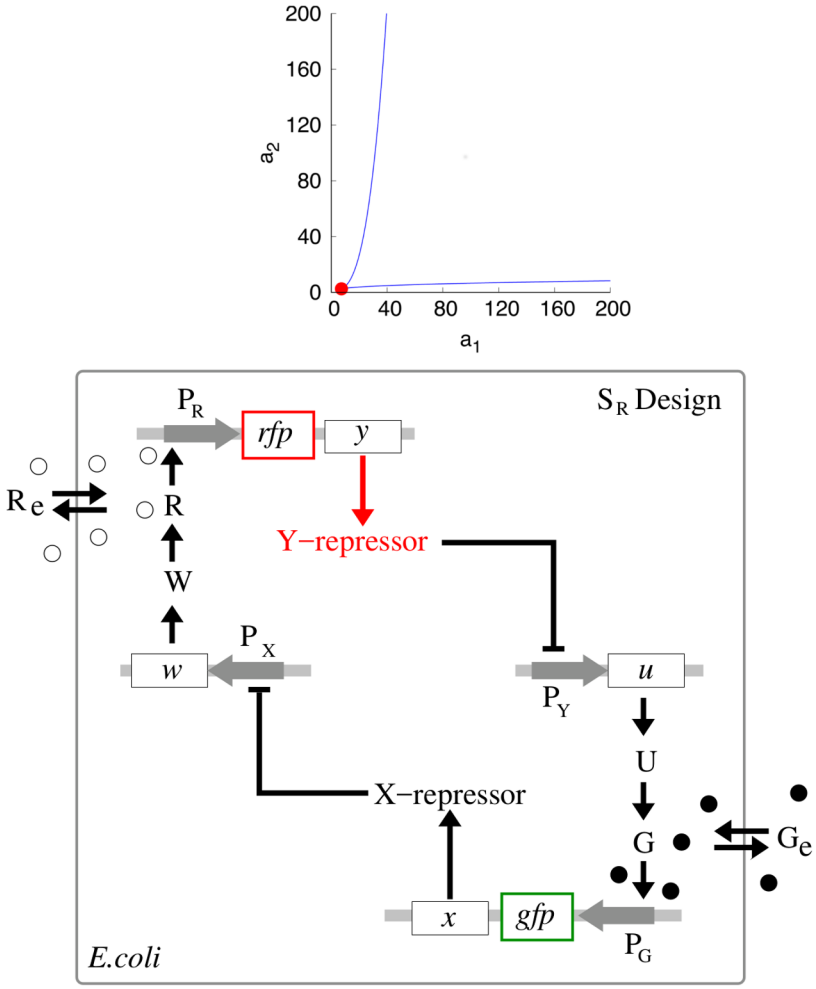

Fig 6. Bistability regions for S and A toggles (top), and a reduced S_R toggle design discovered from the bistability region (bottom). (Top panel). The region between two blue color coded LP-bifurcation loci corresponds to a bistability region for the A toggle model Eqs (9) and (10) at $d = 0$. A red filled circle corresponds to a cusp point (CP). For the S toggle model, bistability exists for all parameter values $a_1 \geq 0$ and $a_2 \geq 0$ at $d = 0$. Other fixed parameter values are given in Eqs (11)–(14). (Bottom panel). The reduced S_R toggle is obtained from the original S toggle (Fig 1) after removal of genes *lacI* and *tetR* from the corresponding plasmids bearing promoters P_Y and P_X, respectively. This reduction procedure corresponds to setting zero values $a_1 = a_2 = 0$ as discussed in the main text.

doi:10.1371/journal.pcbi.1004881.g006

Bistability in Single S and A Toggles

Before comparing population properties of our S design to those of the A design, we remark that, even for isolated cells (when the diffusion constant d is zero), there is a larger range of bistability for the S design compared to the A design. Specifically, a bistability region for a single A toggle in the plane (a_1, a_2) at $d = 0$ is shown in Fig 6(top panel). Similar regions were found in [1, 16]. We also observe that the entire quadrant, $a_1 \geq 0$ and $a_2 \geq 0$, spans a bistability region for the S-model at the fixed parameter values given in Eqs (11)–(14). We have computed the bistablility regions for the S design for three different nonzero values of the promoter leakiness parameter $\gamma = 0.01, 0.1, 1.0$, respectively, while all other parameter values were kept fixed as in the reference set Eqs (11)–(14), and found that in all the three cases, the entire quadrant, $a_1 \geq 0$ and $a_2 \geq 0$, belongs to the computed regions. In contrast, the bistability region for the A

design depends on the promoter leakiness parameter significantly [16], and we also observed computationally that the bistability region was leaving the domain shown in Fig 6 (top panel) as soon as γ was allowed to take on values larger than 0.5, that is, when $\gamma > 0.5$.

Another important observation that follows immediately from Fig 6 (top panel) is that in the case of the S toggle, bistability persists at the origin of the non-negative quadrant in the plane (a_1, a_2), that is, at $a_1 = a_2 = 0$. The observation remains true even for the nonzero values of the leakiness parameters as discussed earlier. Additionally, the property persists for the saturated S design (SI-8.1 Modification of the S Model in S1 Text) with the updated parameter set Eqs (15)–(17). This simply means that the genes *lacI* and *tetR* can be removed from the corresponding plasmids bearing promoters P_Y and P_X, respectively (Fig 1). In this case (Fig 6) (bottom panel), it is enough to keep the genes on the plasmids bearing the corresponding promoters P_G and P_R (Fig 1). We view the reduced S toggle as a minimal design that could be implemented experimentally. The fuller construct S is interesting too, in so far as it is based on the well-characterized and studied Cantor-Collins switch, coupled to quorum-sensing components [4]. We find that the full and reduced designs do not differ much in performance, and, so, we do not consider the minimal design in the rest of the paper.

Bistable Homogeneous Populations of S and A Toggles

Bistable homogeneous populations of S toggles persist within large ranges of the model parameters. For example, panels (A) and (B) in Fig SI-7.6 in S1 Text show scaled levels of LacI and C14-HSL, respectively, for a homogeneous population of S toggle in the G-state, depending on the values of the diffusion (membrane permeability) parameter *d*.

Panels (C)—(F) in Fig SI-7.6 in S1 Text show two stable homogeneous populations of A toggle which coexist while the parameter *d* is allowed to vary. Because the A toggle design does not have any intrinsic symmetry, the levels of the activated repressor proteins, LacI for the G-homogeneous population shown in panels (C) and (E), and TetR for the R-homogeneous population shown panels (D) and (F), differ significantly from one another. Recall that the levels of LacI and TetR in the corresponding G- and R-homogeneous populations consisting of S toggles are identically the same due to mirror symmetry.

Our intensive computational studies confirm that the discussed results on the stable homogeneous populations of S and A toggles, as well as their dependencies on the diffusion parameter *d*, are robust with respect to perturbations in the model parameters, including various combinations in the values of the Hill coefficients, promoter leakiness, and the saturation conditions (SI-8 Modification of the S and A Models to Describe Sequestration of AAA+ protease ClpXP in S1 Text).

The combination of the analyses discussed here can be summarized by saying that under each one of the two designs, S and A, including biological variability in the Hill coefficients, promoter leakiness, and the degradation sequestration conditions, bistable homogeneous stable populations are possible, in either "Red" or "Green" consensus states, and with the same order of magnitude of expression. The difference between these designs, including the sequestration effect for AAA+ proteases ClpXP, become evident, when we study heterogeneous (mixed) populations, as discussed next.

Elimination of (1:1)-Mixed Populations of S Toggles

Fig 7 shows richness of dynamic effects (bifurcations) for a (1:1)-mixed population of S toggles. We see that as soon as the parameter *d* takes on larger values, the (1:1)-mixed state loses its stability via a Branch Point (BP) bifurcation [62] (alternatively called "pitchfork" or "symmetry-

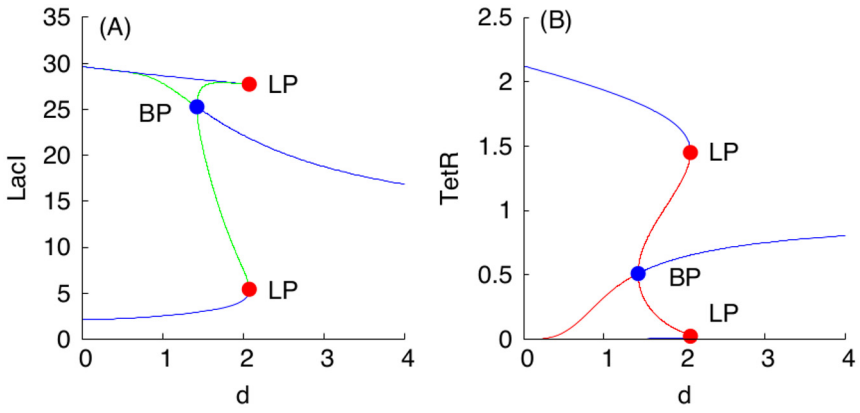

Fig 7. Symmetry breaking in a (1:1)-mixed population of S toggles. Panels (A) and (B) show the dependencies of LacI and TetR levels for the G-subpopulation of a (1:1)-population of S toggles, respectively. Blue color-coded plots correspond to all *unstable* equilibrium solution branches, while green and red color-coded plots correspond to all *stable* equilibrium solution branches. All blue filled BP-labeled points correspond to $d \approx 1.43$. All red filled LP-labeled points correspond to $d \approx 2.07$.

doi:10.1371/journal.pcbi.1004881.g007

breaking" bifurcation [70, 71]), giving rise to two stable (1:1)-mixed non-symmetric states at $d \approx 1.43$. The general symmetry-breaking phenomenon is rigorously studied in [72, 73].

The symmetry-breaking scenario can be described intuitively as follows. Suppose that we start with a mixed population in which 50% of the cells are in "green" state and 50% of the cells are in "red" state, and the nondimensional diffusion coefficient d (which, as we saw, in fact incorporates many of the kinetic parameters in the original system) has a low value. Suppose that we now slowly increase the value of d, and ask what happens to the (1:1)-mixed state. The first event that is observed, at $d \approx 1.43$ corresponding to the BP points in all panels of Fig 7, is that this "pure 50–50 mixed state" loses its stability. A new mixed state arises (Fig 8), in which there are *two* subpopulations, one in which green gene-expression dominates (but with different expression levels of LacI in each of them), and another one which red gene-expression dominates (also with different TetR levels). These two mixed states correspond to the solution branches connecting points marked with labels BP and upper LP, and BP and lower LP, respectively, shown in all panels of Fig 7.

Furthermore, as d is increased a bit more (past $d \approx 2.07$ corresponding to the two points labeled with LP in all panels of Fig 7, respectively), even these mixed states disappear (Fig 7). Thus, even with moderate diffusion, heterogeneous populations cannot be sustained, emphasizing the consensus-forming character of the S design. This is in marked contrast to the A design, as shown next. The loss of stability by the (1:1)-mixed state increases the robustness of the S toggle design towards its self-synchronization by reducing the number of alternative stable states to which the toggle state can settle.

Robustness of (1:1)-Mixed Populations of A Toggles and Saturated S toggles

In contrast to (1:1)-mixed populations of (unsaturated) S toggles described by the S model Eqs (1)–(6), we observe from Fig SI-7.7 in S1 Text that the original (1:1)-mixed A-population cannot be eliminated (made unstable) by increasing the values of the parameter d within a very large parameter interval. In other words, increasing the strength of interactions between the cells does not help to establish synchronization across the given population of identical A toggles. This is in a total agreement with a similar observation reported in [16], where the A model

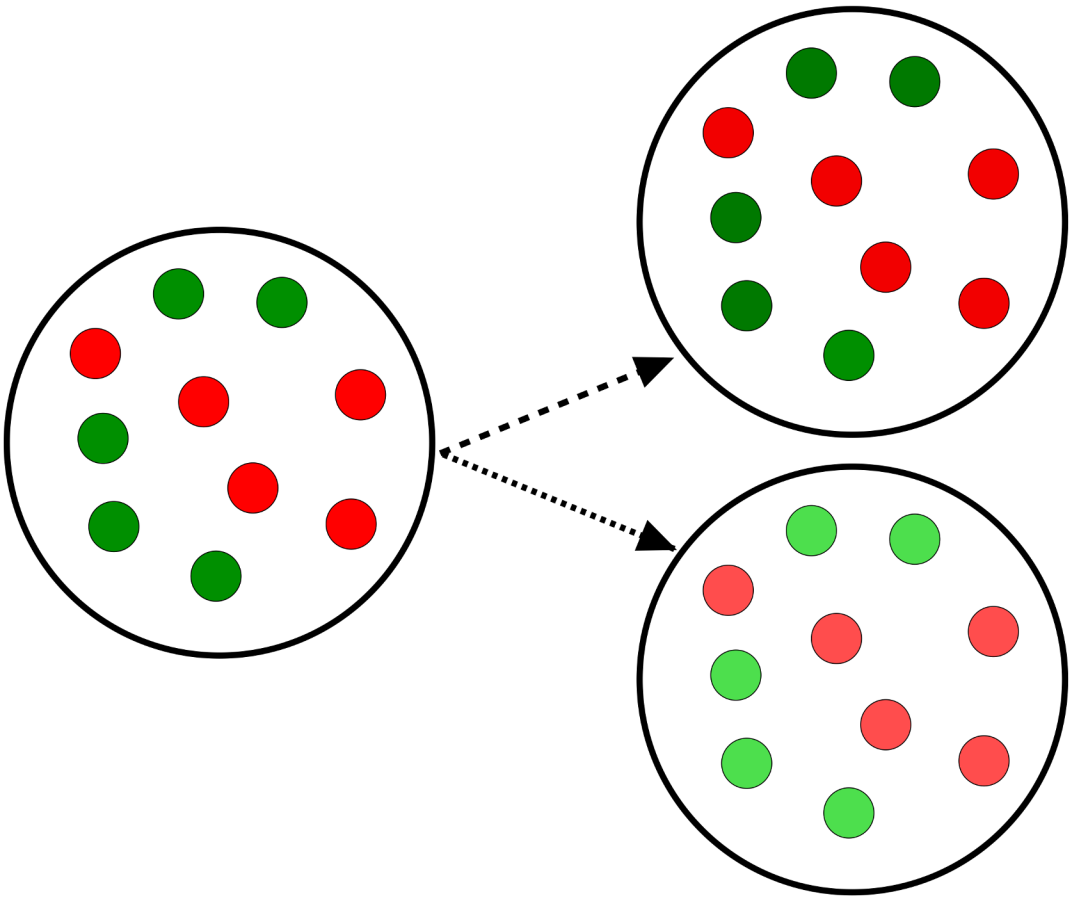

Fig 8. An interpretation of symmetry breaking in a (1:1)-mixed population of S toggles. A new (1:1)-asymmetric mixed state arises, in which there are two subpopulations, one in which *green* gene-expression *dominates* (but with different expression levels of LacI in each of them), and another one which *red* gene-expression *dominates* (also with different TetR levels).

doi:10.1371/journal.pcbi.1004881.g008

is studied in great detail. Specifically, it is found that a strong interaction between A toggles (*e.g.*, high permeability of the membrane to the autoinducer similar to higher values of *d*) results in the suppression of synchronous oscillations, leading to a transition of the population to a stable heterogeneous state, where individual A toggles are locked in different equilibrium states.

Our computational experiments with (1:1)-mixed populations of (saturated) S_m toggles described by the S_m model (SI-8.1) (see SI-8.1 Modification of the S Model in S1 Text) led to dependencies qualitatively indistinguishable from those shown in Fig SI-7.7 in S1 Text. Therefore, we can conclude that the degradation saturation (sequestration) effect may prevent the elimination of the undesired mixed states and synchronization.

(9:1)-Mixed Population of S Toggles

Next, we consider bistable (9:1)-mixed populations of S Toggles, which as discussed in the introduction, we think of as arising from random synchronization errors. We observe that (9:1)-populations of S toggles become quickly extinct as soon as the values of the nondimensional diffusion parameter *d* are slightly increased (Fig 9).

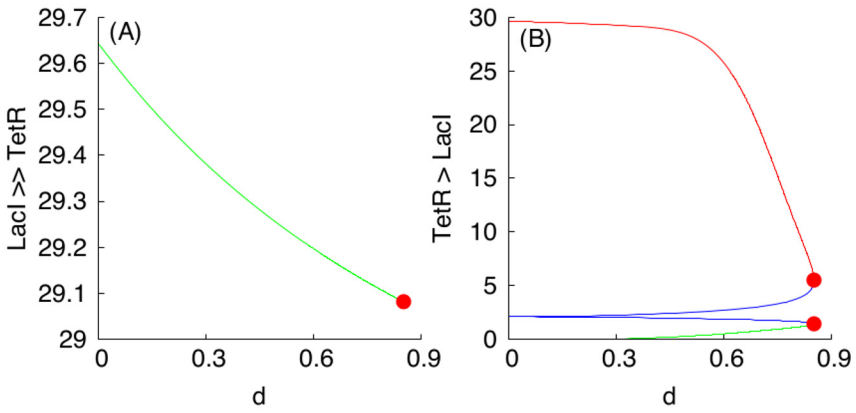

Fig 9. (9:1)-mixed population of S toggles. Panels (A) and (B) correspond to large and small subpopulations of a (9:1)-population of S toggles. All notations and color-coding schemes are as in Fig 7. Red filled circles correspond to the same LP-bifurcation point. In panel (A), projections of stable and unstable solution branches overlap. Because TetR is totally suppressed in the large (90%) subpopulation, the levels of TetR are not shown. Contrarily to panel (A), both TetR and LacI levels are plotted in panel (B) since LacI is only moderately suppressed in the small (10%) R-subpopulation.

doi:10.1371/journal.pcbi.1004881.g009

Robustness of (9:1)- and (1:9)-Mixed Populations of A Toggles and Saturated S Toggles

In contrast to the S design, in the A design, the mixed (9:1)- and (1:9)-heterogeneous populations that might arise from random state switching cannot be eliminated by changes in the values of the parameter d (Fig SI-7.8 in S1 Text). This is again in a total agreement with a similar observation reported in [16].

Using simulations carried out with the S_m model (SI-8.1 Modification of the S Model in S1 Text), we also observed that the sequestration effect results in stable (9:1)-mixed states for the S design existing for large ranges of the diffusion parameter d.

Probing Capabilities of the S Toggle Design for Self-Correction of Spontaneous Synchronization Errors

To probe and compare capabilities of the S toggle and A toggle designs to correct "spontaneous synchronization errors" caused by a random flip of one toggle (or a small fraction of toggles) from a homogeneous population to the state opposite to the transcription signature adopted by the majority of the cells, we have performed simple random tests. In mathematical and computational terms, these random tests can be interpreted as an elementary numerical procedure to evaluate the size of the basin of attraction for the corresponding equilibrium solutions by sampling the corresponding small neighborhoods of the solutions, using random initial conditions, for each parameter value $d \in \{0.01, 10, 100\}$ as follows, (1) find stable G- and R-homogeneous states (for any population size!), (2) flip 10% of population, and (3) explore initial conditions in neighborhood of this state value for the corresponding state variable (for the S design, since symmetric, only the G-homogeneous state needs to be explored).

We can conclude from Fig SI-7.9 in S1 Text that the A toggle does not have any capability for self-correction of spontaneous errors for all tested values of the parameter d (Fig SI-7.9 in S1 Text). The S toggle can self-correct spontaneous synchronization errors for the medium and large values of the parameter d (Fig 10) for all parameters values for which the mixed state becomes unstable, see Fig 9 ((9:1)-Mixed Population of S Toggles.) The rate of the error correction can be to some extend characterized by the observation that the error is corrected within the

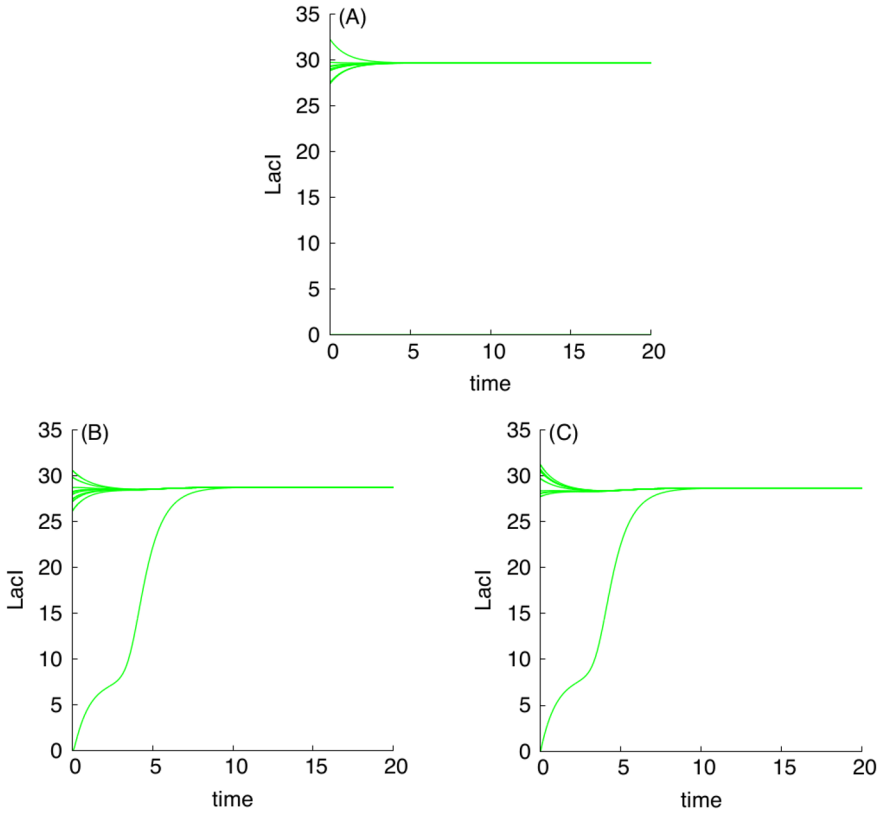

Fig 10. Self-correction of spontaneous errors by S toggles. Panel (A) shows the S toggle which cannot self-correct a (9:1)-spontaneous synchronization error for a small value of the diffusion parameter $d = 0.01$ (a weak coupling between all cells). **Panels (B) and (C)** show the S toggle which can self-correct a (9:1)-spontaneous synchronization error for a medium ($d = 10$) and large ($d = 100$) values of parameter d (a medium and strong coupling between all cells, respectively). For the values of parameter d used in Panels (B) and (C), the mixed states become unstable, see Fig 9.

doi:10.1371/journal.pcbi.1004881.g010

first 10 minutes counted from its onset (Fig 10). Unfortunately, theory does not preclude damped oscillations. Thus, all we can do is to make computational estimates in realistic parameter ranges.

To check how the limited availability of AAA+ proteases ClpXP may negatively impact the self-correctness property by the S design, we have developed an additional S_m model describing saturation (sequestration) of the AAA+ proteases ClpXP (SI-8.1 Modification of the S Model in S1 Text.) We then conducted additional computations to show that the sequestration, while preserving monotonicity and bistability properties, can lead to the loss of the self-correction of spontaneous errors by the S design. Thus, high levels of these proteases are required to implement successfully the S design.

Finally, we note that the reported results on the (9:1)-mixed states for both S and A designs are independent of the number N of cells in the given population with density ρ and can be applied to any population consisting of thousands or even millions of cells, split into two subpopulations comprising 90% and 10% fractions of all cells with different transcription signatures, respectively (Stability and Bifurcation in Cellular Populations.) Specifically, if the given (9:1)-mixed state is unstable for the S design in the model of 10 (identical) cells, it will be unstable in the model describing a larger population of (identical) cells because its stability is determined form an auxiliary system of *four* cells only (SI-6 Exponential Stability of Cellular Populations in S1 Text.) The same is true for the stable (9:1)-mixed state for the A design.

Conclusion

In this study, we have shown how synthetic bistable circuits (toggles), and hosting them, programmable cellular populations, can be designed so as to solve a robust molecular task, the maintenance of a coordinated state, and a "majority-vote" auto-correction of deviations, of a binary switch. Our design was guided by concepts from monotone systems theory [18–23]. Specifically, we have shown how this concept can be used for the design of a new class of monotone synthetic biological toggles, including predictive capabilities describing both dynamic state variables and monotone parametric tendencies caused by parameter perturbations.

To benchmark the new toggle design, termed the S design, and the monotone systems approach, we have compared the S design with the known (and non-monotone) B2-strain from [4], termed the asymmetric or A design in this work. The B2-strain has been previously studied both experimentally [4] and theoretically [16, 17]. Despite a number of remarkable properties of the B2-strain (A design), the A toggle multifunctionality suggests that the design must be tightly controlled to avoid spontaneous switching not only between different expression states, but, as well, between different functions such as a bistable memory and an oscillatory phenotype.

In this respect, modern gene therapy interventions are currently limited to transfected genes to be either in an "on" or "off" state, when the expression of the transfected gene needs to be regulated tightly for the effective treatment of many diseases. To address this challenge, the monotone S toggle design completely excludes any unpredictable chaotic behaviors, as well as undesired stable oscillations. This conclusion is valid (of course, under certain experimentally controllable conditions pointed out in this work) for all parameter values, and provides a strong theoretical guarantee missing from other synthetic biology designs. Some of conditions include: (*i*) a reduced promoter leakiness [51], and (*ii*) unsaturated levels of AAA+ proteases ClpXP.

To achieve an in-depth understanding of dynamic properties of the S toggle design, we have developed biochemically-detailed and biologically-relevant mathematical models to test predictions of monotone systems theory by employing computational bifurcation analysis. To have all results biologically grounded, concrete molecular entities have been used, though the results are general and independent of any specific details.

To investigate the effect of a spontaneous toggle switching within cellular populations, leading to bimodal distributions, we have formalized a concept of spontaneous synchronization errors and tested the toggle design capabilities to self-correct spontaneous synchronization errors by sampling the basin of attraction of the corresponding equilibrium solutions. We found that the S toggle design was able to self-correct (or, auto-correct) synchronization errors, while the non-monotone A toggle design was not.

Because the number of cells in populations is *a priori* unknown, all the above results and conclusions can make sense only if they are made independently of the population size. To justify the above assertion, we have proved a few general theorems on the exponential stability of the equilibrium solutions corresponding to both homogeneous and mixed populations. The simple exponential stability results are independent of the number of cells in the populations and are based on basic first principles of stability analysis resulting from the Schur's formula [63], allowing the characteristic polynomials for the corresponding model linearizations to be computed explicitly.

Using an additional model describing saturation (and sequestration) of AAA+ proteases ClpXP (SI-8 Modification of the S and A Models to Describe Sequestration of AAA+ protease ClpXP in S1 Text), we have observed computationally that even when the above-mentioned

conditions (*i*) and (*ii*) are violated, the S toggle still demonstrates the monotonicity properties. If proteases are in limited supply, however, the conclusions break down, because of the non-monotonicity arising from resource competition. Thus, an important consideration when practically implementing our design is to express these proteases at a high enough level.

We remark that our design is based on a bistable design based on deterministic models. This approach is normally used in synthetic biology design of toggle switches, and our goal was to employ ready technology. On the other hand, in gene regulatory networks bistability, or, to be more precise, multi-modality of steady state distributions, may arise in deterministically monostable systems due to low molecule number effects. Intuitively, a slow switch between two promoter states (modeled in simplest terms by a two-state Markov chain) gives rise to a "bimodal" distribution of gene activation (gene is "on" or "off"); this process then may drive a large-molecule number mRNA and protein process, in effect creating a bimodal protein distribution, though this bimodality would be "averaged out" in a deterministic model that considers a large population. In this context, one may mention the work by Thomas et al. [74] which provides a system with two mutually repressing promoters using noncooperative transcriptional regulation but supplemented by a translational control component in which the protein product of one gene binds and degrades the mRNA of the other gene. Because we use cooperative binding (Hill coefficients 2 and larger), our design is specifically geared to bistability even in low noise situations, and the engineered consensus mechanism is designed to correct for noise-induced transitions. It would be interesting in further work to study consensus designs for toggles based on stochastic bimodality.

Supporting Information

S1 Text. Supplemental Information (SI) materials S1–S8. SI-1 Toggle B2. SI-2 Model Derivation. SI-3 Estimation of Parameter Values. SI-4 Alternative Definitions of Monotone Systems and Order Preservation. SI-5 Symmetry. SI-6 Exponential Stability of Cellular Populations. SI-7 Additional Figures. SI-8 Modification of the S and A Models to Describe Sequestration of AAA+ Protease ClpXP.
(PDF)

Author Contributions

Conceived and designed the experiments: EVN ES. Performed the experiments: EVN EDS. Analyzed the data: EVN EDS. Contributed reagents/materials/analysis tools: EVN EDS. Wrote the paper: EVN EDS.

References

1. Gardner TS, Cantor CR, Collins JJ. Construction of a genetic toggle switch in *Escherichia coli*. Nature. 2000 Jan; 403(6767):339–342. doi: 10.1038/35002131 PMID: 10659857
2. Elowitz MB, Leibler S. A synthetic oscillatory network of transcriptional regulators. Nature. 2000 Jan; 403(6767):335–338. doi: 10.1038/35002125 PMID: 10659856
3. Hasty J, Pradines J, Dolnik M, Collins JJ. Noise-based switches and amplifiers for gene expression. Proc. Natl. Acad. Sci. U.S.A. 2000 Feb; 97(5):2075–80. doi: 10.1073/pnas.040411297 PMID: 10681449
4. Kobayashi H, Kærn M, Araki M, Chung K, Gardner TS, Cantor CR, Collins JJ. Programmable cells: interfacing natural and engineered gene networks. Proc. Natl. Acad. Sci. U.S.A. 2004 Jun; 101 (22):8414–8419. doi: 10.1073/pnas.0402940101 PMID: 15159530
5. Purnick PE, Weiss R. The second wave of synthetic biology: from modules to systems. Nat. Rev. Mol. Cell Biol. 2009 Jun; 10(6):410–422. doi: 10.1038/nrm2698 PMID: 19461664

6. Arpino JA, Hancock EJ, Anderson J, Barahona M, Stan GB, Papachristodoulou A, Polizzi K. Tuning the dials of synthetic biology. Microbiology. 2013 Jul; 159(7):1236–1253. doi: 10.1099/mic.0.067975-0 PMID: 23704788
7. Daniel R, Rubens JR, Sarpeshkar R, Lu TK. Synthetic analog computation in living cells. Nature. 2013 May; 497(7451):619–623. doi: 10.1038/nature12148 PMID: 23676681
8. Carbonell-Ballestero M, Duran-Nebreda S, Montañez R, Solé R, Macía J, Rodríguez-Caso C. A bottom-up characterization of transfer functions for synthetic biology designs: lessons from enzymology. Nucleic Acids Res. 2014 Nov:gku964.
9. Chen Y, Kim JK, Hirning AJ, Josić K, Bennett MR. Emergent genetic oscillations in a synthetic microbial consortium. Science. 2015 Aug; 349(6251):986–989. doi: 10.1126/science.aaa3794 PMID: 26315440
10. Nadell CD, Bassler BL, Levin SA. Observing bacteria through the lens of social evolution. J. Biol. 2008 Sep; 7(7):1–27. doi: 10.1186/jbiol87
11. Miller MB, Bassler BL. Quorum sensing in bacteria. Annu. Rev. Microbiol. 2001 Oct; 55(1):165–199. doi: 10.1146/annurev.micro.55.1.165 PMID: 11544353
12. Pesci EC, Pearson JP, Seed PC, Iglewski BH. Regulation of *las* and *rhl* quorum sensing in *Pseudomonas aeruginosa*. J. Bacteriol. 1997 May; 179(10):3127–3132. PMID: 9150205
13. Lithgow JK, Wilkinson A, Hardman A, Rodelas B, Wisniewski-Dyé F, Williams P, Downie JA. The regulatory locus cinRI in *Rhizobium leguminosarum* controls a network of quorum-sensing loci. Mol. Microbiol. 2000 Jul; 37(1):81–97. doi: 10.1046/j.1365-2958.2000.01960.x PMID: 10931307
14. McAnulla C, Edwards A, Sanchez-Contreras M, Sawers RG, Downie JA. Quorum-sensing-regulated transcriptional initiation of plasmid transfer and replication genes in *Rhizobium leguminosarum biovar viciae*. Microbiol. 2007 Jul; 153(7):2074–2082. doi: 10.1099/mic.0.2007/007153-0
15. Garcia-Ojalvo J, Elowitz MB, Strogatz SH. Modeling a synthetic multicellular clock: repressilators coupled by quorum sensing. Proc. Natl. Acad. Sci. U.S.A. 2004 Jul; 101(30):10955–10960. doi: 10.1073/pnas.0307095101 PMID: 15256602
16. Kuznetsov A, Kærn M, Kopell N. Synchrony in a population of hysteresis-based genetic oscillators. SIAM J. Appl. Math. 2004; 65(2):392–425. doi: 10.1137/S0036139903436029
17. Wang J, Zhang J, Yuan Z, Zhou T. Noise-induced switches in network systems of the genetic toggle switch. BMC Syst. Biol. 2007 Nov; 1(1):50. doi: 10.1186/1752-0509-1-50 PMID: 18005421
18. Smale S. On the differential equations of species in competition. J Math. Biol. 1976 Mar; 3(1):5–7. doi: 10.1007/BF00307854 PMID: 1022822
19. Hirsch MW. The dynamical systems approach to differential equations. Bull. A.M.S. 1984; 11(1):1–64. doi: 10.1090/S0273-0979-1984-15236-4
20. Angeli D, Sontag ED. Monotone control systems. IEEE Trans. Automat. Control. 2003; 48(10):1684–1698. doi: 10.1109/TAC.2003.817920
21. Hirsch M, Smith H. Monotone dynamical systems. Handbook of differential equations: Ordinary differential equations. Amsterdam: Elsevier BV. 2005; 2:239–357.
22. Sontag ED. Monotone and near-monotone biochemical networks. Syst. and Synth. Biol. 2007; 1:59–87. doi: 10.1007/s11693-007-9005-9
23. Smith HL. Monotone dynamical systems: An introduction to the theory of competitive and cooperative systems. Mathematical Surveys and Monographs. Vol. 41. Providence, RI: A.M.S. 2008.
24. Parsek MR, Greenberg EP. Acyl-homoserine lactone quorum sensing in gram-negative bacteria: a signaling mechanism involved in associations with higher organisms. Proc. Natl. Acad. Sci. U.S.A. 2000 Aug 1; 97(16):8789–8793. doi: 10.1073/pnas.97.16.8789 PMID: 10922036
25. Resmi V, Ambika G, Amritkar RE. Synchronized states in chaotic systems coupled indirectly through a dynamic environment. Phys. Rev. E. 2010 Apr; 81(4):046216. doi: 10.1103/PhysRevE.81.046216
26. Sontag ED. Mathematical control theory: deterministic finite dimensional systems. New York: Springer Science & Business Media. 2013.
27. Parsek MR, Val DL, Hanzelka BL, Cronan JE, Greenberg EP. Acyl homoserine-lactone quorum-sensing signal generation. Proc. Natl. Acad. Sci. U.S.A. 1999 Apr; 96(8):4360–4365. doi: 10.1073/pnas.96.8.4360 PMID: 10200267
28. Hooshangi S, Thiberge S, Weiss R. Ultrasensitivity and noise propagation in a synthetic transcriptional cascade. Proc. Natl. Acad. Sci. U.S.A. 2005 Mar; 102(10):3581–3586. doi: 10.1073/pnas.0408507102 PMID: 15738412
29. Tuttle LM, Salis H, Tomshine J, Kaznessis YN. Model-driven designs of an oscillating gene network. Biophys. J. 2005 Dec; 89(6):3873–3883. doi: 10.1529/biophysj.105.064204 PMID: 16183880

30. Stricker J, Cookson S, Bennett MR, Mather WH, Tsimring LS, Hasty J. A fast, robust and tunable synthetic gene oscillator. Nature. 2008 Nov; 456(7221):516–519. doi: 10.1038/nature07389 PMID: 18971928

31. Hussain F, Gupta C, Hirning AJ, Ott W, Matthews KS, Josić K, Bennett MR. Engineered temperature compensation in a synthetic genetic clock. Proc. Natl. Acad. Sci. U.S.A. 2014 Jan; 111(3):972–977. doi: 10.1073/pnas.1316298111 PMID: 24395809

32. Laffend L, Shuler ML. Structured model of genetic control via the *lac* promoter in *Escherichia coli*. Biotechnol. Bioeng. 1994 Mar; 43(5):399–410. doi: 10.1002/bit.260430508 PMID: 18615723

33. Lutz R, Bujard H. Independent and tight regulation of transcriptional units in *Escherichia coli* via the LacR/O, the TetR/O and AraC/I1-I2 regulatory elements. Nucleic Acids Res. 1997 Mar; 25(6):1203–1210. doi: 10.1093/nar/25.6.1203 PMID: 9092630

34. Baumeister R, Flache P, Melefors Ö, von Gabain A, Hillen W. Lack of a 5'non-coding region in Tn 1721 encoded *tetR* mRNA is associated with a low efficiency of translation and a short half-life in *Escherichia coil*. Nucleic Acids Res. 1991 Sep; 19(17):4595–4600. doi: 10.1093/nar/19.17.4595 PMID: 1653948

35. Markiewicz P, Kleina LG, Cruz C, Ehret S, Miller JH. Genetic studies of the lac repressor. XIV. Analysis of 4000 altered Escherichia coli lac repressors reveals essential and non-essential residues, as well as "spacers" which do not require a specific sequence. J. Mol. Biol. 1994 Jul; 240(5):421–33. doi: 10.1006/jmbi.1994.1458 PMID: 8046748

36. Ramos JL, Martínez-Bueno M, Molina-Henares AJ, Terán W, Watanabe K, Zhang X, Gallegos MT, Brennan R, Tobes R. The TetR family of transcriptional repressors. Microbiol. Mol. Biol. Rev. 2005 Jun; 69(2):326–56. doi: 10.1128/MMBR.69.2.326-356.2005 PMID: 15944459

37. Semsey S, Jauffred L, Csiszovszki Z, Erdőssy J, Stéger V, Hansen S, Krishna S. The effect of LacI autoregulation on the performance of the lactose utilization system in *Escherichia coli*. Nucleic Acids Res. 2013 May:gkt351.

38. Gray KM, Garey JR. The evolution of bacterial LuxI and LuxR quorum sensing regulators. Microbiology. 2001 Aug; 147(8):2379–2387. doi: 10.1099/00221287-147-8-2379 PMID: 11496014

39. Shuler ML, Leung S, Dick CC. A mathematical model for the growth of a single bacterial cell. Ann. N Y Acad. Sci. 1979 May; 326(1):35–52. doi: 10.1111/j.1749-6632.1979.tb14150.x

40. Neidhardt FC, Ingraham JL, Schaechter M. Physiology of the Bacterial Cell: A Molecular Approach. Massachusetts: Sinauer Associates, Inc., Publishers Sunderland. 1990.

41. Kim BG, Shuler ML. A structured, segregated model for genetically modified *Escherichia coli* cells and its use for prediction of plasmid stability. Biotechnol. Bioeng. 1990 Sep; 36(6):581–92. doi: 10.1002/bit.260360605 PMID: 18595116

42. Shu J, Shuler ML. Prediction of effects of amino acid supplementation on growth of *E. coli* B/r. Biotechnol. Bioeng. 1991 Apr; 37(8):708–15. doi: 10.1002/bit.260370804 PMID: 18600666

43. Laffend L, Shuler ML. Ribosomal protein limitations in *Escherichia coli* under conditions of high translational activity. Biotechnol. Bioeng. 1994 Mar; 43(5):388–98. doi: 10.1002/bit.260430507 PMID: 18615722

44. Bailey JE. Mathematical modeling and analysis in biochemical engineering: past accomplishments and future opportunities. Biotechnol. Prog. 1998 Jan; 14(1):8–20. doi: 10.1021/bp9701269 PMID: 9496667

45. Domach MM, Leung SK, Cahn RE, Cocks GG, Shuler ML. Computer model for glucose-limited growth of a single cell of *Escherichia coli* B/r-A. Biotechnol. Bioeng. 2000 Mar 20; 67(6):827–40. doi: 10.1002/(SICI)1097-0290(20000320)67:6%3C827::AID-BIT18%3E3.0.CO;2-N PMID: 10699861

46. Nikolaev EV, Burgard AP, Maranas CD. Elucidation and structural analysis of conserved pools for genome-scale metabolic reconstructions. Biophys. J. 2005 Jan; 88(1):37–49. doi: 10.1529/biophysj.104.043489 PMID: 15489308

47. Nikolaev EV, Atlas JC, Shuler ML. Computer models of bacterial cells: from generalized coarse-grained to genome-specific modular models. J. Phys.: Conf. Ser. 2006; 46(1):322–326.

48. Atlas JC, Nikolaev EV, Browning ST, Shuler ML. Incorporating genome-wide DNA sequence information into a dynamic whole-cell model of *Escherichia coli*: application to DNA replication. IET Syst. Biol. 2008 Sep; 2(5):369–382. doi: 10.1049/iet-syb:20070079 PMID: 19045832

49. Nikolaev EV. The elucidation of metabolic pathways and their improvements using stable optimization of large-scale kinetic models of cellular systems. Metab. Eng. 2010 Jan; 12(1):26–38. doi: 10.1016/j.ymben.2009.08.010 PMID: 19733253

50. Lodish H, Berk A, Kaiser C, Krieger M., Bretscher A, Ploegh H., Amon A, Scott M. Molecular cell biology. New York: Macmillan. 2012

51. Penumetcha P, Lau K, Zhu X, Davis K, Eckdahl TT, Campbell AM. Improving the Lac system for synthetic biology. Bios. 2010 Mar; 81(1):7–15. doi: 10.1893/011.081.0104

52. Stephanopoulos G, Aristidou AA, Nielsen J. Metabolic engineering: principles and methodologies. New York: Academic press. 1998.

53. Dockery JD, Keener JP. A mathematical model for quorum sensing in *Pseudomonas aeruginosa*. Bull. Math. Biol. 2001 Jan; 63(1):95–116. doi: 10.1006/bulm.2000.0205 PMID: 11146885

54. Bressloff PC. Stochastic processes in cell biology. New York: Springer. 2014.

55. Dong YH, Wang LH, Xu JL, Zhang HB, Zhang XF, Zhang LH. Quenching quorum-sensing-dependent bacterial infection by an N-acyl homoserine lactonase. Nature. 2001 Jun; 411(6839):813–817. doi: 10.1038/35081101 PMID: 11459062

56. Waldherr S, Allgower F. Network-level dynamics of diffusively coupled cells. Decision and Control (CDC), 2012 IEEE 51st Annual Conference 2012; 5517–5522.

57. Farrell CM, Baker TA, Sauer RT. Altered specificity of a AAA+ protease. Mol. cell. 2007 Jan; 25 (1):161–166. doi: 10.1016/j.molcel.2006.11.018 PMID: 17218279

58. Khibnik AI, Kuznetsov YA, Levitin VV, Nikolaev EV. Continuation techniques and interactive software for bifurcation analysis of ODEs and iterated maps. Phys. D: Nonlinear Phenomena. 1993 Jan; 62(1–4):360–71. doi: 10.1016/0167-2789(93)90294-B

59. Govaerts W, Kuznetsov YA, Dhooge A. Numerical continuation of bifurcations of limit cycles in MATLAB. SIAM J. Sci. Comput. 2005; 27(1):231–252. doi: 10.1137/030600746

60. Doedel EJ. Numerical Continuation Methods for Dynamical Systems. Lecture notes on numerical analysis of nonlinear equations. Netherlands: Springer 2007:1–49.

61. Bindel D, Friedman M, Govaerts W, Hughes J, Kuznetsov YA. Numerical computation of bifurcations in large equilibrium systems in MATLAB. J. Comput. App. Math. 2014 May; 261:232–48. doi: 10.1016/j.cam.2013.10.034

62. Kuznetsov YA. Elements of applied bifurcation theory. New York: Springer Science & Business Media. 2013.

63. Gantmakher FR. The theory of matrices. A.M.S.: Chelsea Publishing Company. 1959.

64. Hirsch MW. Differential equations and convergence almost everywhere in strongly monotone semiflows. Contemp. Math. 1983; 17:267–285. doi: 10.1090/conm/017/706104

65. Hirsch MW. Systems of differential equations that are competitive or cooperative II: Convergence almost everywhere. SIAM J. Math. Anal. 1985 May; 16(3):423–439. doi: 10.1137/0516030

66. Hadeler KP, Glas D. Quasimonotone systems and convergence to equilibrium in a population genetic model. J. Math. Anal. Applic. 1983 Sep; 95(2):297–303. doi: 10.1016/0022-247X(83)90108-7

67. Zaslavsky T. A mathematical bibliography of signed and gain graphs and allied ares. Electronic Journal of Combinatorics 1998; DS8

68. Dhooge A, Govaerts W, Kuznetsov YA. MATCONT: a MATLAB package for numerical bifurcation analysis of ODEs. ACM Transactions on Mathematical Software (TOMS). 2003 Jun; 29(2):141–64. doi: 10.1145/779359.779362

69. Wang L, Sontag ED. Singularly perturbed monotone systems and an application to double phosphorylation cycles. J. Nonlin. Sci. 2008 Oct; 18(5):527–50. doi: 10.1007/s00332-008-9021-2

70. Golubitsky M, Stewart I. Singularities and groups in bifurcation theory. New York: Springer Science & Business Media. 2012.

71. Nikolaev EV. Bifurcations of limit cycles of differential equations admitting an involutive symmetry. Sbornik: Mathematics. 1995; 186(4):611. doi: 10.1070/SM1995v186n04ABEH000033

72. Nikolaev E, Shnol E. Bifurcations of cycles in systems of differential equations with a finite symmetry group-I. J. Dynamic. Cont. Syst. 1998; 4(3):315–341. doi: 10.1023/A:1022832331959

73. Nikolaev E, Shnol E. Bifurcations of cycles in systems of differential equations with a finite symmetry group-II. J. Dynamic. Cont. Syst. 1998; 4(3):343–363. doi: 10.1023/A:1022884316030

74. Thomas P, Popović N, Grima R. Phenotypic switching in gene regulatory networks. Proc. Natl. Acad. Sci. U.S.A. 2014; 111(19):6994–6999. doi: 10.1073/pnas.1400049111 PMID: 24782538

Quorum-Sensing Synchronization of Synthetic Toggle Switches: A Design based on Monotone Dynamical Systems Theory

Evgeni V. Nikolaev, Eduardo D. Sontag*

Department of Mathematics and Center for Quantitative Biology, Rutgers, The State University of New Jersey, Piscataway, NJ 08854-8019, The United States

*Corresponding Author: eduardo.sontag@rutgers.edu

Supporting Information

SI-1 Toggle B2

Kobayashi et al [1] consider a number of genetic toggle switches, interfaced with a QS signaling pathway. Specifically, their *E. coli* strain "B2" (Fig. SI-1.1) detects as well as produces (through the synthetase encoded by the expressed gene luxI, which converts common precursor metabolites) acyl-homoserine lactone (AHL) signaling molecules. AHL is a QS signaling pathway from *Vibrio fischeri*. Functionally, toggle B2 enables an *E. coli* population to measure population density through AHL, because AHL signaling can be reversibly transported to the medium via diffusion, contributing to the AHL density in the culture [1]. To achieve an in-depth understanding of dynamic properties of coupled QS and toggle constructs, Kuznetsov et al. [2] developed and studied a mechanistic mathematical model of a population (or, equivalently, an ensemble) comprising N toggles, see Fig. 1 (bottom panel), corresponding to Toggle B2. Their study revealed important multiple functions, namely bistability as well as stable oscillations, that an ensemble of Toggles B2 was capable of exhibiting. Analytical conditions for bistability were found, and a time separation was introduced to obtain a stable limit cycle for a population of interacting cells.

In bistable circuits (toggles), transitions such as those caused by fluctuations due to low copy numbers of species per cell, or due to local environmental "noise" can force individual cells to change expression state at random [1]. This noise effect can spontaneously lead to the emergence of heterogeneous (mixed) populations consisting of cells in different expression states, which appear as bimodal population distributions when the corresponding protein levels are measured [1]. To investigate the effect of a spontaneous toggle switching in single and coupled cellular systems, leading to bimodal population distributions, Wang et al. [3] developed models for a single cell and a multi-cellular toggle system comprising N cells, respectively. In their models, the dynamics of the repressor proteins LacI and λ CI is described by the two ODE equations developed in [4]. The AI-interfacing employed in the population model [3] corresponds to a signaling pathway which is slightly different from the signaling pathway in Toggle B2

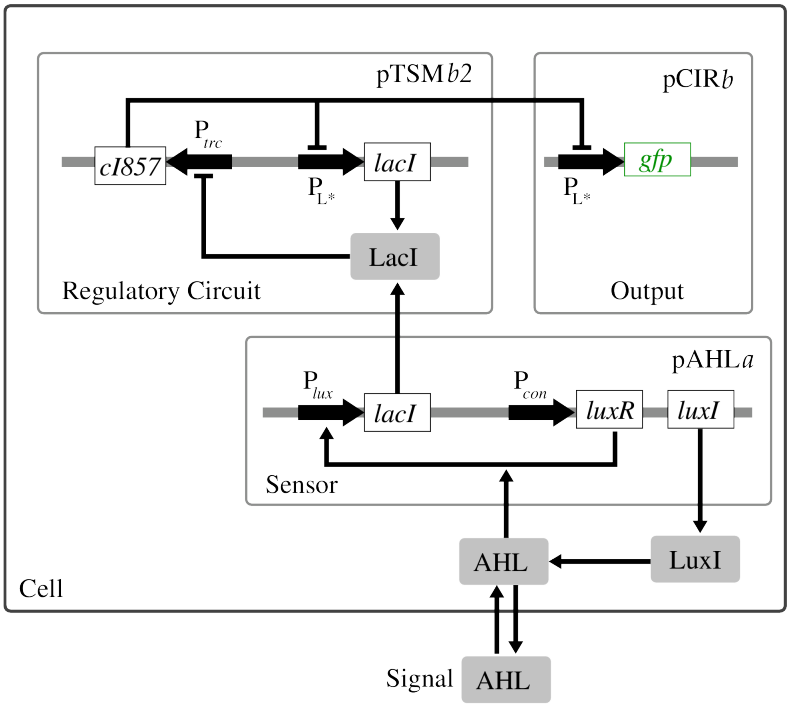

Figure SI-1.1. Toggle B2: Density-Dependent Gene Activation. *Notations and abbreviations.* Plasmids: pTSM*b2*, pCIR*b* and pAHL*a*; genes: *gfp*, *cI857*, *lacI*, *luxR*, and *luxI*; promoters: P_{trc}, P_{L^*}, and P_{lux}; AHL, acyl-homoserine lactone. Figure adapted from Fig. 6(A) in [1].

(Fig. SI-1.1) as suggested in [1] and described earlier. The main difference is in the description of the expression of the gene that encodes LuxI, see [3] for more details.

SI-2 Model Derivation

Here, we describe the main assumptions and steps used to derive mass-balance equations for the S- and A-models formulated in the main text.

SI-2.1 SI-2.1 Mass-Balance Equations

The derivation of the S- and A-models includes the development of two modules:

I. A transcription-translation module describing biosyntheis of repressor proteins.

II. A metabolic module describing biosynthesis of autoinducers.

A general and systematic discussion of both modules can be found in [5, 6]. The derivation of the first module for the A-model, relevant to our work, is given in [2]. Because one of our modeling objectives is to ultimately describe how the analysis of the mathematical models can be mechanistically interpreted in terms of tuning synthetic toggle "dials" by implementable experimental interventions as reviewed in [7], including modifications of ribosome-binding sites (RBS), carboxy-terminal tags, *etc.*, [4, 8, 9], we will derive mass-balance equations at the level of molecular detail sufficient to suggest plausible modeling predictions.

A transcription-translation module can be described by a basic two-stage model [2,5,6],

$$\frac{dn_x}{dt} = n_A k_x - r_x n_x, \tag{SI-2.1a}$$

$$\frac{dn_{\rm X}}{dt} = k_{\rm X} n_x - r_{\rm X} n_{\rm X}. \tag{SI-2.1b}$$

Here, n_x is the number of mRNA transcripts per cell for gene x, and $n_{\rm X}$ is the number of protein molecules per cell; n_A is the number of active promoters from which the mRNA of gene x is transcribed at an average rate k_x; $k_{\rm X}$ is the averaged translation rate; r_x and $r_{\rm X}$ are the effective first-order rate constants associated with degradation of the mRNA and proteins, respectively.

Since mRNA molecules are usually degraded rapidly compared to other cellular processes, a quasi-steady state for the equation (SI-2.1a) can often be assumed [2], yielding

$$n_x = \frac{n_A k_x}{r_x}. \tag{SI-2.2}$$

Using (SI-2.2) in the right-hand side of the equation (SI-2.1b), we obtain

$$\frac{dn_{\rm X}}{dt} = k_{\rm X} \frac{k_x\, n_A}{r_x} - r_{\rm X}\, n_{\rm X}. \tag{SI-2.3}$$

The ratio $b_x = k_{\rm X}/r_x$ in equation (SI-2.3) is called a burst parameter of the protein X [2]. Using b_x in (SI-2.3) yields

$$\frac{dn_{\rm X}}{dt} = b_x k_x n_A - r_{\rm X} n_{\rm X}. \tag{SI-2.4}$$

Assuming log-phase growth of *E. coli*, the volume $V(t)$ of the growing bacterium can be approximated by the expression $V(t) = V_0 \exp(\lambda t)$, and equation (SI-2.4) can be rewritten in a concentration form,

$$\frac{d[{\rm X}]}{dt} = b_x k_x [{\rm P_A}] - (r_{\rm X} + \mu)\,[{\rm X}]. \tag{SI-2.5}$$

Here, $[{\rm X}](t) = n_{\rm X}(t)/V(t)$ and $[{\rm P_A}](t) = n_A(t)/V(t)$.

The concentration of activate promoters, $[{\rm P_A}]$, can be computed, using an appropriate Hill function [6]. For example, we use

$$[{\rm P_{YA}}] = \frac{[{\rm P_Y}]}{1 + ([{\rm Y}]/K_{\rm Y})^{n_{\rm Y}}} \tag{SI-2.6}$$

for the repressor protein Y binding to the promoter $\rm P_Y$ with the dissociation constant $K_{\rm Y}^{n_{\rm Y}}$. In (SI-2.6), $[{\rm P_Y}]$ is the total concentration of all promoters $\rm P_Y$, while $[{\rm P_{YA}}]$ is the concentration of active promoters not bound with the repressor protein Y. Recall that the cooperativity described by the Hill exponent $n_{\rm Y}$ can arise from [4–6]:

(i). Multimerization of represssor proteins;

(ii). Cooperative binding of repressor multimers to multiple operator sites in the promoter.

Analogously, we use a Hill-function

$$[{\rm P_{GA}}] = [{\rm P_G}] \frac{([{\rm G}]/K_{\rm G})^{n_{\rm G}}}{1 + ([{\rm G}]/K_{\rm G})^{n_{\rm G}}} \tag{SI-2.7}$$

for the autoinducer G binding to the promoter P_G with the dissociation constant $K_G^{n_G}$ and the Hill exponent n_G. The concentration of all active promoters P_A can now be obtained from (SI-2.6) and (SI-2.7) as

$$P_A = P_{YA} + P_{GA}. \tag{SI-2.8}$$

Using expression (SI-2.8), the equation (SI-2.5) can finally be updated as

$$\frac{d[X]}{dt} = \frac{b_x k_x [P_Y]}{1 + ([Y]/K_Y)^{n_Y}} + b_x k_x [P_G] \frac{([G]/K_G)^{n_G}}{1 + ([G]/K_G)^{n_G}} - (r_X + \mu)[X]. \tag{SI-2.9}$$

Here, all parameters are described below in Table SI-3.2.

Similar mass balanced equations can be derived for the repressor protein Y, and synthases U and W. For example, the mass balance equation for the synthase U is

$$\frac{d[U]}{dt} = \frac{b_u k_u [P_Y]}{1 + ([Y]/K_Y)^{n_Y}} - (r_U + \mu)[U]. \tag{SI-2.10}$$

Analogously, we can write down a mass balance equation for the autoinducer concentration [G], that is, [C14-HSL], governed by the synthase U (CinI),

$$\frac{d[G]}{dt} = k_G [U] + D_G (G_e - G) - (r_G + \mu)[G]. \tag{SI-2.11}$$

Here, k_G is the maximum production rate of C14-HSL by CinI (Table SI-3.4), D_G is the export rate of C14-HSL (Table SI-3.4), and $[G_e]$ is the extracellular concentration of C14-HSL.

Assuming that the concentration of the enzyme U reaches its quasi-steady state rapidly [10], one can obtain from (SI-2.10) that

$$[U] = \frac{b_u k_u}{r_U + \mu} \times \frac{[P_Y]}{1 + ([Y]/K_Y)^{n_Y}}. \tag{SI-2.12}$$

Using (SI-2.12) in the equation (SI-2.11) yields

$$\frac{d[G]}{dt} = \frac{b_u\, k_u\, k_G}{r_U + \mu} \times \frac{[P_Y]}{1 + ([Y]/K_Y)^{n_Y}} - (r_G + \mu)[G]. \tag{SI-2.13}$$

Here, the definitions and the values of all parameters are given in Table SI-3.4. A similar mass balanced equation can be derived for the second autoinducer R (C4-HSL), and we omit the details.

SI-2.2 SI-2.2 Nondimensionalization

To nondimensionalize mass balance equations, as for example, the mass balance equations (SI-2.9) and (SI-2.13), we use the following dimensionless state variables, which are similar to those introduced in [2],

$$t' = (r_d + \mu)\, t, \quad x = \frac{[X]}{K_X}, \quad y = \frac{[Y]}{K_Y}, \quad g = \frac{[G]}{K_G}, \quad g_e = \frac{[G_e]}{K_G}, \quad r = \frac{[R]}{K_R}, \quad r_e = \frac{[R_e]}{K_R}. \tag{SI-2.14}$$

Here, we assume that all protein degradation rates can be set experimentally so that the following equalities can be obtained *approximately* [8],

$$r_{\rm X} \,=\, r_{\rm X} \,=\, r_{\rm U} \,=\, r_{\rm W} \,=\, r_d = \frac{\ln 2}{\tau_{1/2}}, \quad \tau_{1/2} \,=\, 4\,\text{min}. \tag{SI-2.15}$$

The procedure of setting all protein degradation rates or, equivalently, all protein half-lives approximately equal to a prescribed value close to mRNA half-lives [8] is required to balance the toggle [4]. We discuss the balancing procedure and relevant experimental interventions in Sect. SI-2.2.

Using the dimensionless variables (SI-2.14), all original modeling mass balances can be nondimensionalized, yielding the S- and A-models formulated in the main text, where the prime is dropped from dimensionless time t'. In this case, dimensional and dimensionless parameters are related to one another as:

1. For the dimensionless rates, we obtain:

$$a_1 = \frac{b_x\, k_x\, [\mathrm{P_Y}]}{K_{\rm X}\,(r_d+\mu)}, \quad a_2 \,=\, \frac{b_y\, k_y\, [\mathrm{P_X}]}{K_{\rm Y}\,(r_d+\mu)}, \quad a_3 \,=\, \frac{b_x\, k_x\, [\mathrm{P_G}]}{K_{\rm X}\,(r_d+\mu)}, \tag{SI-2.16a}$$

$$a_4 = \frac{b_y\, k_y\, [\mathrm{P_R}]}{K_{\rm Y}\,(r_d+\mu)}, \quad a_5 \,=\, \frac{b_u\, k_u\, k_{\rm G}\, [\mathrm{P_Y}]}{K_{\rm G}\,(r_d+\mu)^2}, \quad a_6 \,=\, \frac{b_w\, k_w\, k_{\rm R} [\mathrm{P_X}]}{K_{\rm R}\,(r_d+\mu)^2}. \tag{SI-2.16b}$$

2. For dimensionless diffusion and degradation parameters, we obtain:

$$d_g = \frac{D_{\rm G}}{r_d+\mu}, \quad d_r \,=\, \frac{D_{\rm R}}{r_d+\mu}, \quad \delta_g \,=\, \frac{r_{\rm G}+\mu}{r_d+\mu}, \quad \delta_r \,=\, \frac{r_{\rm R}+\mu}{r_d+\mu}, \quad \delta_e \,=\, \frac{\mu_e}{r_d+\mu}, \tag{SI-2.17a}$$

Molecular and biophysical parameter values used in the expressions (5) - (6) will be estimated in Sect. SI-2.2, while dimensionless parameters will be estimated in Sect. SI-2.2 In this section, we only mention that due to [8], we can set

$$K_{\rm X} \,=\, K_{\rm Y} \,=\, 40\,\text{monomers per cell}. \tag{SI-2.18}$$

We could not find any estimation of values for the two parameters $K_{\rm G}$ for C14-HSL and $K_{\rm R}$ for C4-HSL in the literature despite the fact that more and more precise measurements of kinetic parameters become available [11]. We estimate the order of magnitude of $K_{\rm G}$ and $K_{\rm R}$ as follows.

In the detailed experimental results on the C4-HSL-mediated quorum sensing regulatory system of the opportunistic Gram-negative bacterium *Aeromonas hydrophila*, the concentration of C4-HSL was found to be of order of magnitude equal to $10\,\mu$M [12]. In *E.coli* biology, it is convenient to use nM units [13], because relative to the effective *E. coli* volume [14], the value of 1 nM corresponds to one molecule per cell. This fact is widely used in the literature [8]. Therefore, the above estimate of $10\,\mu$M corresponds to 10^4 C4-HSL signaling molecules per cell.

Another *ad-hoc* rule of *E.coli* biology used in a number of studies with the Cornell *E.coli* computer model [15–18], resulting in a number of relevant predictions such as ribosomal-protein limitations, *lac*-control, plasmid stability, and *etc.* [14, 19–24], is that, the coarse-grained estimation for the dissociation equilibrium constant to be used in the Hill function can be calculated as 25% of the intracellular modifier (reference) concentration. In our case, this yields a coarse-grade estimate of 0.25×10^4 C4-HSL signaling molecules per cell,

$$K_{\rm G} \,=\, K_{\rm R} \,=\, 2.5 \times 10^3\,\text{molecules per cell}. \tag{SI-2.19}$$

The values for other parameters will be estimated below.

SI-2.3 Toggle Balancing (Symmetrization)

As it was observed experimentally [4,8], synthetic circuits can operate and deliver the engineered traits only if special molecular constrains are fulfilled,

(i) repressor protein half-lives are close to mRNA halflifes [8];

(ii) repressor protein half-lives are approximately equal [4,8].

Constrain *(ii)* is required for "balancing" the given circuit [4]. Moreover, both works suggest experimental interventions to fulfill the above constraints [4,8]. Such and similar interventions are termed a "tuning dials" in the review [7].

It is mathematically convenient for us to generalize the above balancing procedure by the procedure of "symmetrization" of two antagonistic, mutually repressing toggle subsystems by selecting synthetic (tuned) parameter values that would make two antagonist subsystems symmetric to one another. In other words, we assume that an *ideal* S toggle has mirror symmetry corresponding to permutations between the two antagonistic subsystems. Symmetry usually helps with analytical analysis of nonlinear mathematical models.

Specifically, we "symmetrize" (balance) biosynthesis kinetic rates, using constraints

$$a_1 = a_2, \quad a_3 = a_4 \quad \text{and} \quad a_5 = a_6. \tag{SI-2.20}$$

Appropriate molecular interventions, which can be used to set the relationships (SI-2.20) approximately under certain experimental conditions, are reviewed in [7]. Similarly, we symmertize "diffusion" parameters,

$$d_g = d_r = d, \tag{SI-2.21}$$

and the autoinducer "degradation" or "utilization" ("load") parameters,

$$\delta_g = \delta_r = \delta_e = \delta. \tag{SI-2.22}$$

SI-3 Estimation of Parameter Values

SI-3.1 Toggle Parameters

In our estimations, we use general biochemical calculations [25, 26]. First, we collect generic prokaryotic and specific *E.coli* parameter values in Table SI-3.1.

Table SI-3.1. Generic prokaryotic and *E. coli* specific values of model parameters

Name	Description	Value	Unit	Reference
r_{mRNA}	Rate of transcription by RNA polymerase in prokaryotes	80	bp/sec	[27]
τ_{mRNA}	Typical half-life time for 80% of genes in *E. coli*	3 - 8	min	[28]
r_{aa}	Rate of translation by the ribosome in prokaryotes	20	aa/sec	[27][a]
k_{P}	Rate of translation by the ribosome in prokaryotes	1.71	sec^{-1}	estimated in (SI-3.3)
T	*E. coli* replication period under specific nutrition conditions	25	min	[14]
μ	Intracellular specific dilution rate due to *E. coli* cell growth	$\ln 2/T$	min^{-1}	[14]
μ_e	Extracellular dilution rate due to flow	0.1	min^{-1}	[29]
ρ	Total volume fraction of cells in chamber	0.8	$-$	[30]
N	Number of *E. coli* cells in an overnight population culture	10^9 (OD600 = 1)	cells/ml	[14]

[a]This estimate is smaller than the estimate 33 aa/sec used in [11].

A general rate of translation of protein P in prokaryotes (k_{P})**.** Suppose that an mRNA transcript of protein P contains n_{aa} amino acids. Then, for one ribosome to transcribe P from its mRNA transcript, assuming a translation rate of 20 amino acids per second (Table SI-3.1), it will take time

$$t_{\mathrm{P}} \;=\; \frac{n_{\mathrm{aa}}}{20}. \tag{SI-3.1}$$

The above estimates yields the rate per ribosome which is

$$\frac{1 \text{ molecule}}{\mathrm{t_P}} \;=\; \frac{20}{\mathrm{n_{aa}}} \,\mathrm{sec}^{-1}. \tag{SI-3.2}$$

Given that the coding region of protein P is $n_{\mathrm{aa}} \times 3$ nucleotides long, and that a ribosome can attach every 35 nucleotides, we can estimate that $n_{\mathrm{aa}} \times 3/35$ ribosomes can be attached per mRNA molecule. We, thus, obtain

$$k_{\mathrm{P}} \;= \frac{20}{n_{\mathrm{aa}}} \times \frac{n_{\mathrm{aa}} \times 3}{35} \;=\; 1.71 \text{ protein molecules } \mathrm{sec}^{-1}. \tag{SI-3.3}$$

To illustrate our parameter estimation procedure, we derive parameter values for the Lac-repressor subsystem only. Parameter values for all other subsystems can be derived similarly.

k_x : **Fully induced strength of promoters** $\mathrm{P_Y}$ ($\mathrm{P_{tet}}$) **and** $\mathrm{P_G}$**.** One *lacI* mRNA transcript is 1204 bases long (Table SI-3.2). To transcribe one molecule of *lacI* mRNA from one gene with a rate of 80 bases per second (Table SI-3.2) takes

$$\frac{1204 \text{ bases}}{80 \text{ bases/sec}} \;=\; 15.05 \text{ sec}. \tag{SI-3.4}$$

Table SI-3.2. Parameter values of the LacI-repressor subsystem.

Name	Description	Value	Unit	Reference
Transcription:				
L_{lacI}	Size of *lacI* gene	1204	bp	[31]
Γ_x	Repressed strength of promoter P_{tet}	5.0×10^{-4}	molecules/cell/sec	[8]
k_x	Fully induced transcription rate[a]	6.65×10^{-2}	species/cell/sec	estimated in (SI-3.5)
K_Y	The number of TetR to repress[b] P_{tet}	40	monomers/cell	estimated in (SI-2.18)
K_G	The number of C14-HSL to activate[c] P_{cin}	2.5×10^3	molecules/cell	estimated in (SI-2.19)
$\tau_{1/2,lacI}$	Half-life of *lacI* mRNA	3.8	min	[32]
r_x	Rate of *lacI* mRNA degradation	3.04×10^{-3}	sec^{-1}	estimated in (SI-3.7)
n_Y	The number of subunits in TetR	2		[33]
n_G	Hill coefficient of C14-HSL	3		a reference value[d]
Translation:				
L_{LacI}	Size of one subunit in tetrameric LacI	360	aa/subunit	[34]
k_X	Rate of LacI translation	1.71	molecules/cell/sec	estimated in (SI-3.3)
$\tau_{1/2,LacI}$	Half-life of LacI protein	4	min	[8]
r_X	Rate of LacI degradation	1.16×10^{-3}	sec^{-1}	estimated in (SI-3.7)

[a] Fully induced strength of promoters P_{tet} and P_{cin},
[b] For the sake of brevity, "to repress" means "to half-maximally repress."
[c] For the sake of brevity, "to activate" means "to half-maximally activate."
[d] The Hill coefficients for C6-HSL and C12-HSL are estimated in the range of values 1 - 2 in [35, 36], while these are estimated to be equal to 4 for C4-HSL and C14-HSL in [37]. We use a compromising *reference* value equal to 3 and also explore other values in our computational studies.

Then, per gene the estimate (SI-3.4) yields

$$k_x = \frac{1}{15.05 \text{ sec}} = 6.65 \times 10^{-2} \text{ lacI mRNA (molecules/cell/sec)}. \quad \text{(SI-3.5)}$$

The estimate (SI-3.4) is one order of magnitude less than the estimate 0.5 lacI mRNA (molecules/cell/sec) provided in [8].

r_x : **Rate of *lacI* mRNA degradation.** The calculation of degradation rates for proteins is based on the known protein half-lives,

$$r_x = \frac{\ln 2}{t_{1/2}}. \quad \text{(SI-3.6)}$$

We obtain (Table SI-3.2),

$$r_x = \frac{\ln 2}{3.8 \times 60 \text{ sec}} = 3.04 \times 10^{-3} \text{ sec}^{-1}. \quad \text{(SI-3.7)}$$

r_X : **Rate of LacI (X) degradation.** We obtain (Table SI-3.2),

$$r_d = r_X = \frac{\ln 2}{4 \times 60 \text{ sec}} = 2.89 \times 10^{-3} \text{ sec}^{-1}. \quad \text{(SI-3.8)}$$

We use the estimate (SI-3.8) for all proteins in the model.

Table SI-3.3. Parameter values of the TetA-repressor subsystem.

Name	Description	Value	Unit	Reference
Transcription:				
L_{tetR}	Size of *tetR* gene	905	bp	[38]
Γ_y	Repressed strength of promoter P_{lac}	5×10^{-4}	molecules/cell/sec	estimated in Table SI-3.2
k_y	Fully induced transcription rate[a]	8.87×10^{-2}	molecules/cell/sec	estimated
K_X	The number of LacI to repress[b] P_{lac}	40	monomers/cell	estimated in Table SI-3.2[d]
K_R	The number of C4-HSL to activate[c] P_{rhl}	5×10^4	monomers/cell	estimated in Table SI-3.2
$\tau_{1/2,tetR}$	Half-life of *tetR* mRNA	0.5	min	[39]
r_y	Rate of *tetR* mRNA degradation	2.31×10^{-2}	sec^{-1}	estimated
n_X	The number of subunits in LacI	2		[33]
n_R	Hill coefficient of C4-HSL	4		estimated in Table SI-3.2
Translation:				
L_{TetR}	Size of one subunit in tetrameric TetR	207	aa/subunit	[38]
k_Y	Rate of TetR translation	1.71	molecules/cell/sec	estimated in (SI-3.3)
$\tau_{1/2,TetR}$	Half-life of TetR protein	4	min	estimated Table SI-3.2
r_Y	Rate of TetR degradation	1.16×10^{-3}	sec^{-1}	estimated

[a]Fully induced strength of promoters P_{lac} and P_{tet},
[b]For the sake of brevity, "to repress" means "to half-maximally repress."
[c]For the sake of brevity, "to activate" means "to half-maximally activate."
[d] Equilibrium dissociation constant for LacI is 7.7×10^{-8} M [40].

Table SI-3.4. Parameter values of the 3-OH-C14-HSL/CinI-signaling subsystem.

Name	Description	Value	Unit	Reference
Transcription:				
L_{cinI}	Size of *cinI* gene[a]	663	bp	estimated
Γ_u	Repressed strength of promoter P_{lac}	5×10^{-4}	molecules/cell/sec	estimated in Table SI-3.2
k_u	Fully induced strength of promoter P_{tet}	13.27×10^{-2}	molecules/cell/sec	estimated
$\tau_{1/2,cinI}$	Half-life of *cinI* mRNA	6.6	min	arbitrary[b]
r_u	Rate of *cinI* mRNA degradation	1.75×10^{-3}	sec^{-1}	estimated
Translation:				
L_{CinI}	Size of CinI aa-sequence	221	aa	http://string-db.org
k_U	Rate of CinI translation	1.71	molecules/cell/sec	estimated in Table SI-3.2
$\tau_{1/2,CinI}$	Half-life[a] of CinI protein	4	min	[8]
r_U	Rate of protein CinI degradation	1.16×10^{-3}	sec^{-1}	estimated in Table SI-3.2
Signaling:				
k_G	Maximal production rate of CinI	2	min^{-1}	[41]
r_G	Degradation rate of C14-HSL	0.002	hr^{-1}	[42][c]
D_G	Export rate of C14-HSL	2.1	min^{-1}	[43]

[a]The coding region of the gene has been estimated from its protein sequence size provided in the same table as $221 \times 3 = 663$.
[b]This estimate corresponds to a general (or typical) pattern for mRNA half-lives in *E. coli* [44]. Note that [8] use a generic half-life parameter value of 2 min.
[c]Data for 3-OH-C12-HSL is used.

Table SI-3.5. Parameter values of the C4-HSL/RhlI-signaling subsystem.

Name	Description	Value	Unit	Reference
Transcription:				
L_{rhlI}	Length of *rhlI* gene	603	bp	[45]
Γ_w	Repressed strength of promoter P_{lac}	5×10^{-4}	molecules/cell/sec	estimated in Table SI-3.2
k_w	Fully induced strength of promoter P_{lac}	13.27×10^{-2}	molecules/cell/sec	estimated
$\tau_{1/2,rhlI}$	Half-life of *rhlI* mRNA	6.6	min	[46][a]
r_w	Rate of *lacI* mRNA degradation	1.75×10^{-3}	sec^{-1}	estimated
Translation:				
L_{LacI}	Length of RhlI protein aa-sequence	196	aa	[47]
k_{W}	Rate of RhlI translation	1.71	molecules/cell/sec	estimated in Table SI-3.2
$\tau_{1/2,\mathrm{RhlI}}$	Half-life of RhlI protein	4	min	estimated in Table SI-3.2
r_X	Rate of LacI degradation	1.16×10^{-3}	sec^{-1}	estimated
Signaling:				
k_{R}	Maximal production rate of C4-HSL by RhlI	16	min^{-1}	[41]
r_{R}	Degradation rate of C4-HSL	0.02	hr^{-1}	[42]
D_{R}	Export rate of C4-HSL	3.0	min^{-1}	[43]

[a]The half-life data for *lasI* mRNA is used because the degradation of *rhlI* is positively regulated by *LasI* [46] and, so, could have a longer half-life. This estimate is in line with a general (or typical) pattern for mRNA half-lives in *E. coli* [44]. Note that [8] use a genetic half-life parameter value of 2 min (Table SI-3.4).

SI-3.2 Dimensionless parameter values

Using data from Table SI-3.1 and the estimate (SI-3.8), we obtain

$$\mu = \frac{\ln 2}{25 \times 60} = 0.46 \times 10^{-3}\,\mathrm{sec}^{-1},\ r_d + \mu = 3.35 \times 10^{-3}\,\mathrm{sec}^{-1}. \tag{SI-3.9}$$

To estimate rates a_i, $i = 1 \ldots 6$, defined in (5), we assume that the equalities $b_x = b_y = b_u = b_w = 10$ can be approximately set by using RBS-related interventions [7]. Also, to avoid competition for ribosomes, only a few plasmids bearing promoters P_X, P_Y, P_G, and P_R can be used. By selecting $[P_X] = [P_Y] = [P_G] = [P_R] = 1$ copies per cell, we obtain

$$a_1 = a_3 = \frac{10 \times \left(6.65 \times 10^{-2}\right) \times 1}{40 \times (3.35 \times 10^{-3})} = 4.96 \approx 5, \tag{SI-3.10a}$$

$$a_2 = a_4 = \frac{10 \times \left(8.87 \times 10^{-2}\right) \times 2}{40 \times (3.35 \times 10^{-3})} = 6.61 \approx 7, \tag{SI-3.10b}$$

$$a_5 = a_6 = \frac{10 \times \left(13.27 \times 10^{-2}\right) \times (2/60) \times 2}{(2.5 \times 10^3) \times (3.35 \times 10^{-3})^2} = 3.15 \approx 3. \tag{SI-3.10c}$$

Next, from (6), we obtain

$$d_g = \frac{2.1/60}{3.35 \times 10^{-3}} = 10.44, \tag{SI-3.11a}$$

$$d_r = \frac{3/60}{3.35 \times 10^{-3}} = 14.40, \tag{SI-3.11b}$$

$$\delta_g = \delta_r \approx \frac{\mu}{r_d + \mu} = \frac{0.46 \times 10^{-3}}{3.35 \times 10^{-3}} = 0.14, \tag{SI-3.11c}$$

$$\delta_e = \frac{0.1/60}{3.35 \times 10^{-3}} = 0.50. \tag{SI-3.11d}$$

We find the estimated values of the parameters to be of the same order of magnitude as the corresponding parameter values estimated and used in [2–4, 8, 35–37]. Not enough is yet known about molecular interactions inside host cells to obtain highly precise descriptions [7]; it is common to computationally evaluate the effect of different values for rate parameters and even for Hill exponents [2–4, 8]. Following [2, 4, 8], where genetic circuits built from similar elements have been studied, we have explored sets of parameter values which are close to the estimates given in (SI-3.10) and (SI-3.11), which ensure bistability in both S- and A-models, see the main text.

SI-4 Alternative Definitions of Monotone Systems and Order Preservation

We defined monotonicity using graph partitions because this is the easiest way to present the concept. However, the usual definition found in textbooks is not phrased in that form. We explain here how our definition is equivalent to the usual one as well as to another property. For further remarks on these equivalences, see [48]. A signed graph (such as the species influence graph obtained by looking at signs of Jacobain entries) G is said to be *balanced* (see Harary [49]) if every undirected closed loop in the graph G has a net positive sign, that is to say, an even number, possibly zero, of negative arrows. Equivalently, any two (undirected) paths between two nodes must have the same net sign. By undirected loops or paths, we mean that one is allowed to transverse an edge either forward or backward. A *spin assignment* Σ for the graph G is an assignment, to each node v_i, of a number σ_i equal to "+1" or "−1" (a "spin," to borrow from statistical mechanics terminology). If there is an edge from node v_j to node v_i, with label $J_{ij} \in \{\pm 1\}$, we say that this edge is *consistent with the spin assignment* Σ provided that:

$$J_{ij}\sigma_i\sigma_j = 1$$

which is the same as saying that $J_{ij} = \sigma_i\sigma_j$, or that $\sigma_i = J_{ij}\sigma_j$. An equivalent formalism is that in which edges are labeled by "0" or "1," instead of 1 and −1 respectively, and edge labels J_{ij} belong to the set $\{0, 1\}$, in which case consistency is the property that $J_{ij} \oplus \sigma_i \oplus \sigma_j = 0$ (sum modulo two). One says that Σ *is a consistent spin assignment for the graph* G (or simply that G is consistent) if every edge of G is consistent with Σ. In other words, for any pair of vertices v_i and v_j, if there is a positive edge from node v_j to node v_i, then v_j and v_i must have the same spin, and if there is a negative edge connecting v_j to v_i, then v_j and v_i must have opposite spins. (If there is no edge from v_j to v_i, this requirement imposes no restriction on their spins.) It is easy to see that if there is a consistent spin assignment for G, then the graph is balanced. Conversely, if G is balanced then there is a consistent spin assignment for G: to see this, simply label one node arbitrarily, and follow paths to label other nodes consistently. (If the graph is not connected, repeat the procedure in each connected component.)

For any spin assignment Σ, let A_1 be the subset of nodes labeled +1, and let A_{-1} be the subset of nodes labeled −1. The set of all nodes is partitioned into A_1 and A_{-1}. Conversely, any partition of the set of nodes into two subsets can be thought of as a spin assignment. With this interpretation, a consistent spin assignment is the same as a partition of the node set into two subsets A_1 and A_{-1} in such a manner that all edges between elements of A_1 are positive, all edges between elements of A_{-1} are positive, and all edges between a node in A_1 and a node in A_{-1} are negative. In summary, our definition of monotonicity, given in terms of partitions of state variables, amounts to the same as the requirement that there exist at least one consistent spin assignment for its associated graph G, or equivalently, that its graph G is balanced.

Supposing that a system is monotone, with a consistent spin assignment $\Sigma = \{\sigma_i, i = 1, \ldots, n\}$, we introduce following the relation among vectors $x \in \mathbb{R}^n_{\geq 0}$:

$$x \preceq y$$

means that

$$\sigma_i x_i \leq \sigma_i y_i \;\; i = 1, \ldots, n\,.$$

This is a componentwise inequality that requires $x_i \leq y_i$ if node i has been assigned a positive spin, and $x_i \geq y_i$ if instead node i has been assigned a negative spin. Let $y(t)$ and $z(t)$ be any two solutions of the system $dx/dt = f(x)$, and suppose that $\sigma_i y_i(0) \leq \sigma_i z_i(0)$ for each $i = 1, \ldots, n$. Then, *Kamke's Theorem* states that $\sigma_i y_i(t) \leq \sigma_i z_i(t)$ for all $t \geq 0$ and coordinate $i = 1, \ldots, n$. This is the usual definition of monotonicity: if states start at time zero in a certain order, then they must remain forever in the same order. Conversely, a flow that preserves an order of this type must be monotone in the sense that we have defined the concept. See the textbook [50] for a proof, and [51] for extensions with systems with external inputs.

The order preservation property has a variety of important implications for our model. For parameters viewed as constant states, it allows us to conclude the monotonicity of stable branches in bifurcation diagrams, as illustrated by the results described in Monotone Parametric Dependencies in the S design. A different implication concerns the domain of attraction of equilibria. Suppose that we consider an initial state $x(0)$ that is coordinate-wise less, in the monotone order, than a given equilibrium E (in a possibly multistable system). Comparing to E the solution $x(t)$ starting from this initial state $x(0)$, we know that $x(t)$ must remain less than E for all times. Thus, an equilibrium to which $x(t)$ converges must be upper bounded by E. In particular, if the equilibrium E is minimal (with respect to the coordinate-wise order), it follows that this trajectory converges to E. Similar conclusions apply to maximal equilibria E and initial states $x(0)$ that are coordinate-wise larger than E. One obtains in this manner a rich amount of information about the basin of attraction of equilibria in monotone systems.

SI-5 Symmetry

In this section, we formalize the symmetry of

- a single S toggle embedded into an environment ($N = 1$),
- a population of N-identical S toggles interacting via a common environment ($N \geq 2$).

SI-5.1 Symmetry of the S Model

As is routine in physics and engineering, symmetry-based simplifications often lead to important insights into complex phenomena [52], and we also use symmetry to discuss bifurcations in S toggle populations. We observe that under a special condition imposed on the parameter values,

$$a_1 = a_2,\ a_3 = a_4,\ a_5 = a_6,\ d_g = d_r,\ \delta_g = \delta_r, \tag{SI-5.1}$$

a single S toggle embedded into an external environment is described by the S model (1) with $N = 1$ which has a $\mathbb{Z}_2$-symmetry group generated by involution $\mathcal{I}$ [52–54],

$$\mathcal{I} : (x, y, g, r, g_e, r_e) \longrightarrow (y, x, r, g, r_e, g_e). \tag{SI-5.2}$$

Consider the fixed-point subspace $\mathrm{Fix}\,(\mathbb{Z}_2) \in \mathbb{R}^6$ of the group $\mathbb{Z}_2$, see [52],

$$\mathrm{Fix}\,(\mathbb{Z}_2) = \{z = (x, y, g, r, g_e, r_e) \in \mathbb{R}^6 \,|\, \mathcal{I}z \equiv z\}. \tag{SI-5.3}$$

We ignore the trivial equilibria that belong to $\mathrm{Fix}\,(\mathbb{Z}_2)$, that is, equilibria of the S model (1) for which the following equalities hold, $x = y$, $g = r$, and $g_e = r_e$, corresponding to identically the same levels of LacI and TetR, and C14-HSL and C4-HSL, respectively. Let us denote the equilibrium of the S model (1) by z_0, and let us assume that $z_0 \notin \mathrm{Fix}\,(\mathbb{Z}_2)$. Now, because the S model is invariant with respect to the involution (SI-5.2), and because $z_0 \notin \mathrm{Fix}\,(\mathbb{Z}_2)$, we obtain that both z_0 and $\mathcal{I}\,z_0$, $\mathcal{I}\,z_0 \neq z_0$, are different equilibria of the S model (1), see [52, 53]. The equilibria z_0 and $\mathcal{I}\,z_0$ are called relative equilibria [55]. All bifurcations for the relative equilibria occur simultaneously at the same values of free parameters. We generalize G- and R-homogeneous populations states as relative equilibria, which means that as soon as the S toggle has a G-state, it will also have the corresponding R-state, implying bistability.

The general case of $N \geq 2$ is slightly more complicated as a population of identical S toggles has a symmetry group obtained after combinations of permutations among all cells in the given population and the toggle involution (SI-5.2), which we denote $\mathcal{G} = \mathbb{Z}_2 \times \mathbf{S}_N$ for brevity. Here, $\mathbf{S}_N$ is a symmetric group of order $N \geq 1$, and $\mathbb{Z}_2$ is the toggle involution (SI-5.2) applied to all toggles simultaneously. For example, for $N = 2$, we will have one permutation,

$$\mathcal{P} : (x_1, y_1, g_1, r_1, x_2, y_2, g_2, r_2, g_e, r_e) \longrightarrow (x_2, y_2, g_2, r_2, x_1, y_1, g_1, r_1, g_e, r_e), \tag{SI-5.4}$$

and the involution,

$$\mathcal{I} : (x_1, y_1, g_1, r_1, x_2, y_2, g_2, r_2, g_e, r_e) \longrightarrow (y_1, x_1, r_1, g_1, y_2, x_2, r_2, g_2, r_e, g_e). \tag{SI-5.5}$$

SI-5.2 Symmetry Breaking

The symmetry-breaking (pitchfork) bifurcation discussed around Fig. 7 in the main text has co-dimension one for all typical systems with $\mathbb{Z}_2$-symmetry [52,53]. To understand the symmetry-breaking occurring at the BP-point shown in Fig. 7, we need first to define the symmetry of the original symmetric (1:1)-mixed state. We observe that the original symmetric (1:1)-mixed state is invariant with respect to transformation g,

$$g = \mathcal{P} \circ \mathcal{I} = \mathcal{I} \circ \mathcal{P}, \quad g \circ g = \mathrm{id} \tag{SI-5.6}$$

where id is the identity. Here, $\mathcal{P}$ and $\mathcal{I}$ are as defined in (SI-5.4) and (SI-5.5), respectively. The transformation (SI-5.6) forms subgroup $\Sigma_{(1:1)}$ of the group $\mathbb{Z}_2 \times \mathbf{S}_2$, see SI-5.1 Symmetry of the S Model, which consists of two elements, that is, $\Sigma_{(1:1)} = \{\mathrm{id}, g\}$. The subgroup $\Sigma_{(1:1)}$ is called the *isotropy* subgroup [52] of the original (1:1)-mixed state. We further observe that the two (1:1)-states bifurcating from the original $\Sigma_{(1:1)}$-symmetric (1:1)-state at the BP-point (Fig. 7) are not invariant with respect to the isotropy subgroup $\Sigma_{(1:1)}$. Indeed, they are mapped one to one another by the transformation (SI-5.6). This observation motivates using the "symmetry-breaking" terminology [52] with respect to the loss of the isotropy subgroup symmetry by the (1:1)-mixed state at the BP-point. Due to the isotropy subgroup $\Sigma_{(1:1)}$ of the original (1:1)-mixed state, involution g defined in (SI-5.6) maps panel (A) to panel (D), and panel (B) to panel (C) within Fig. 7 of the main text. That is, $g : \mathrm{LP}_1 \to \mathrm{LP}_2$, $g : \mathrm{LP}_2 \to \mathrm{LP}_1$, and $g : \mathrm{BP} \to \mathrm{BP}$, see the coordinates of the three critical points, BP, LP_1, and LP_2, at the end of the caption of Fig. 7.

SI-5.3 A Remark on Bifurcations in Symmetric vs. Non-Symmetric Models

Mathematical models are idealizations of complex phenomena, based on certain assumptions, and there is a long established tradition to use symmetries in mathematical physics to clarify and explain complex phenomena. We use symmetry as another mathematical simplification alternative to simplifications arising from biological assumptions.

For our modeling studies with the S model, it may be difficult and even impossible to construct identical promoters which would correspond to identical values of parameters, that is, for example, $a_3 \neq a_4$. Therefore, it is required to discuss an appropriate interpretation of bifurcation diagrams computed for the S model.

First of all, we note that all LP-points will typically persist under small non-symmetric perturbations. However, all BP-points corresponding to pitchfork bifurcations will typically disappear under non-symmetric perturbations. They will typically be replaced by LP-bifurcation points. In such cases, in the small vicinity of the original BP point after a non-symmetric perturbation, we will typically have three branches of solutions, one branch of solutions which do not change their stability, and other two branches of solutions, stable and unstable, which will emanate from or collide with one another at the LP bifurcation point. Outside of the small vicinity of the perturbed BP-point, the bifurcation diagrams for both symmetric and non-symmetric models will be typically qualitatively the same. Such situations are mathematically very well studied and are described in the corresponding literature [52, 53].

SI-6 Exponential Stability of Cellular Populations

A systematic analysis of dynamical mathematical models begins with finding equilibrium solutions followed by the analysis of their exponential stability [56]. The next step is often to carry out (local) bifurcation analysis of the equilibrium solutions, allowing for the exploration of "stability boundaries" in the parameter space [53]. Both stability and bifurcation analyses rely on the computation of the eigenvalues from the corresponding model linearizations [53].

A nontrivial specificity of the computation of eigenvalues for the stability and bifurcation analyses of the A- and S-population models is that both models with $N > 1$ are invariant with respect to the action or the given linear representation of the *symmetric* group $\mathbf{S}_N$ of permutations among N-cells [52]. It is known that irreducible representations of groups enforce *multiple* eigenvalues of matrices that commute with their linear representations, a well-known fact following from Schur's Lemma in the representation theory of Lie groups [52].

To take into account the necessity to deal with multiple eigenvalues in the situations when the value of N is *a priori* unknown, we have developed a general approach to the analysis of exponential stability [56] in arbitrary populations of identical cells, independently of N, as described below.

A conceptually similar reduction approach (without any discussion of the multiplicity problem) on the exponential orbital stability of periodic solutions in systems of identical and slightly different oscillators coupled via a medium was developed by E. E. Shnol [57]. In his work, an averaging technique over the entire cellular population was used in both cases of homogeneous and mixed populations. Later, G. Katriel [58] has rediscovered the reduction result for homogeneous populations only, using Floquet Theory [59]. We note that the Schur's formula [60] can also be used to compute multipliers of periodic solutions in systems of coupled oscillators, using the linearizations of the corresponding Poincaré maps, in the very similar way as it is done for the case of equilibrium solutions in this work.

SI-6.1 A General Population Model of Identical Cells

In this SI, we use Schur's formula [60] to compute explicitly the characteristic polynomials for the corresponding model linearizations. The most important implication of Schur's formula is that it can be easily seen that the values of the eigenvalues are independent of $N \geq 2$.

To describe the general exponential stability analysis, we first introduce an appropriate notation as follows. Let S and z be "generalized" global (extracellular) and local (intracellular) state variables, respectively, $\dim S = m \geq 1$ and $\dim z = k \geq 2$. Using the generalized variables, both the S-model (1) and the A-model (2) can then be rewritten in the following general form, which we call a G-model,

$$\frac{dS}{dt} = H_0(S) + \frac{\rho}{N}\sum_{i=1}^{N} H(S, z_i), \qquad 0 \leq \rho \leq 1, \tag{SI-6.1a}$$

$$\frac{dz_i}{dt} = h(S, z_i), \quad i = 1, \ldots N. \tag{SI-6.1b}$$

The G-model (SI-6.1) includes $m + Nk$ equations.

SI-6.2 A Homogeneous Population

In the case of a homogeneous population of identical cells, we have $z_i(t) \equiv z(t)$. As a result, the G-model (SI-6.1) reduces to a system of $(m+k)$-differential equations,

$$\frac{dS}{dt} = H_0(S) + \rho H(S,z), \qquad 0 \le \rho \le 1, \tag{SI-6.2a}$$

$$\frac{dz}{dt} = h(S,z). \tag{SI-6.2b}$$

Observe that the model (SI-6.2) describes a *single* cell placed in a "free", non-constant medium.

Definition 1. *Let* (S_0, z_0) *be an equilibrium solution of the model* (SI-6.2). *Then,* (S_0, z_0) *corresponds to a homogeneous population equilibrium solution,*

$$(S_0, z_0, \ldots, z_0) = (S_0, N{\times}z_0)\,, \tag{SI-6.3}$$

of the full G-model (SI-6.1) *for any* $N \ge 2$. *Notation* $N{\times}z_0$ *means that* z_0 *is repeated* N*-times in* $(S_0, z_0, \ldots, z_0)$.

Although the model (SI-6.2) is sufficient to study the *existence* of homogeneous population equilibrium solutions (SI-6.3), it is not enough to establish the exponential *stability* of the corresponding solutions (SI-6.3). Let (S_0, Nz_0) be a homogeneous population equilibrium solution of the G-model (SI-6.1) with any fixed $N \ge 2$. To analyze the exponential stability of $(S_0, N{\times}z_0)$ in the "full" G-model (SI-6.1), we need to compute the eigenvalues of the corresponding Jacobian matrix $\mathbf{J}_N$,

$$\mathbf{J}_N = \begin{pmatrix} \mathbf{A} & \frac{\rho}{N}\mathbf{B} & \frac{\rho}{N}\mathbf{B} & \ldots & \frac{\rho}{N}\mathbf{B} \\ \mathbf{C} & \mathbf{D} & \mathbf{O} & \ldots & \mathbf{O} \\ \mathbf{C} & \mathbf{O} & \mathbf{D} & \ldots & \mathbf{O} \\ \vdots & \vdots & \vdots & \ddots & \vdots \\ \mathbf{C} & \mathbf{O} & \mathbf{O} & \ldots & \mathbf{D} \end{pmatrix}. \tag{SI-6.4}$$

In (SI-6.4), each of three matrices, $\mathbf{B}$, $\mathbf{C}$, and $\mathbf{D}$, is repeated N-times; $\mathbf{A}$ and $\mathbf{D}$ are square matrices of sizes m and k, respectively; $\mathbf{B}$ and $\mathbf{C}$ are rectangular matrices of sizes $m \times k$ and $k \times m$, respectively,

$$\mathbf{A} = \frac{\partial H_0}{\partial S} + \rho\frac{\partial H}{\partial S}, \quad \mathbf{B} = \frac{\partial H}{\partial z}, \quad \mathbf{C} = \frac{\partial h}{\partial S}, \quad \mathbf{D} = \frac{\partial h}{\partial z}. \tag{SI-6.5}$$

All partial derivatives in the expressions (SI-6.5) are evaluated at (S_0, z_0) which depends on all G-model parameters with the one important exception that they are *independent* of N because (S_0, z_0) is obtained using (SI-6.2). Notation $\mathbf{O}$ corresponds to zero submatrices of appropriate sizes.

We call a square matrix *stable* if all its eigenvalues have strictly negative real parts. The following theorem holds for J_N.

Theorem 1. (I). *Statements* (a), (b), *and* (c) *are equivalent.*

(a). *The matrix* $\mathbf{J}_N$ *is stable for all* $N \ge 2$.

(b). *The matrix* $\mathbf{J}_1$ *and its submatrix* $\mathbf{D}$ *are both stable.*

(c). *The matrix* $\mathbf{J}_2$ *is stable.*

(II). *The matrix* $\mathbf{J}_N$ *has typically* k *different eigenvalues, each of multiplicity* $N-1$ *in the following sense. Let* $\{\lambda_1,\dots,\lambda_{m+k}\}$ *be the set of eigenvalues of matrix* $\mathbf{J}_1$*, and let* $\{\mu_1,\dots,\mu_k\}$ *be the set of eigenvalues of its submatrix* $\mathbf{D}$*, Then,*

$$\{\lambda_1,\dots,\lambda_{m+k},(N-1)(\mu_1,\dots,\mu_k)\} \tag{SI-6.6}$$

is the set of all eigenvalues of matrix $\mathbf{J}_N$ *for any* $N\geq 2$*, where* $\{\mu_1,\dots,\mu_k\}$ *is repeated* $(N-1)$*-times.*

Proof. Let λ be a complex number, $\lambda\in\mathbb{C}$. Consider a new matrix $\mathbf{M}_\lambda=\mathbf{J}_N-\lambda\mathbf{I}_{m+Nk}$, where $\mathbf{I}_{m+Nk}$ is the identity matrix of size $m+nk$. To find eigenvalues of $\mathbf{J}_N$, we need to write down the corresponding characteristic equation $P(\lambda)=0$, $P(\lambda)=\det\mathbf{M}_\lambda$. Let us represent matrix $\mathbf{M}_\lambda$ in the form

$$\mathbf{M}_\lambda=\begin{pmatrix}\mathbf{A}_\lambda & \mathbb{B}\\ \mathbb{C} & \mathbb{D}_\lambda\end{pmatrix}. \tag{SI-6.7}$$

Here, matrices $\mathbf{A}_\lambda=\mathbf{A}-\lambda\mathbf{I}_m$, $\mathbb{B}=\frac{1}{N}(\mathbf{B},\dots,\mathbf{B})$, $\mathbb{C}=(\mathbf{C},\dots,\mathbf{C})^{\mathrm{T}}$, and $\mathbb{D}_\lambda=\mathrm{diag}\,(\mathbf{D}_\lambda,\dots,\mathbf{D}_\lambda)$ with $\mathbf{D}_\lambda=\mathbf{D}-\lambda\mathbf{I}_k$. Next, assume for a moment that $\mathbb{D}_\lambda^{-1}$ exists. Then, Schur's formula can be used to compute $\det\mathbf{M}_\lambda$ [60],

$$\det\mathbf{M}_\lambda=\det\mathbb{D}_\lambda\cdot\det\left(\mathbf{A}_\lambda-\mathbb{B}\mathbb{D}_\lambda^{-1}\mathbb{C}\right). \tag{SI-6.8}$$

Next, we compute

$$\mathbb{B}\mathbb{D}_\lambda^{-1}\mathbb{C}=\mathbb{B}\left(\mathbb{D}_\lambda^{-1}\mathbb{C}\right)=\frac{1}{N}(\mathbf{B},\dots,\mathbf{B})\begin{pmatrix}\mathbf{D}_\lambda^{-1}\mathbf{C}\\ \mathbf{D}_\lambda^{-1}\mathbf{C}\\ \cdots\\ \mathbf{D}_\lambda^{-1}\mathbf{C}\end{pmatrix}=\mathbf{B}\mathbf{D}_\lambda{}^{-1}\mathbf{C}. \tag{SI-6.9}$$

For the determinant of the block diagonal $\mathbb{D}_\lambda$, we obtain $\det\mathbb{D}_\lambda=(\det\mathbf{D}_\lambda)^N$. Substituting (SI-6.9) into (SI-6.8) yields

$$\det\mathbf{M}_\lambda=(\det\mathbf{D})^n\cdot\det\left(\mathbf{A}_\lambda-\mathbf{B}\mathbf{D}_\lambda^{-1}\mathbf{C}\right). \tag{SI-6.10}$$

Using the Schur's formula for the product $\det\mathbf{D}\cdot\det\left(\mathbf{A}_\lambda-\mathbf{B}\mathbf{D}_\lambda^{-1}\mathbf{C}\right)$ in the "backward" direction, we can rewrite (SI-6.10) in the following equivalent form

$$\det\mathbf{M}_\lambda\;=\;(\det\mathbf{D}_\lambda)^{N-1}\cdot\det\begin{pmatrix}\mathbf{A}_\lambda & \mathbf{B}\\ \mathbf{C} & \mathbf{D}_\lambda\end{pmatrix}. \tag{SI-6.11}$$

The expression (SI-6.11) can now be rewritten simply as

$$P(\lambda)\;=\;(\det\mathbf{D}-\lambda\mathbf{I}_k)^{N-1}\cdot\det(\mathbf{J}_1-\lambda\mathbf{I}_{m+k}). \tag{SI-6.12}$$

Recall that the expression (SI-6.12) has been proven under a restrictive condition $\det\mathbb{D}_\lambda\neq 0$, see above, which means that λ is not an eigenvalue of the matrix $\mathbf{D}$. This restriction can be

removed, for example, as follows. Let λ_0 be an eigenvalue of the matrix $\mathbf{D}$. Then, we obtain for the polynomial $P(\lambda)$ by continuity

$$P(\lambda_0) \;=\; \lim_{\lambda\to\lambda_0} P(\lambda) \;=\; \lim_{\lambda\to\lambda_0} \left(\det \mathbf{D} - \lambda \mathbf{I}_k\right)^{N-1} \cdot \det\left(\mathbf{J}_1 - \lambda \mathbf{I}_{m+k}\right) \;=\; 0. \tag{SI-6.13}$$

It follows from (SI-6.13) that (SI-6.12) holds for all $\lambda \in \mathbb{C}$.

Finally, we observe from (SI-6.12) that to compute all eigenvalues of the Jacobian matrix $\mathbf{J}_N$ for any $N \geq 2$, it is sufficient to compute the eigenvalues of either two smaller matrices, $\mathbf{D}$ and $\mathbf{J}_1$, or one matrix $\mathbf{J}_2$. The latter may be practically slightly easier than computing the eigenvalues for $\mathbf{D}$ and $\mathbf{J}_1$ separately. The proof of the theorem follows. □

Consider a differential equation

$$\frac{dz}{dt} \;=\; h(S_0, z), \tag{SI-6.14}$$

where S_0 is a fixed parameter corresponding to the equilibrium $(S_0, N \times z_0)$ of the full G-model (SI-6.1). In contrast to equation (SI-6.2), equation (SI-6.14) describes a single cell placed into a constant environment, which can be interpreted as an environment shaped by the large population of cells and which does not "sense" any changes in a single cell. Additionally, consider a cascade model

$$\frac{dS}{dt} \;=\; H_0(S) + \rho H(S, z_1), \quad 0 \leq \rho \leq 1, \tag{SI-6.15a}$$

$$\frac{dz_j}{dt} \;=\; h(S, z_j), \quad j = 1, 2. \tag{SI-6.15b}$$

Observe that the variable z_2 is absent from the first equation (SI-6.15a) and, hence, (SI-6.15) cannot be obtained from (SI-6.1) by simply setting $N = 2$.

Then, using the definition of exponential stability [56], the first statement of Theorem 1 can be reformulated as the following corollary which admits an intuitive interpretation of the fact why the case of $N = 2$ is sufficient to study the exponential stability of homogeneous population solutions.

Corollary 1. *Let* $(S_0, N \times z_0)$ *be an equilibrium solution of the G-model* (SI-6.1). *Then, statements* (a) - (*d*) *are equivalent.*

(a). $(S_0, N \times z_0)$ *is exponentially stable in the G-model* (SI-6.1) *for any* $N \geq 2$.

(b). (S_0, z_0) *is exponentially stable in the reduced model* (SI-6.2), *and* z_0 *is exponentially stable in the single-cell model* (SI-6.14).

(c). (S_0, z_0, z_0) *is exponentially stable in the G-model* (SI-6.1) *at* $N = 2$.

(*d*). (S_0, z_0, z_0) *is exponentially stable in the cascade model* (SI-6.15).

A comparison of Statements *(a)* and *(b)* of Corollary 1 leads to a conclusion that the given population consisting of identical cells is stable with respect to any small perturbation if and only if *(i)* the population is stable with respect to any small *uniform* perturbation of the entire population described by system (SI-6.1) and, simultaneously, *(ii)* a majority of *unperturbed* cells forces a single *slightly perturbed* cell to re-join back the unperturbed majority.

Indeed, system (SI-6.14) used in Statement *(b)* means that the entire population does not sense small perturbations in a single cell because S_0 is fixed in (SI-6.14).

Note that both conditions in Statement *(b)* can be reformulated, using the cascade model (SI-6.15) from statement (*d*). Finally, because the stability property is independent of the number N of identical cells in the population, the simple case of $N = 2$ can be used as given by statement *(c)*.

SI-6.3 A Mixed Population Split into Two Subpopulations

Suppose now that the given population consisting of N, $N \geq 4$, identical cells is split into two different subpopulations of sizes $N_1 \geq 2$ and $N_2 \geq 2$, respectively, where $N = N_1 + N_2$. We always assume that each subpopulation consists of at least two cells. Then, the two different homogeneous subpopulations can be described by two state variables z_1 and z_2, respectively, where $z_1 \neq z_2$, that is, $z_{i_p}(t) \equiv z_1(t)$ for some subset of indexes i_p, $p = 1, \ldots, N_1$, and $z_{i_q}(t) \equiv z_2(t)$, for another subset of indexes i_q, $q = 1, \ldots, N_2$. It follows that the equation (SI-6.1a) from the G-model (SI-6.1) simplifies as follows

$$\frac{dS}{dt} = H_0(S) + \frac{\rho}{N}\sum_{i=1}^{N} H(S, z_i) = \rho\Big(\beta_1 H(S, z_1) + \beta_2 H(S, z_2)\Big). \tag{SI-6.16}$$

In (SI-6.16), β_j is the fraction of the j-th subpopulation, $\beta_j = N_j/N$, $j = 1, 2$, $\beta_1 + \beta_2 = 1$. In this case, the entire G-model (SI-6.1) reduces to the following three equations

$$\dot{S} = H_0(S) \, + \, \rho\Big(\beta_1 H(S, z_1) \, + \, \beta_2 H(S, z_2)\Big), \quad \beta_j \in \mathbb{Q}, \quad \beta_1 \, + \, \beta_2 = 1, \tag{SI-6.17a}$$

$$\dot{z_j} = h(S, z_j), \quad j = 1, 2. \tag{SI-6.17b}$$

Definition 2. *Let (S_0, z_{10}, z_{20}), $z_{10} \neq z_{20}$, be a non-uniform equilibrium solution of the reduced system* (SI-6.17). *Then, (S_0, z_{10}, z_{20}), $z_{10} \neq z_{20}$ corresponds to a mixed population equilibrium solution,*

$$(S_0, z_{10}, \ldots, z_{10}, z_{20}, \ldots, z_{20}) = (S_0, N_1 z_{10}, N_2 z_{20}), \tag{SI-6.18}$$

of the full G-model (SI-6.1). *The solution* (SI-6.18) *describes a mixed population of N identical cells, split into two (non-identical) subpopulations of sizes $N_1 > 0$ and $N_2 > 0$, respectively, $N_1 + N_2 = N$. Notation $N_j z_{j0}$ means that z_{j0} is repeated N_j-times in $(S_0, z_{10}, \ldots, z_{10}, z_{20}, \ldots, z_{20})$, $j = 1, 2$.*

Due to the condition $\beta_1 + \beta_2 = 1$ used in (SI-6.17a), there formally exists a *continuum* of different fractions $\beta_1 : \beta_2$, $\beta_1 \in \mathbb{R}$ and $\beta_2 \in \mathbb{R}$. Of course, in the *biological* sense, only rational values $\beta_1 \in \mathbb{Q}$ and $\beta_2 \in \mathbb{Q}$ are allowable, leading to infinitely many fractional $(\beta_1 : \beta_2)$-configurations in the subdivision of the original population into two different subpopulations. Simple examples of such situations can be easily presented (Fig. SI-6.1).

For the sake simplicity of the exponential stability analysis, we will always assume that both β_1 and β_2 are real numbers, that is, $\beta_j \in \mathbb{R}$, $j = 1, 2$.

Let $(S_0, N_1 z_{10}, N_2 z_{20})$ be a mixed population equilibrium solution of the G-model (SI-6.1) with any fixed $N \geq 4$, see (SI-6.3). To analyze the exponential stability of $(S_0, N_1 z_{10}, N_2 z_{20})$, we

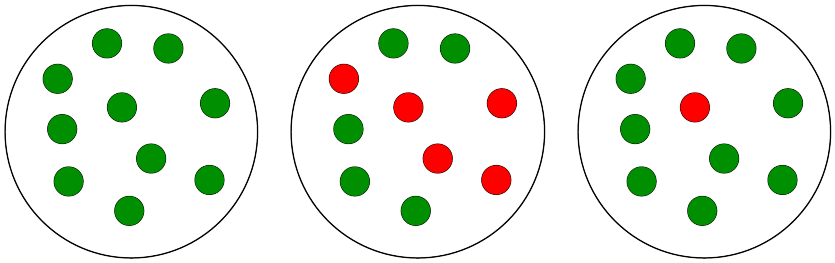

Figure SI-6.1. Examples of $(p:q)$-populations. The left panel corresponds to the case of a (10:0)-homogeneous population; the middle panel corresponds to the case of a (5:5)- or, equivalently, (1:1)-mixed population, and the right panel corresponds to a (9:1)-mixed population.

need to compute the eigenvalues of the corresponding Jacobian matrix $\mathbf{J}_N$ obtained from the G-model (SI-6.1),

$$\mathbf{J}_N = \begin{pmatrix} \mathbf{A} & \frac{\rho}{N}\mathbf{B}_1 & \dots & \frac{\rho}{N}\mathbf{B}_1 & \frac{\rho}{N}\mathbf{B}_2 & \dots & \frac{\rho}{N}\mathbf{B}_2 \\ \mathbf{C_1} & \mathbf{D}_1 & \dots & \mathbf{D}_1 & \mathbf{O} & \dots & \mathbf{O} \\ \vdots & \dots & \ddots & \dots & \vdots & \ddots & \vdots \\ \mathbf{C_1} & \mathbf{O} & \dots & \mathbf{D}_1 & \mathbf{O} & \dots & \mathbf{O} \\ \mathbf{C}_2 & \mathbf{O} & \dots & \mathbf{O} & \mathbf{D}_2 & \dots & \mathbf{O} \\ \vdots & \vdots & \vdots & \vdots & \vdots & \ddots & \vdots \\ \mathbf{C}_2 & \mathbf{O} & \dots & \mathbf{O} & \mathbf{O} & & \mathbf{D}_2 \end{pmatrix}. \tag{SI-6.19}$$

In the matrix (SI-6.19), submatrices $\mathbf{B}_i$, $\mathbf{C}_i$, and $\mathbf{D}_i$, are repeated N_j-times; $\mathbf{A}$ and $\mathbf{D}_i$ are square matrices of sizes m, and k, respectively; $\mathbf{B}_i$ and $\mathbf{C}_i$ are rectangular matrices of sizes $m \times k$ and $k \times m$, respectively, and

$$\mathbf{A} = \frac{\partial H_0}{\partial S} + \sum_{j=1}^{2} \rho_j \frac{\partial H(S_0, z_{j0})}{\partial S}, \tag{SI-6.20a}$$

$$\mathbf{B}_j = \frac{\partial H(S_0, z_{j0})}{\partial z}, \quad \mathbf{C}_j = \frac{\partial h(S_0, z_{j0})}{\partial S}, \quad \mathbf{D}_j = \frac{\partial h(S_0, z_{j0})}{\partial z}, \quad j = 1, 2. \tag{SI-6.20b}$$

Consider the Jacobian matrix $\mathbf{Q}_2$ of size $m + 2k$ for the system (SI-6.17), computed at (S_0, z_{10}, z_{20}),

$$\mathbf{Q}_2 = \begin{pmatrix} \mathbf{A} & \rho_1\mathbf{B}_1 & \rho_2\mathbf{B}_2 \\ \mathbf{C}_1 & \mathbf{D}_1 & \mathbf{O} \\ \mathbf{C}_2 & \mathbf{O} & \mathbf{D}_2 \end{pmatrix} \tag{SI-6.21}$$

Theorem 2. (I). *Statements* (a) *and* (b) *are equivalent.*

(a). *The matrix* $\mathbf{J}_N$ *is stable for all* $N \geq 4$, *and with any* $N_1 \geq 2$ *and* $N_2 \geq 2$ *such that* $N_1 + N_2 = N$.

(b). *Matrix* $\mathbf{Q}_2$, *and its two submatrices,* $\mathbf{D}_1$ *and* $\mathbf{D}_2$, *are stable.*

(II). *Matrix* $\mathbf{J}_N$ *has typically* $2k$ *different multiple eigenvalues in the following sense. Let* $\{\lambda_1, \dots, \lambda_{m+2k}\}$ *be the set of eigenvalues of* $\mathbf{Q}_2$, *let* $\{\mu_1, \dots, \mu_k\}$ *be the set of eigenvalues of* $\mathbf{D}_1$, *and let* $\{\sigma_1, \dots, \sigma_k\}$ *be the set of eigenvalues of* $\mathbf{D}_2$. *Then,*

$$\{\lambda_1, \dots, \lambda_{m+k},\ (N_1 - 1)\,(\mu_1, \dots, \mu_k)\,,\ (N_2 - 1)\,(\sigma_1, \dots, \sigma_k)\}\,, \tag{SI-6.22}$$

is the set of all eigenvalues of the matrix $\mathbf{J}_N$ *for any* $N \geq 4$. *In* (SI-6.22), *the set* $\{\mu_1, \ldots, \mu_k\}$ *is repeated* $(N_1 - 1)$*-times, and the set* $\{\sigma_1, \ldots, \sigma_k\}$ *is repeated* $(N_2 - 1)$*-times. To have a nonzero value of multiplicity* $N_j - 1$ *in* (SI-6.22), *condition* $N_j \geq 2$ *and, hence,* $N \geq 4$, *are natural requirements,* $j = 1, 2$. *In other words, the latter two conditions guarantee that both matrices* D_1 *and* D_2 *exist. Otherwise, Theorem 2 does not make any sense.*

Proof. The proof Theorem 2 can be carried out, using a simple modification of the proof of Theorem 1. For this reason, we only provide a brief sketch of the proof for Theorem 2. Similarly to the proof of Theorem 1, we need to write down a characteristic equation $P(\lambda) = 0$ Here $P(\lambda) = \det \mathbf{M}_\lambda$, and matrix $\mathbf{M}_\lambda$ can be defined as in (SI-6.7), using appropriate submatrices,

$$\mathbf{A}_\lambda = \mathbf{A} - \lambda \mathbf{I}_m, \tag{SI-6.23a}$$

$$\mathbb{B} = \frac{1}{N} (\mathbf{B}_1, \ldots, \mathbf{B}_1, \mathbf{B}_2, \ldots, \mathbf{B}_2), \tag{SI-6.23b}$$

$$\mathbb{C} = (\mathbf{C}_1, \ldots, \mathbf{C}_1, \mathbf{C}_2, \ldots, \mathbf{C}_2)^{\mathrm{T}}, \tag{SI-6.23c}$$

$$\mathbb{D}_\lambda = \mathrm{diag}\,(\mathbf{D}_{\lambda 1}, \ldots, \mathbf{D}_{1\lambda}, \mathbf{D}_{2\lambda}, \ldots, \mathbf{D}_{2\lambda}), \quad \mathbf{D}_{i\lambda} = \mathbf{D}_i - \lambda \mathbf{I}_k. \tag{SI-6.23d}$$

In the above submatrix definitions, the matrices with index j are repeated N_j-times, $i, j = 1, 2$. In this case, $\det \mathbf{M}_\lambda$ can also be computed using Schur's formula, see (SI-6.8). However, (SI-6.9) should be replaced by

$$\mathbb{B}\mathbb{D}_\lambda^{-1}\mathbb{C} = \rho_1 \mathbf{B}_1 \mathbf{D}_{1\lambda}^{-1} \mathbf{C}_1 + \rho_2 \mathbf{B}_2 \mathbf{D}_{2\lambda}^{-1} \mathbf{C}_2. \tag{SI-6.24}$$

For the block diagonal matrix $\mathbb{D}_\lambda$, we obtain $\det \mathbb{D}_\lambda = (\det \mathbf{D}_{1\lambda})^{N_1} \cdot (\det \mathbf{D}_{2\lambda})^{N_2}$. Now, similarly to (SI-6.10), we will have

$$\det \mathbf{M}_\lambda = (\det \mathbf{D}_1)^{N_1} \cdot (\det \mathbf{D}_2)^{N_2} \cdot \det \Big(\mathbf{A}_\lambda - \rho_1 \mathbf{B}_1 \mathbf{D}_{1\lambda}^{-1} \mathbf{C}_1 - \rho_2 \mathbf{B}_2 \mathbf{D}_{2\lambda}^{-1} \mathbf{C}_2 \Big). \tag{SI-6.25}$$

Using the Schur's formula in the "backward" direction, we will then have

$$P(\lambda) = (\det \mathbf{D}_1 - \lambda \mathbf{I}_k)^{N_1 - 1} \cdot (\det \mathbf{D}_2 - \lambda \mathbf{I}_k)^{N_2 - 1} \cdot \det \mathbf{Q}_2. \tag{SI-6.26}$$

The rest can be proved as in the proof for Theorem 1. The proof of Theorem 2 follows. □

Consider the following cascade model

$$\frac{dS}{dt} = H_0(S) + \rho \Big(\beta_1 H(S, z_1) + \beta_2 H(S, z_3) \Big), \quad \beta_1 + \beta_2 = 1, \tag{SI-6.27a}$$

$$\frac{dz_j}{dt} = h(S, z_j), \quad j = 1, \ldots, 4. \tag{SI-6.27b}$$

Variables z_2 and z_4 are absent from the first equation (SI-6.27a) and, hence, the cascade system (SI-6.27) cannot be obtained from the G-model (SI-6.1) by simply setting $N = 4$. Now, Theorem 2 can be reformulated in terms its Corollary 2 as follows.

Corollary 2. *Let* $(S_0, N_1 \times z_{10}, N_2 \times z_{20})$ *be a mixed population equilibrium solution of the G-model* (SI-6.1). *Then, Statements* (a) - (c) *are equivalent.*

(a). $(S_0, N_1 \times z_{10}, N_2 \times z_{20})$ *is exponentially stable in the G-model* (SI-6.1) *for any* $N \geq 4$, *and with any* $N_1 \geq 2$ *and* $N_2 \geq 2$ *such that* $N_1 + N_2 = N$.

(b). (S_0, z_{10}, z_{20}) *is exponentially stable in the reduced model* (SI-6.17), *and each* z_{j0} *is exponentially stable in the single-cell model* (SI-6.14), $j = 1, 2$.

(c). $(S_0, z_{10}, z_{10}, z_{20}, z_{20})$ *is exponentially stable in the cascade model* (SI-6.27).

SI-6.4 A Mixed Population Split into Several Subpopulations

The case of a mixed population split into two subpopulations with densities $\rho_1 = \beta_1\rho$ and $\rho_2 = \beta_2\rho$ can be generalized to the case of a mixed population split into L-different subpopulations with densities $\rho_1, \dots, \rho_L$, where $\rho_1 + \dots + \rho_L = \rho$, $L \geq 3$ as follows.

Let subpopulation j consist of N_j cells, and let subpopulation j correspond to variable z_j, that is, we have $z_{j'}(t) \equiv z_j(t)$, where $j' \in \{i_1, i_2, \dots, i_{N_j}\} \subset \{1, 2, \dots N\}$, $j = 1, \dots, L$. In this case, the G-model (SI-6.1) reduces to the following equations

$$\dot{S} = H_0(S) \; + \; \sum_{j=1}^{L} \rho_j H(S, z_j), \quad \sum_{j=1}^{L} \rho_j = \rho, \tag{SI-6.28a}$$

$$\dot{z_j} = h(S, z_j), \quad \rho_j = \beta_j\rho, \quad \beta_j = \frac{N_j}{N}, \quad j = 1, \dots, L. \tag{SI-6.28b}$$

Definition 3. *Let $(S_0, z_{10}, \dots, z_{L0})$ be a non-uniform equilibrium solution of the system* (SI-6.28)*, where $z_{j0} \neq z_{j'0}$ for all $j \neq j'$. Then, $(S_0, z_{10}, \dots, z_{L0})$, corresponds to a mixed population equilibrium solution,*

$$(S_0, N_1 z_{10}, \dots, N_L z_{L0}), \tag{SI-6.29}$$

of the full G-model (SI-6.1)*. The solution* (SI-6.29) *describes a mixed population of N identical cells, which is split into L subpopulations of the corresponding sizes $N_j \geq 2$, $N_1 + \dots + N_L = N$. Notation $N_j z_{j0}$ means that z_{j0} is repeated N_j-times in the vector-form solution of the the full G-model* (SI-6.1)*, $N_j \geq 2$, $j = 1, \dots, L$.*

Consider the Jacobian matrix $\mathbf{Q}_L$ for the reduced system (SI-6.28), computed at $(S_0, z_{10}, \dots, z_{L0})$,

$$\mathbf{Q}_L = \begin{pmatrix} \mathbf{A} & \rho_1\mathbf{B}_1 & \dots & \rho_L\mathbf{B}_L \\ \mathbf{C}_1 & \mathbf{D}_1 & \dots & \mathbf{O} \\ \vdots & \vdots & \ddots & \vdots \\ \mathbf{C}_L & \mathbf{O} & \dots & \mathbf{D}_L \end{pmatrix}. \tag{SI-6.30}$$

In (SI-6.30), all submatrices are defined as in (SI-6.20), where $j = 1, 2$ should be replaced by $j = 1, \dots, L$. Below, we formulate Theorem 3 and Corollary 3 without any proof because they are similar to Theorem 2 and Corollary 1, respectively.

Theorem 3. (I). *Statements* (a) *and* (b) *are equivalent.*

(a). *The Jacobian $\mathbf{J}_N$ computed for the G-model at the given equilibrium* (SI-6.29) *is stable for all $N \geq 2L$, and with any $N_j \geq 2$, $j = 1, \dots, L$, such that $N_1 + \dots N_L = N$.*

(b). *Matrix $\mathbf{Q}_L$ and its submatrices $\mathbf{D}_j$, $j = 1, \dots, L$, are stable.*

(II). *Matrix $\mathbf{J}_N$ has typically kL different multiple eigenvalues in the following sense. Let $\{\lambda_1, \dots, \lambda_{m+kL}\}$ be the set of eigenvalues of $\mathbf{Q}_L$, and let $\{\mu_1^{(j)}, \dots, \mu_k^{(j)}\}$ be the set of eigenvalues of $\mathbf{D}_j$, $j = 1, \dots, L$. Then,*

$$\left\{\lambda_1, \dots, \lambda_{m+k}, \; (N_1 - 1)\left(\mu_1^{(1)}, \dots, \mu_k^{(1)}\right), \dots, (N_L - 1)\left(\mu_1^{(N_L)}, \dots, \mu_k^{(N_L)}\right)\right\} \tag{SI-6.31}$$

is the set of all eigenvalues of the matrix $\mathbf{J}_N$ for any $N \geq 2L$. In (SI-6.31)*, each set $\{\mu_1^{(j)}, \dots, \mu_k^{(j)}\}$ is repeated $(N_j - 1)$-times with all $N_j \geq 2$, $j = 1, \dots, K$.*

Consider the following cascade model

$$\frac{dS}{dt} = H_0(S) + \sum_{j=1}^{L} \rho_j H(S, z_{2j-1}), \quad \sum_{j=1}^{L} \rho_j = \rho, \tag{SI-6.32a}$$

$$\frac{dz_j}{dt} = h(S, z_j), \quad j = 1, \ldots, 2L. \tag{SI-6.32b}$$

State variables z_{2j} with even indeces are absent from the first equation (SI-6.32a) of the cascade model (SI-6.32).

Corollary 3. *Let* $(S_0, N_1 z_{10}, \ldots, N_L z_{L0})$ *be a mixed equilibrium solution of the G-model* (SI-6.1)*, where* $N_{j0} \neq N_{j'0}$ *for all* $j \neq j'$*. Then, Statements* (a) - (c) *are equivalent.*

(a). $(S_0, N_1 z_{10}, \ldots, N_L z_{L0})$ *is exponentially stable in the G-model* (SI-6.1) *for any* $N \geq 2L$*, and with any* $N_j \geq 2$*,* $j = 1, \ldots, L$*, such that* $N_1 + \ldots N_L = N$*.*

(b). $(S_0, z_{10}, \ldots, z_{L0})$ *is exponentially stable in the reduced model* (SI-6.28)*, and each* z_{j0} *is exponentially stable in the single-cell model* (SI-6.14)*,* $j = 1, \ldots, L$*.*

(c). $(S_0, z_{10}, z_{10}, z_{20}, z_{20}, \ldots, z_{L0}, z_{L0})$ *is exponentially stable in the cascade model* (SI-6.32)*.*

SI-7 Additional Figures

Figure SI-7.1

In accordance with predictions from Fig. 3, we observe that an increase in the values of δ_g lead to suppressed levels in x_1 (LacI) as well as to elevated levels in y_1 (TetR). This is illustrated in Fig. SI-7.1. The almost constant dependencies in Fig. SI-7.1 (C) and (D) can be explained by suppressed levels of TetR and C4-HSL in the G-population.

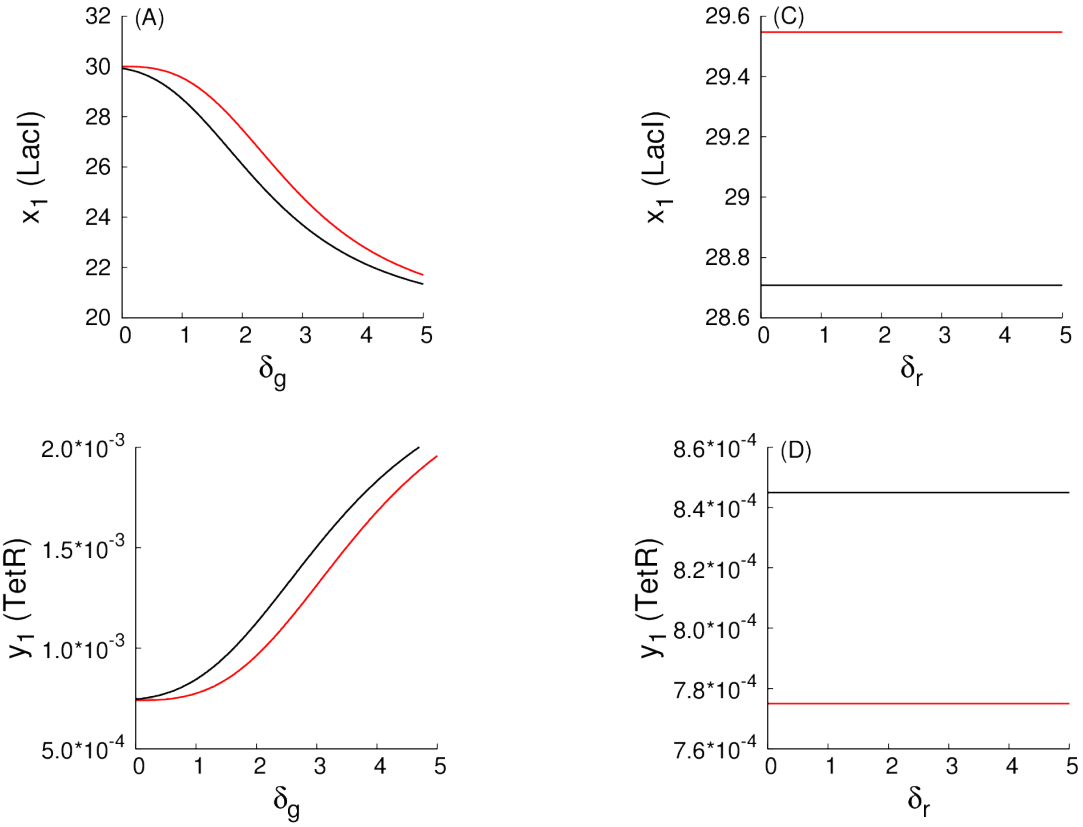

Figure SI-7.1. Examples of monotone parametric dependencies for the repressor-protein levels in the G-homogeneous state. Red solid curves correspond to a weak coupling among all toggles ($d = 0.1$), while black solid curves correspond to a strong coupling among all toggles ($d = 10$).

Analogously (Fig. SI-7.1), an increase in the values of δ_g should also lead to suppressed levels in g_1 (C14-HSL) as well as to elevated levels in r_1 (C4-HSL), while an increase in the values of δ_r should lead to elevated levels in g_1 (C14-HSL) and, simultaneously, to decreased levels in r_1 (C4-HSL). This is illustrated in Fig. SI-7.2. Constant dependencies in Fig. SI-7.2 (C) can be explained by suppressed levels of TetR and C4-HSL in the G-population.

Figure SI-7.2

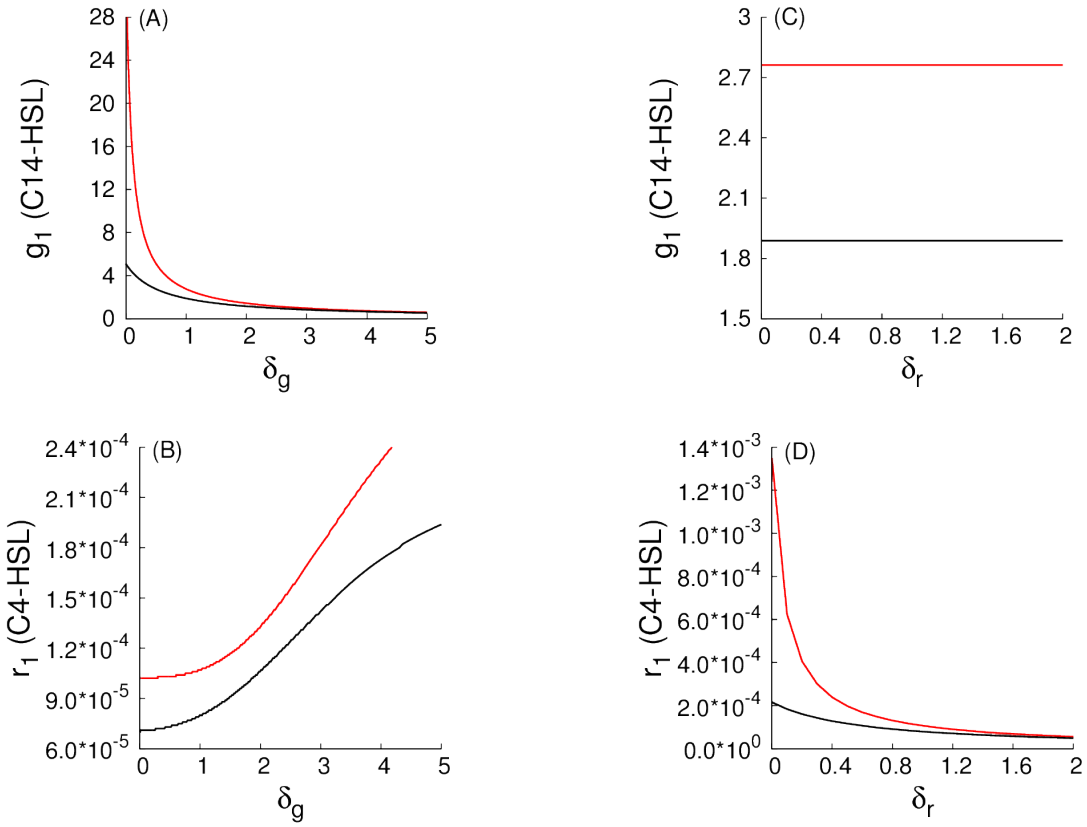

Figure SI-7.2. Examples of monotone parametric dependencies for the signaling species levels in the G-homogeneous state. Red solid curves correspond to a weak coupling among all toggles ($d = 0.1$), while black solid curves correspond to a strong coupling among all toggles ($d = 10$).

Figure SI-7.3

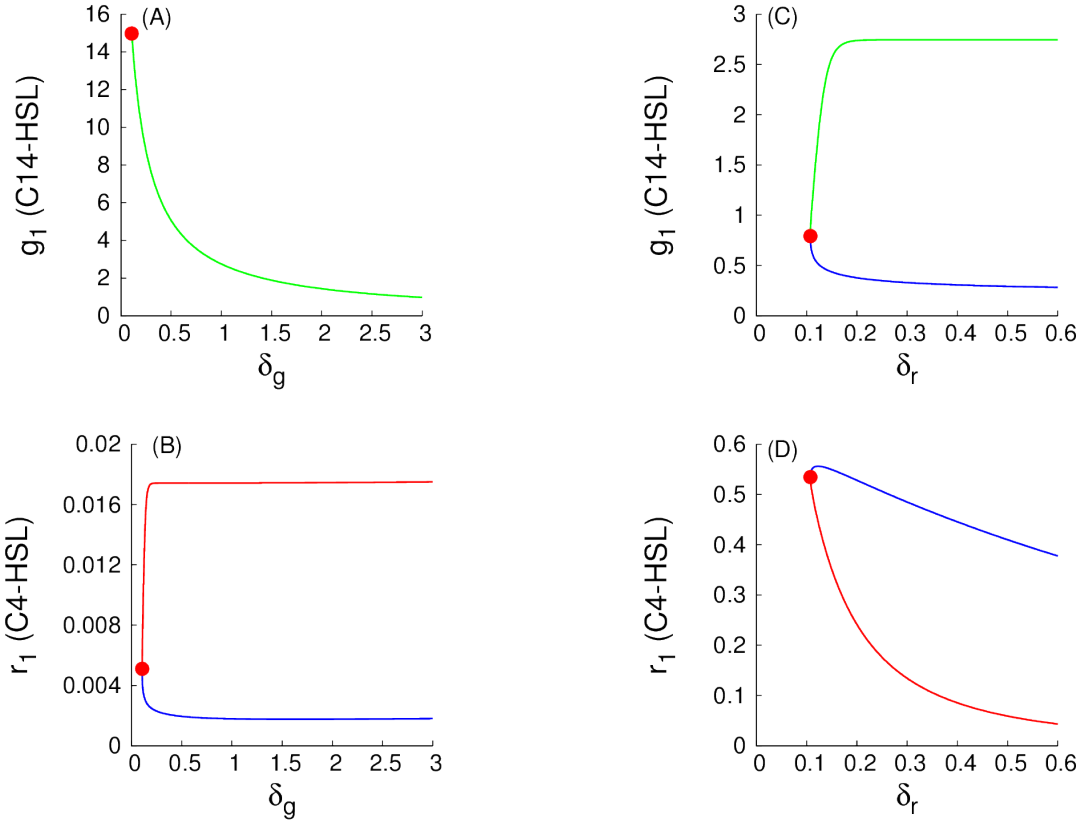

Figure SI-7.3. Examples of monotone parametric dependencies for the signaling species levels in the (1:1)-mixed state. All explanations are as in Fig. 5.

Figure SI-7.4

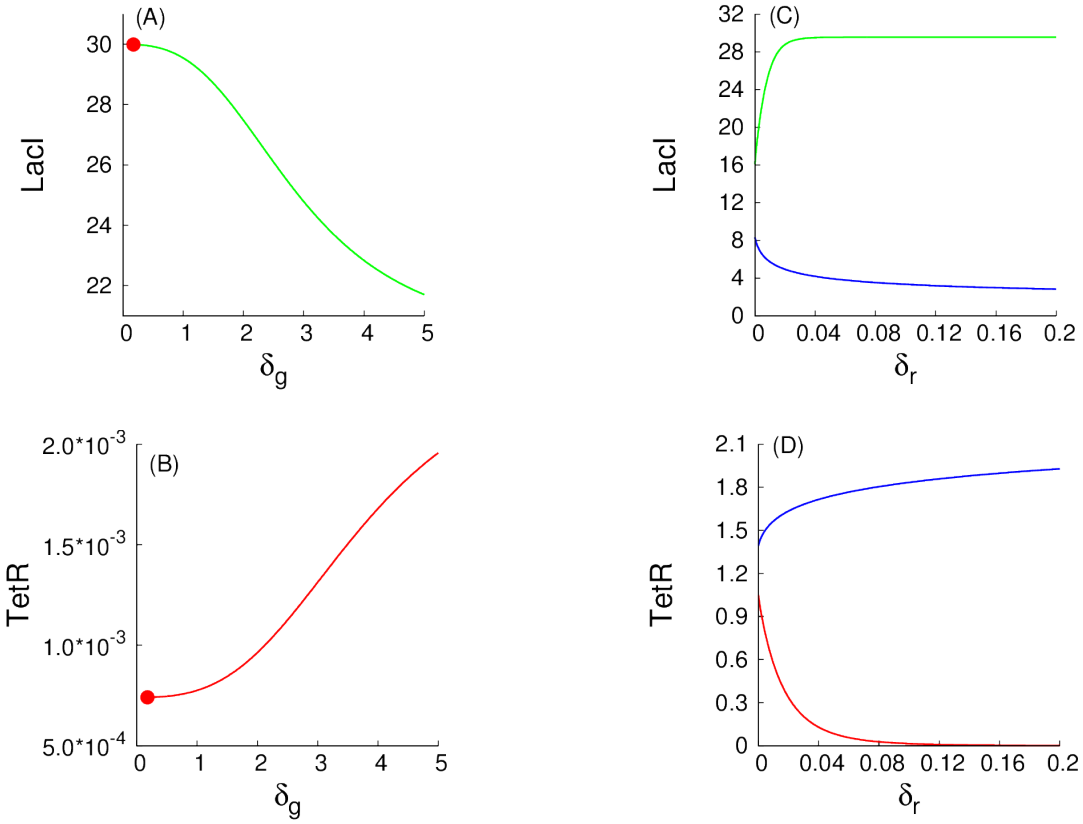

Figure SI-7.4. Examples of monotone parametric dependencies for the repressor-protein levels in the (9:1)-mixed state (a 90% large G-subpopulation.) Green and red solid curves correspond to stable solution branches, while all blue curves correspond to unstable solution branches. Red filled circles correspond to an LP-bifurcation point. In panels (A) and (B), projections of stable and unstable solution branches coincide and, so, only the stable solution branches are shown.

The monotone parametric dependencies for a (9:1)-mixed state corresponding to a spontaneous synchronization error are illustrated in Fig. SI-7.4 for a large G-subpopulation comprising 90% of all cells, and in Fig. SI-7.5 for a small R-subpopulation comprising 10% of all cells in the given (9:1)-mixed state.

We observe that LP-bifurcation points are present in both panels (A) and (B), and are absent from both panels (C) and (D) in Fig. SI-7.4 and Fig. SI-7.5. To explain this observation we have to recall the difference between parameters δ_g and δ_r. As discussed earlier, a decrease in the values of δ_g can be interpreted in terms of the improved communication between the toggles within the large subpopulation, while a decrease in the values of δ_r can be interpreted in terms of the improved communication between the toggles within the small subpopulation.

Figure SI-7.5

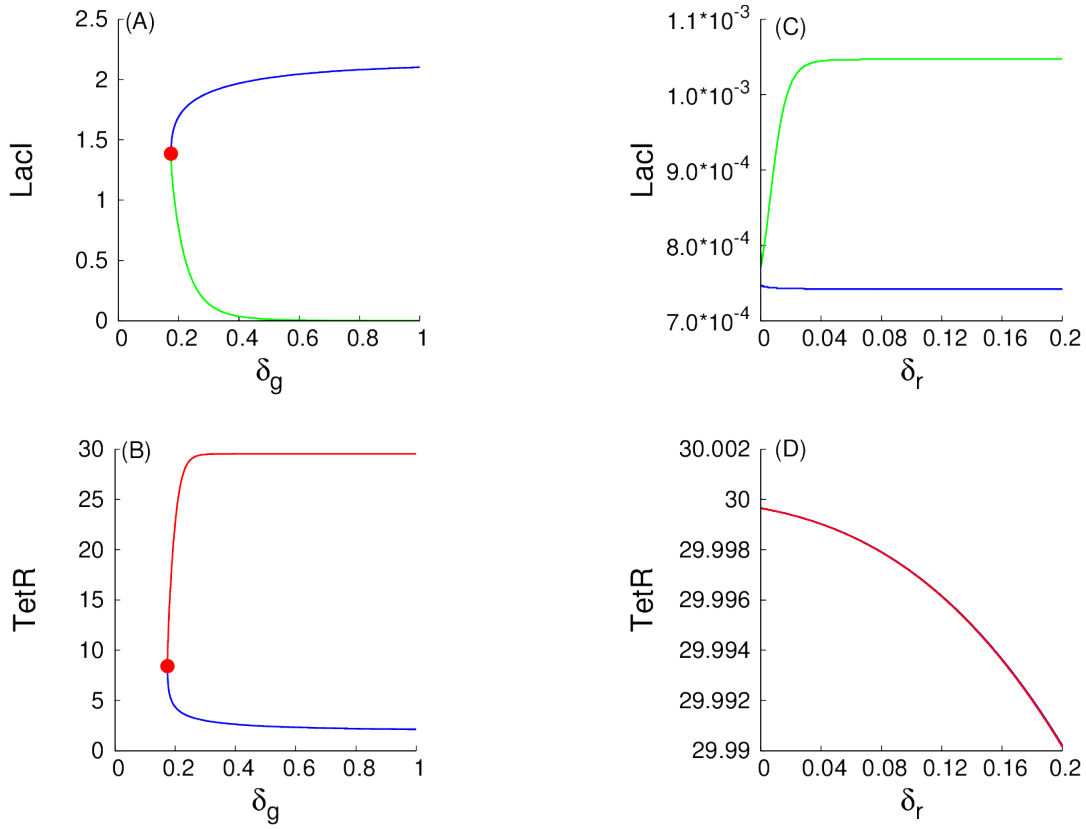

Figure SI-7.5. Examples of monotone parametric dependencies for the repressor-protein levels in the (9:1)-mixed state (a 10% small R-subpopulation.) Green and red solid curves correspond to stable solution branches, while all blue curves correspond to unstable solution branches. In panel (D), projections of stable and unstable solution branches coincide. Red filled circles in panels (A) and (B) correspond to an LP-bifurcation point.

Figure SI-7.6

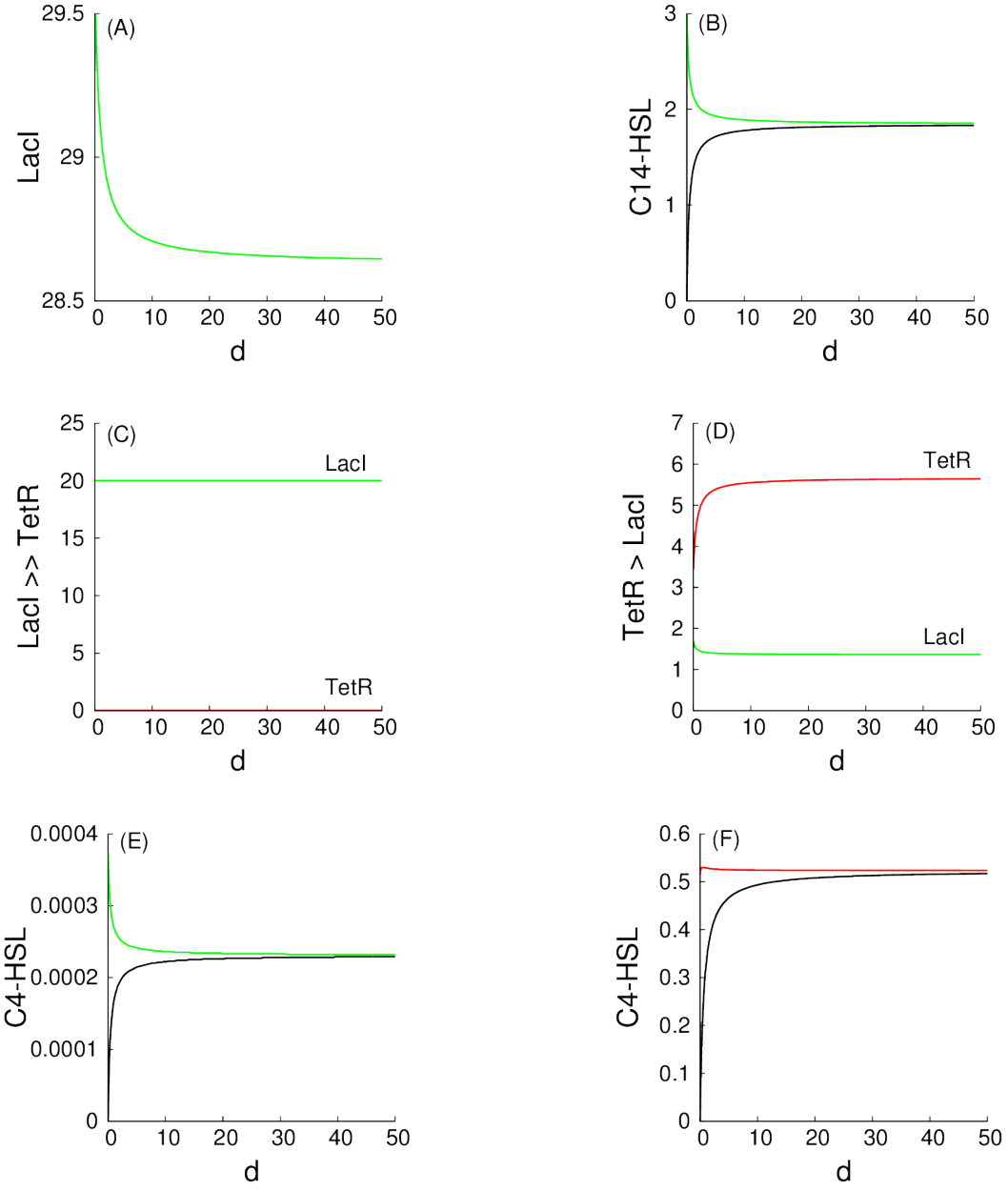

Figure SI-7.6. Homogeneous populations of S and A toggles. Dependencies of G-homogeneous populations on the values of the parameter d are shown. Top panels (A) and (B) correspond to a G-homogeneous population of S toggles. Panel (A) presents (dimensionless) levels of the activated LacI, while levels of the repressed TetR are of order of magnitude about 10^{-3} and are not shown. Panel (B) presents levels of C14-HSL. The green curve corresponds to the intracellular levels, while the black plot corresponds to extracellular levels of C14-HSL, respectively. Panels (C) and (E) present levels of the activated LacI and C4-HSL obtained for the A toggle settled at the G-state (LacI > TetR). Panels (D) and (F) present levels of the activated TetR and C4-HSL obtained for the A toggle settled at the R-state (TetR > LacI).

We observe from Fig. SI-7.6 that the intracellular and extracellular levels of the QS signaling molecule C14-HSL become asymptotically indistinguishable from one another as $d \to \infty$. The asymptotic behavior of the S toggle for large values of d can be analytically understood after introducing a small parameter $\varepsilon = d^{-1}$ into the S-model (1) which becomes a singularly-perturbed problem [61]. Setting formally $\varepsilon = 0$ in the singularly-perturbed problem as required by the theory of singular perturbations [61], the differential equations (SI-8.1c) and (SI-8.1d) can be reduced to elementary algebraic equations $g = g_e$ and $r = r_e$, respectively.

Figure SI-7.7

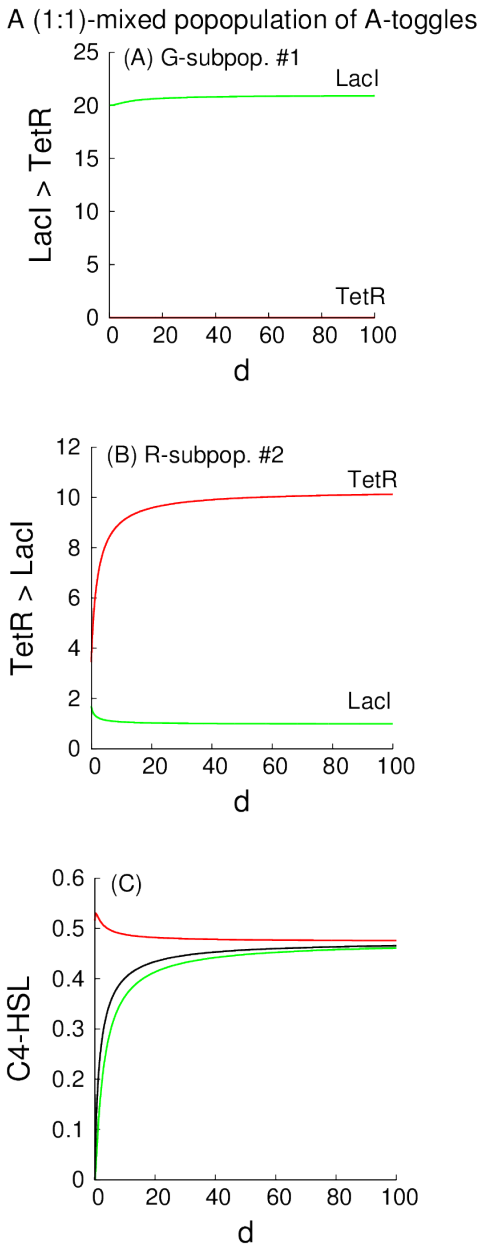

Figure SI-7.7. A (1:1)-mixed population of A toggles. Green and red color coded curves in panels (A) and (B) correspond to the intracellular concentrations of LacI and TetR, respectively, while a black color-coded curve in panel (C) corresponds to the extracellular concentration of C4-HSL. In panel (C), the green color-coded curve corresponds to the concentration of C4-HSL within the G-subpopulation, that is, LacI > TetR as in panel (A), while the red color-coded curve corresponds to the R-subpopulation, that is, TetR > LacI as in panel (B).

Figure SI-7.8

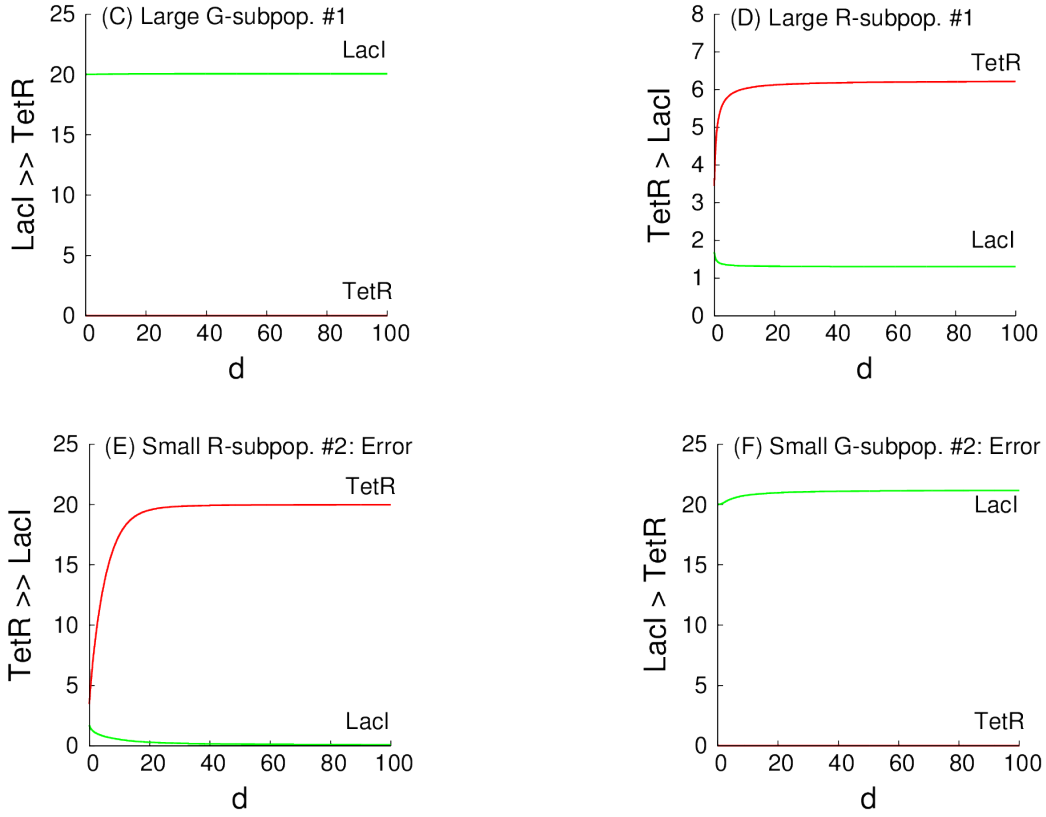

Figure SI-7.8. A (9:1)- and (1:9)-mixed population of A toggles. Here, all notations and color-coding schemes are as in Fig. 9. Panels (A) and (B) correspond to the (9:1)-mixed population, within which the transcription signature LacI $\gg$ TetR dominates in proportion 9:1 (*i.e.*, with 90% of green cells and 10% of red cells), while panels (C) and (D) correspond to the (1:9)-mixed population, within which the opposite transcription signature TetR $\gg$ LacI as well dominates in proportion 9:1 (*i.e.*, with 90% of red cells and 10% of green cells.)

Figure SI-7.9

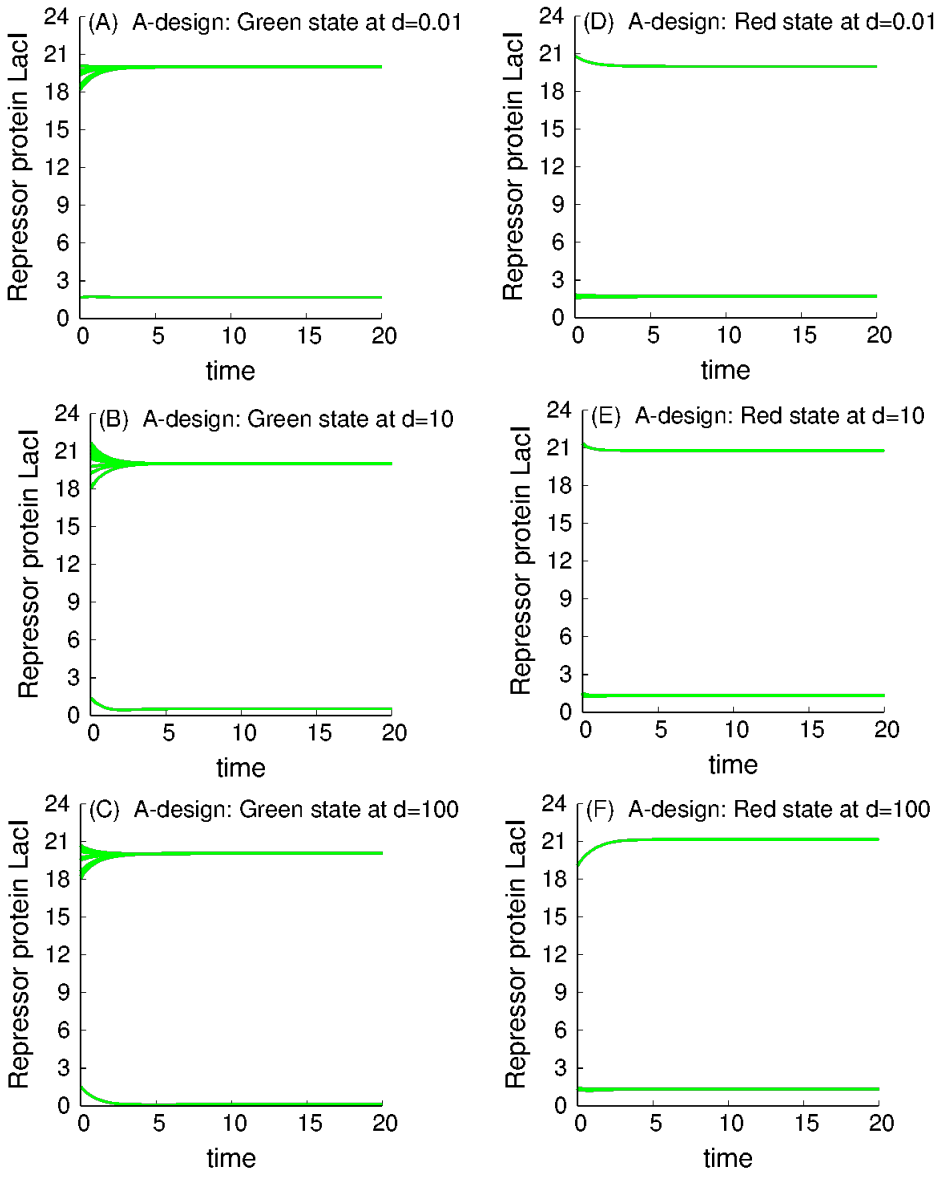

Figure SI-7.9. Lack of any self-correction capability for spontaneous errors by A toggles. The left panels correspond to the reference (10:0)-state (G-state), while the right panels correspond to the reference (0:10)-state (R-state). The initial conditions in the left panels correspond to nine "green" cells and one "red" cell. The initial conditions in the right panels correspond to one "green" cell and nine "red" cells.

SI-8 Modification of the S and A Models to Describe Sequestration of AAA+ protease ClpXP

To probe competition and sequestration effects for AAA+ proteases ClpXP in the context of our monotone theory-based modeling studies described in the main text, we have modified S and A models by adding the corresponding Michaelis-Menten type degradation [37]. Because all scaling procedures used for this case are similar to the scaling procedures described in detail earlier, we omit laborious technical details.

SI-8.1 Modification of the S Model

A dimensionless modified S_m model is

$$\frac{dx_i}{dt} = \gamma_x + \frac{a_1}{1+y_i^{n_Y}} + \frac{a_3\, g_i^{n_G}}{1+g_i^{n_G}} - \delta\, x_i - \frac{k_{ssrA}\, x_i}{1 + Z_i}, \tag{SI-8.1a}$$

$$\frac{dy_i}{dt} = \gamma_y + \frac{a_2}{1+x_i^{n_X}} + \frac{a_4 r_i^{n_R}}{1+r_i^{n_R}} - \delta\, y_i - \frac{k_{ssrA}\, y_i}{1 + Z_i}, \tag{SI-8.1b}$$

$$\frac{dg_i}{dt} = \gamma_g + \frac{a_5}{1+y_i^{n_Y}} + d\Big(g_e - g_i\Big) - \delta_g\, g_i, \tag{SI-8.1c}$$

$$\frac{dr_i}{dt} = \gamma_r + \frac{a_6}{1+x_i^{n_X}} + d\Big(r_e - r_i\Big) - \delta_r\, r_i, \quad i = 1, \ldots, N, \tag{SI-8.1d}$$

$$\frac{dg_e}{dt} = \frac{\rho}{N}\sum_{i=1}^{N} d\Big(g_i - g_e\Big) - \delta_e\, g_e, \quad 0 \le \rho \le 1, \tag{SI-8.1e}$$

$$\frac{dr_e}{dt} = \frac{\rho}{N}\sum_{i=1}^{N} d\Big(r_i - r_e\Big) - \delta_e\, r_e. \tag{SI-8.1f}$$

Here, all state variables are as defined for the original (non-modified) S model (1), see the main text. New parameters in (SI-8.1b) and (SI-8.1b) include: k_{ssrA}, a maximal degradation rate for ssrA tagged proteins, δ is an intracellular dilution rate due to cell growth. A new term Z_i used in (SI-8.1b) and (SI-8.1b) is

$$Z_i = x_i/K_{MX} + y_i/K_{MY}. \tag{SI-8.2}$$

(SI-8.2) assumes that the degradation kinetics of all ssrA-tagged proteins via ClpXP is the same and, hence, can be described with the same Michaelis-Menten equation [37]. Parameters, K_{MY} and K_{MY}, used in (SI-8.2) are scaled Michaelis constants. All other parameters in (SI-8.1a) - (SI-8.1f) are as defined for the original (non-modified) S model (1).

SI-8.2 Modification of the A Model

A dimensionless modified A_m model is

$$\frac{dx_i}{dt} = \gamma_x + \frac{a_1}{1+y_i^{n_Y}} + \frac{a_4\, r_i^{n_R}}{1+r_i^{n_R}} - \delta\, x_i - \frac{k_{ssrA}\, x_i}{1 + Z_i}, \tag{SI-8.3a}$$

$$\frac{dy_i}{dt} = \gamma_y + \frac{a_2}{1+x_i^{n_X}} - \delta\, y_i - \frac{k_{ssrA}\, y_i}{1 + Z_i}, \tag{SI-8.3b}$$

$$\frac{dr_i}{dt} = \gamma_r + \frac{a_6}{1+x_i^{n_X}} + d\Big(r_e - r_i\Big) - \delta_r\, r_i, \quad i = 1, \ldots, N, \tag{SI-8.3c}$$

$$\frac{dr_e}{dt} = \frac{\rho}{N}\sum_{i=1}^{N} d\Big(r_i - r_e\Big) - \delta_e\, r_e. \tag{SI-8.3d}$$

Here, all state variables and parameters are as defined for the S_m model (SI-8.1).

SI-8.3 Reference parameter values

For the sake of simplicity and as an important extreme situation, we assume that the reference number of AAA+ protease ClpXP molecules per cell is of the same order of magnitude as the reference number of ssrA-tagged protein molecules, *i.e.*, LacI and TetR (SI-2.2 Nondimensionalization). In other words, we assume that the number of AAA+ protease ClpXP molecules per cell is about 40 monomers per cell, that is, ssrA-tagged LacI and TetR should compete for AAA+ protease ClpXP. A set of all dimensionless parameter values used in the modified models can be found in Table SI-8.1, and is computed based on the data obtained from [37].

Table SI-8.1. Dimensionless parameter values used in the computational modeling.

Name	Description of dimensionless parameters	Value
k_{ssrA}	a maximal degradation rate for ssrA tagged proteins	10.0
K_{MX}	a parameter reciprocal to the non-monotonicity degree for LacI	33.0
K_{MY}	a parameter reciprocal to the non-monotonicity degree for TetR	33.0
δ	an intracellular dilution rate due to cell growth	0.7

References

1. Kobayashi H, Kærn M, Araki M, Chung K, Gardner TS, Cantor CR, et al. Programmable cells: interfacing natural and engineered gene networks. Proceedings of the National Academy of Sciences of the United States of America. 2004;101(22):8414–8419.
2. Kuznetsov A, Kærn M, Kopell N. Synchrony in a population of hysteresis-based genetic oscillators. SIAM Journal on Applied Mathematics. 2004;65(2):392–425.
3. Wang J, Zhang J, Yuan Z, Zhou T. Noise-induced switches in network systems of the genetic toggle switch. BMC systems biology. 2007;1(1):50.
4. Gardner TS, Cantor CR, Collins JJ. Construction of a genetic toggle switch in *Escherichia coli*. Nature. 2000;403(6767):339–342.
5. Bolouri H. Computational modeling of gene regulatory networks: a primer. World Scientific; 2008.
6. Sauro HM. Enzyme kinetics for systems biology. Future Skill Software; 2011.
7. Arpino JA, Hancock EJ, Anderson J, Barahona M, Stan GBV, Papachristodoulou A, et al. Tuning the dials of synthetic biology. Microbiology. 2013;159(Pt 7):1236–1253.
8. Elowitz MB, Leibler S. A synthetic oscillatory network of transcriptional regulators. Nature. 2000;403(6767):335–338.
9. Farrell CM, Baker TA, Sauer RT. Altered specificity of a AAA+ protease. Molecular cell. 2007;25(1):161–166.
10. Cornish-Bowden A. Fundamentals of enzyme kinetics. John Wiley & Sons; 2013.
11. Tuttle LM, Salis H, Tomshine J, Kaznessis YN. Model-driven designs of an oscillating gene network. Biophysical journal. 2005;89(6):3873–3883.
12. Garde C, Bjarnsholt T, Givskov M, Jakobsen TH, Hentzer M, Claussen A, et al. Quorum sensing regulation in *Aeromonas hydrophila*. Journal of molecular biology. 2010;396(4):849–857.
13. Neidhardt FC, Ingraham JL, Schaechter M. Physiology of the Bacterial Cell: A Molecular Approach. Sinauer Associates Sunderland, MA; 1990.
14. Domach M, Leung S, Cahn R, Cocks G, Shuler M. Computer model for glucose-limited growth of a single cell of *Escherichia coli* B/r-A. Biotechnology and bioengineering. 2000;67(6):827–840.
15. Shuler M, Leung S, Dick C. A mathematical model for the growth of a single bacterial cell. Annals of the New York Academy of Sciences. 1979;326(1):35–52.
16. Shuler M. Single-cell models: promise and limitations. Journal of biotechnology. 1999;71(1):225–228.
17. Castellanos M, Wilson DB, Shuler ML. A modular minimal cell model: purine and pyrimidine transport and metabolism. Proceedings of the National Academy of Sciences of the United States of America. 2004;101(17):6681–6686.

18. Nikolaev EV, Atlas JC, Shuler ML. Computer models of bacterial cells: from generalized coarsegrained to genome-specific modular models. In: Journal of Physics: Conference Series. vol. 46. IOP Publishing; 2006. p. 322.

19. Kim BG, Shuler M. A structured, segregated model for genetically modified *Escherichia coli* cells and its use for prediction of plasmid stability. Biotechnology and bioengineering. 1990;36(6):581–592.

20. Shu J, Shuler M. Prediction of effects of amino acid supplementation on growth of *E. coli* B/r. Biotechnology and bioengineering. 1991;37(8):708–715.

21. Laffend L, Shuler M. Ribosomal protein limitations in *Escherichia coli* under conditions of high translational activity. Biotechnology and bioengineering. 1994;43(5):388–398.

22. Laffend L, Shuler M. Structured model of genetic control via the *lac* promoter in *Escherichia coli*. Biotechnology and bioengineering. 1994;43(5):399–410.

23. Bailey JE. Mathematical modeling and analysis in biochemical engineering: past accomplishments and future opportunities. Biotechnology progress. 1998;14(1):8–20.

24. Atlas J, Nikolaev E, Browning S, Shuler M. Incorporating genome-wide DNA sequence information into a dynamic whole-cell model of *Escherichia coli*: Application to DNA replication. Systems Biology, IET. 2008;2(5):369–382.

25. Segel IH. Biochemical Calculations: How To Solve Mathematical Problems In General Biochemistry. Wiley; 1976.

26. Bhattacharya BS, Sweby PK, Minihane AM, Jackson KG, Tindall MJ. A mathematical model of the sterol regulatory element binding protein 2 cholesterol biosynthesis pathway. Journal of Theoretical Biology. 2014;p. 150–162.

27. Lodish H, Berk A, Kaiser CA, Krieger M, Bretscher A, Ploegh H, et al. Molecular cell biology. Macmillan; 2012.

28. Bernstein JA, Khodursky AB, Lin PH, Lin-Chao S, Cohen SN. Global analysis of mRNA decay and abundance in Escherichia coli at single-gene resolution using two-color fluorescent DNA microarrays. Proceedings of the National Academy of Sciences. 2002;99(15):9697–9702.

29. Prindle A, Selimkhanov J, Li H, Razinkov I, Tsimring LS, Hasty J. Rapid and tunable post-translational coupling of genetic circuits. Nature. 2014;.

30. Thomas PW, Stone EM, Costello AL, Tierney DL, Fast W. The quorum-quenching lactonase from *Bacillus thuringiensis* is a metalloprotein. Biochemistry. 2005;44(20):7559–7569.

31. Raj M. PCR Amplification, and Sequence Comparison of lacI gene in WT *E. coli* C29 cells and a presumptive *lacI* Knockout *E. coli* C29 cells to Determine the Difference in the Basal Expression Level of *lacZ* in Lac Operon. J Exp Microbiol Immunol. 2004;6:13–19.

32. Semsey S, Jauffred L, Csiszovszki Z, Erdőssy J, Stéger V, Hansen S, et al. The effect of LacI autoregulation on the performance of the lactose utilization system in *Escherichia coli*. Nucleic acids research. 2013;p. gkt351.

33. Ramos JL, Martínez-Bueno M, Molina-Henares AJ, Terán W, Watanabe K, Zhang X, et al. The TetR family of transcriptional repressors. Microbiology and Molecular Biology Reviews. 2005;69(2):326–356.

34. Markiewicz P, Kleina LG, Cruz C, Ehret S, Miller JH. Genetic studies of the lac repressor. XIV. Analysis of 4000 altered *Escherichia coli* lac repressors reveals essential and non-essential residues, as well as" spacers" which do not require a specific sequence. Journal of molecular biology. 1994;240(5):421–433.

35. Daniel R, Rubens JR, Sarpeshkar R, Lu TK. Synthetic analog computation in living cells. Nature. 2013;497(7451):619–623.

36. Carbonell-Ballestero M, Duran-Nebreda S, Montañez R, Solé R, Macía J, Rodríguez-Caso C. A bottom-up characterization of transfer functions for synthetic biology designs: lessons from enzymology. Nucleic acids research. 2014;42(22):14060–14069.

37. Chen Y, Kim JK, Hirning AJ, Josić K, Bennett MR. Emergent genetic oscillations in a synthetic microbial consortium. Science. 2015;349(6251):986–989.

38. Postle K, Nguyen TT, Bertrand KP. Nucleotide sequence of the repressor gene of the TN10 tetracycline resistance determinant. Nucleic acids research. 1984;12(12):4849–4863.

39. Baumeister R, Flache P, Melefors Ö, von Gabain A, Hillen W. Lack of a 5'non-coding region in Tn 1721 encoded *tetR* mRNA is associated with a low efficiency of translation and a short half-life in *Escherichia coil*. Nucleic acids research. 1991;19(17):4595–4600.

40. Wang Y, Tegenfeldt JO, Reisner W, Riehn R, Guan XJ, Guo L, et al. Single-molecule studies of repressor–DNA interactions show long-range interactions. Proceedings of the National Academy of Sciences of the United States of America. 2005;102(28):9796–9801.

41. Pai A, You L. Optimal tuning of bacterial sensing potential. Molecular systems biology. 2009;5(1).

42. Chen CC, Riadi L, Suh SJ, Ohman DE, Ju LK. Degradation and synthesis kinetics of quorum-sensing autoinducer in *Pseudomonas aeruginosa* cultivation. Journal of biotechnology. 2005;117(1):1–10.

43. Flynn JM, Levchenko I, Seidel M, Wickner SH, Sauer RT, Baker TA. Overlapping recognition determinants within the ssrA degradation tag allow modulation of proteolysis. Proceedings of the National Academy of Sciences. 2001;98(19):10584–10589.

44. Selinger DW, Saxena RM, Cheung KJ, Church GM, Rosenow C. Global RNA half-life analysis in *Escherichia coli* reveals positional patterns of transcript degradation. Genome research. 2003;13(2):216–223.

45. Ochsner UA, Reiser J. Autoinducer-mediated regulation of rhamnolipid biosurfactant synthesis in *Pseudomonas aeruginosa*. Proceedings of the National Academy of Sciences. 1995;92(14):6424–6428.

46. Takaya A, Tabuchi F, Tsuchiya H, Isogai E, Yamamoto T. Negative regulation of quorum-sensing systems in *Pseudomonas aeruginosa* by ATP-dependent Lon protease. Journal of bacteriology. 2008;190(12):4181–4188.

47. Brint JM, Ohman DE. Synthesis of multiple exoproducts in *Pseudomonas aeruginosa* is under the control of RhlR-RhlI, another set of regulators in strain PAO1 with homology to the autoinducer-responsive LuxR-LuxI family. Journal of Bacteriology. 1995;177(24):7155–7163.

48. Sontag ED. Monotone and near-monotone biochemical networks. Systems and Synthetic Biology. 2007;1:59–87.

49. Harary F. On the notion of balance of a signed graph. Michigan Mathematical Journal. 1953;2:143?146.

50. Smith H. Monotone dynamical systems: An introduction to the theory of competitive and cooperative systems, Mathematical Surveys and Monographs, vol. 41. Providence, RI: AMS; 1995.

51. Angeli D, Sontag ED. Monotone control systems. IEEE Trans Automat Control. 2003;48(10):1684–1698.

52. Golubitsky M, Schaeffer DG, Stewart I. Singularities and groups in bifurcation theory. vol. 2. Springer New York; 1988.

53. Kuznetsov YA. Elements of applied bifurcation theory. vol. 112. Springer Science & Business Media; 2013.

54. Nikolaev EV. Bifurcations of limit cycles of differential equations admitting an involutive symmetry. Sbornik: Mathematics. 1995;186(4):611.

55. Krupa M. Bifurcations of relative equilibria. SIAM journal on mathematical analysis. 1990;21(6):1453–1486.

56. Sontag ED. Mathematical control theory: deterministic finite dimensional systems. vol. 6. Springer; 2013.

57. Shnol E. The synchronization of oscillators which interact via a medium. Journal of Applied Mathematics and Mechanics. 1987;51(1):9–13.

58. Katriel G. Synchronization of oscillators coupled through an environment. Physica D: Nonlinear Phenomena. 2008;237(22):2933–2944.

59. Hartman P. Ordinary differential equations. Wiley, New York; 1964.

60. Gantmakher FR. The theory of matrices. vol. 131. American Mathematical Soc.; 1959.

61. Vasil'eva AB, Butuzov VF, Kalachev LV. The boundary function method for singular perturbation problems. SIAM; 1995.